3-1972

An Investigation of the Thermal Conductivity, Electrical Resistivity, and Thermoelectric Power of Thorium Nitride-Uranium Nitride Alloys

Samuel Cavin Weaver
University of Tennessee, Knoxville

To the Graduate Council:

I am submitting herewith a dissertation written by Samuel Cavin Weaver entitled "An Investigation of the Thermal Conductivity, Electrical Resistivity, and Thermoelectric Power of Thorium Nitride-Uranium Nitride Alloys." I have examined the final electronic copy of this dissertation for form and content and recommend that it be accepted in partial fulfillment of the requirements for the degree of Doctor of Philosophy, with a major in Materials Science and Engineering.

J. E. Spruiell, Major Professor

We have read this dissertation and recommend its acceptance:

Earl McHayes, E. E. Stooksbury, Howard L Davis, John W. Prader, S. L. Oliver

Accepted for the Council:

Carolyn R. Hodges

Vice Provost and Dean of the Graduate School

(Original signatures are on file with official student records.)

February 25, 1972

To the Graduate Council:

I am submitting herewith a dissertation written by Samuel Cavin Weaver, entitled, "An Investigation of the Thermal Conductivity, Electrical Resistivity, and Thermoelectric Power of Thorium Nitride-Uranium Nitride Alloys." I recommend that it be accepted in partial fulfillment of the requirements for the degree of Doctor of Philosophy, with a major in Metallurgical Engineering.

J. E. Spruiell
Major Professor

We have read this dissertation
and recommend its acceptance:

Carl J. Mathews

E. E. Hansbury

Harold L. Davis

John W. Prados

Ben F. Oliver

Accepted for the Council:

Hilton A. Smith
Vice Chancellor for
Graduate Studies and Research

AN INVESTIGATION OF THE THERMAL CONDUCTIVITY, ELECTRICAL RESISTIVITY, AND THERMOELECTRIC POWER OF THORIUM NITRIDE-URANIUM NITRIDE ALLOYS

A Dissertation

Presented to

the Graduate Council of

The University of Tennessee

In Partial Fulfillment

of the Requirements for the Degree

Doctor of Philosophy

---

by

Samuel Cavin Weaver

March 1972

ACKNOWLEDGMENTS

The author wishes to acknowledge Dr. J. E. Spruiell for his assistance, continuous encouragement, and guidance throughout the author's graduate studies at the University of Tennessee for the past seven years. His aid and assistance in writing the Master's Thesis and this Dissertation were most valuable.

Dr. D. L. McElroy, the author's research group leader at Oak Ridge National Laboratory, provided the author with the opportunity to do this research. Dr. McElroy recognized the value of this work from the initial concept and much of the technical direction is a result of his guidance. The opportunity to work with him was extremely gratifying and sincerely enjoyable.

To Dr. J. L. Scott, the author's previous research group leader at Oak Ridge National Laboratory, the author is sincerely grateful. Dr. Scott has been a constant source of encouragement to the author's graduate studies during his entire study program at the University of Tennessee.

Dr. T. G. Kollie of the Physical Properties Group at Oak Ridge National Laboratory spent many, many hours providing detailed technical assistance to the author. Among other things, the use of the PDP-8 Computer CODAS system would not have been possible without his valuable help. His assistance and encouragement were invaluable.

Dr. R. K. Williams is gratefully acknowledged for his assistance in both the experimental data taking and in the evaluation of the data. He advised on much of the mathematical treatment of the data and some of the data treatment was actually devised and published by him.

Mr. J. P. Moore developed the guarded thermal conductivity apparatus used in the experiments in this study. His technical guidance in the experimental techniques was essential to the success of the data taken.

Dr. W. Fulkerson is acknowledged for his assistance in the areas of sample preparation and technical discussions. Thanks are extended to Mr. J. R. Ritts for his nuclear physics calculations which demonstrated the practical value of this work.

Mr. W. W. Ewing assisted the author during nearly all of the experimental work and did much of the sample preparation and equipment assembly. His assistance was most valuable. The author is thankful for the assistance of Mr. R. S. Graves who also assisted in some of the experimental work.

The author wishes to extend thanks to the following persons who assisted in the research and preparation of this document: Mrs. Edith Jones who typed this manuscript; Mr. R. A. Potter and Dr. V. J. Tennery for their assistance in preparing (Th-U)N powder metallurgy samples; Mr. G. D. Stohler for the metallography work; and to Mr. W. W. Proaps and Mr. W. Colwell for their assistance in preparing the drawings.

The author wishes to thank the Oak Ridge National Laboratory for the opportunity provided under its educational assistance program. The research was sponsored by the Atomic Energy Commission under contract with Union Carbide Corporation.

The author gratefully acknowledges his parents, Mr. and Mrs. S. L. Weaver, who have been a constant source of inspiration throughout his life.

Special thanks and appreciation are reserved for the author's wife, Carol, for her continuing encouragement and inspiration during the difficult years as a graduate student.

ABSTRACT

Thermal conductivity, electrical resistivity, and thermoelectric power measurements were made on thorium nitride (ThN), (Th-2% U)N, and (Th-5% U)N; electrical resistivity and thermoelectric power measurements were made on uranium nitride (UN). Results from the experiments indicated that ThN behaves very nearly as a pure metal in its transport properties. Thermal conductivities, λ, were high, electrical resistivities, ρ, were low, and thermoelectric power, S, measurements were nearly zero. Uranium nitride, which antiferromagnetic below 50 °K and has a lower thermal conductivity, had a much higher electrical resistivity and a large positive thermoelectric power.

The thermal conductivity of ThN is much higher than nuclear fuels currently being considered for use in liquid metal fast breeder reactors. At nuclear reactor operating temperatures of interest, λ for ThN is approximately 20 times that of UO_2. Even when alloyed with UN, ThN retained a thermal conductivity greater than any other ceramic fuel currently being considered. Calculations were presented which illustrate the potential of ThN alloyed with UN or plutonium nitride (PuN) as fuels in proposed reactor concepts. The results suggested ThN would have a significant economic advantage and a predicted fuel performance which exceeds other fuels being considered.

The electrical resistivity measurements showed ThN and the (Th-U)N alloys to have a linear dependence with temperature above about 100 °K. Below 100 °K, the slope changed to near zero at 0 °K. Small additions of UN to ThN of 2 and 5% caused a very large increase in ρ.

This probably resulted because the antiferromagnetic UN exhibits a large ρ. In addition to changing the residual resistivity at 4.2 °K, $d\rho/dT$ was reduced by alloying.

The thermoelectric power of ThN is very small. However, alloying with UN, which has a large value for S, caused a significant change in the S of (Th-U)N alloys.

The data treatment permitted a separation of λ into a lattice conductivity, λ_L, and an electronic contribution to the thermal conductivity, λ_e. The results showed both of these contributions to be significant over the temperature range studied. The ability to separate the components accurately allowed a prediction of λ at temperatures greatly exceeding the range of actual experimental measurements. The data treatment also resulted in a calculation for the Lorenz function which was found to be very near the Sommerfeld value at temperatures of 300 °K and above.

A significant aspect of the study was the development of a technique to make high quality samples. None of the standard fabrication techniques were satisfactory, so a zone melting technique was developed which converted the metal directly into the nitride. This technique produced high-purity, high-density samples approximately 100 times as fast as any of the other more conventional techniques. The fabricated samples were nearly 100% dense with very large grains of approximately 0.3 cm diameter. High-density, large-grained samples would be expected to show superior in-reactor performance to either small-grained or low-density samples.

Another important aspect of the study was the use of the PDP-8 computer to take and analyze some of the data. By using the computer

system, the data were taken approximately 1000 times faster in the case of high temperature ρ measurements. This is very important for a material such as UN which has a large value for S and exhibits significant Peltier heating on reversing the electrical current. In the case of UN, this was the only way accurate data could be obtained above 1200 °K.

TABLE OF CONTENTS

CHAPTER		PAGE
I.	INTRODUCTION AND THEORETICAL BACKGROUND	1
	Background and Practical Importance of Study	1
	Theories of Thermal Conductivity	16
	Lattice Thermal Conductivity	18
	Electronic Thermal Conductivity	24
	Theories of Electrical Resistivity	30
	Theories of Thermoelectric Power	33
II.	REVIEW OF EXPERIMENTAL MEASUREMENTS	37
	Properties of the Uranium-Thorium-Nitrogen System	37
	Electrical Resistivity	44
	Thermal Conductivity	47
	Thermoelectric Power	52
III.	EXPERIMENTAL DETAILS	55
	Sample Preparation	55
	Uranium Nitride Fabrication	55
	Thorium Nitride and (Thorium-Uranium) Nitride Fabrication	55
	Measurement Techniques	73
	Electrical Resistivity Knife Edge	73
	Electrical Resistivity Apparatus	76
	Guarded Longitudinal Heat Flow Apparatus	78
	Calibration of Equipment	85
	CODAS System and Circuitry	87

CHAPTER PAGE

Error Analysis 90

IV. RESULTS AND DISCUSSION 93

High-Temperature Electrical Resistivity 93

Low-Temperature Electrical Resistivity 98

Thermal Conductivity 109

Total Thermal Conductivity 109

Lattice Thermal Conductivity 114

Electronic Thermal Conductivity 126

Thermal Conductivity Extrapolated to High Temperatures 131

Weidemann-Franz-Lorenz Ratio 134

Thermoelectric Power 137

V. CONCLUSIONS AND RECOMMENDATIONS 145

Conclusions 145

Recommendations 146

BIBLIOGRAPHY 148

APPENDIXES 154

Appendix A 155

Appendix B 175

VITA 198

LIST OF TABLES

TABLE		PAGE
1.	Results of Calculations on Proposed Reactor Concepts Using Various Combinations of Nitride Fuels	7
2.	Summary of Some Properties of Interest in ThN	43
3.	Techniques of Sample Preparation	56
4.	Chemical Analysis of Samples	57
5.	Results of Spectrographic Analysis of Specimens	58
6.	Comparison of Thermal Conductivity of Nb-10% W as Measured on Equipment Used in Study with Previous Measurements by Moore	86
7.	Comparison of Voltage Readings from 6-Dial Potentiometer with CODAS	89
8.	Summary of Measurement Errors for (Th-U)N Alloys in the Guarded Thermal Conductivity Apparatus	91
9.	Summary of Data Taken on (Th-U)N System	94
10.	Comparison of Results for Curve Fitting of ThN Data Using Various Temperature Ranges	125
A1.	Electrical Resistivity of UN as Taken from the 6-Dial Potentiometer	156
A2.	Electrical Resistivity of UN from Room Temperature to 1700 °K Using CODAS	157
A3.	Electrical Resistivity Data for ThN, Sample Th-13 . . .	158
A4.	Electrical Resistivity Data for (Th-2% U)N, Sample Th-16	159

TABLE PAGE

A5. Electrical Resistivity Data for (Th–5% U)N, Sample Th-15 160

A6. Electrical Resistivity Data for (Th–5% U)N, Sample Th-21 161

A7. Thermal Conductivity Data for ThN, Sample Th-13 162

A8. Thermal Conductivity Data for (Th–2% U)N, Sample Th-16 163

A9. Thermal Conductivity Data for (Th–5% U)N, Sample Th-15 164

A10. Thermal Conductivity Data for (Th–5% U)N, Sample Th-21 165

A11. Thermoelectric Power Measurements of Uranium Nitride 166

A12. Thermoelectric Power of ThN, Sample AC-6 167

A13. Thermoelectric Power of (Th–1% U)N, Sample AC-1 168

A14. Thermoelectric Power of (Th–2% U)N, Sample AC-15 169

A15. Thermoelectric Power of (Th–5% U)N, Sample AC-5 170

A16. Thermoelectric Power of ThN, Sample Th-13 171

A17. Thermoelectric Power of (Th–2% U)N, Sample Th-16 172

A18. Thermoelectric Power of (Th–5% U)N, Sample Th-15 173

A19. Thermoelectric Power of (Th–5% U)N, Sample Th-21 174

B1. Smoothed Electrical Resistivity Values for UN 176

B2. Smoothed Electrical Resistivity Values for ThN from 298 to 1273 °K 177

B3. Smoothed Values of Electrical Resistivity 178

B4. Extrapolated Electrical Resistivity Data 179

TABLE PAGE

B5. Comparison of Electrical Resistivity Values with that Calculated from the Bloch-Gruneisen Equation, Assuming θ = 286°K 180

B6. Change in Impurity Electrical Resistivity as Calculated from Bloch-Gruneisen Equation 181

B7. Smoothed Values of Thermal Conductivity 182

B8. Two Component Separation of (Th-2% U)N and ThN, Samples Th-16 and Th-13 183

B9. Two Component Separation of (Th-5% U)N and ThN, Samples Th-15 and Th-13 184

B10. Two Component Separation of (Th-5% U)N and ThN, Samples Th-21 and Th-13 185

B11. Error Analysis for Two Component Separation of (Th-2% U)N and ThN, Samples Th-16 and Th-13 186

B12. Error Analysis for Two Component Separation of (Th-5% U)N and ThN, Samples Th-15 and Th-13 187

B13. Error Analysis for Two Component Separation of (Th-5% U)N and ThN, Samples Th-21 and Th-13 188

B14. Lattice Component of Thermal Resistivity of ThN and (Th-U)N Alloys 189

B15. Extrapolated Thermal Conductivity Data 190

B16. Weidemann-Franz-Lorenz Ratio of Arc Cast Samples 191

B17. Weidemann-Franz-Lorenz Ratio of Arc Cast Sample Expressed as Fraction of Sommerfeld Value 192

B18. Weidemann-Franz-Lorenz Ratio of Zone Melted Samples . . 193

B19. Weidemann-Franz-Lorenz Ratio of Zone Melted Samples Expressed Fraction of Sommerfeld Values 194

TABLE PAGE

B20. Smoothed Values of Thermoelectric Power for UN from 100 to 1700 °K 195

B21. Smoothed Values of Thermoelectric Power from Arc Cast Samples 196

B22. Smoothed Values of Thermoelectric Power of (Th-U)N for Zone Melted Samples 197

LIST OF FIGURES

FIGURE PAGE

1. Thermal Conductivities of Some Potential Nuclear Fuels 3

2. Curves Showing the Relationship Between Operating Fuel Centerline Temperatures and Linear Heat Ratings. These curves assume the fuel is in the shape of a solid right circular cylinder and that the surface temperature of the fuel is at 1000 °K 5

3. Ratio of Linear Heat Rating with Central Hole, H_c, to Linear Heat Rating of Solid Pellet, H_o, as Function of Volume of Fuel Removed by Hole 11

4. Curves Showing the Effect of Annulus Size in Cylindrical Fuel Pellets on Maximum Operation Temperature of the Fuel 14

5. Schematic Representation of the Lattice Thermal Resistivity of a Nonmagnetic Metal. (1) Phonon-electron resistance. (2) Phonon-boundary resistance. (3) Phonon-impurity resistance. (4) Three-phonon Umklapp Resistance. (5) Higher order Umklapp Resistance. (6) Summation curve 23

6. Schematic Representation of the Lorenz Function Showing Deviations from L_o. (1) Pure, defect-free metal with no electron-electron scattering. (2)(3) Effects of increasing impurity content. (4) Effect of electron-electron inelastic scattering at high temperatures. (5) Effect of ambipolar enhancement 28

FIGURE PAGE

7. Schematic Diagram of Two Metals with Junctions at Two Different Temperatures T_1 and T_2 to Illustrate Thermoelectric Effect 35

8. The Uranium-Nitrogen Binary System After Benz and Bowman 38

9. The Thorium-Nitrogen Binary System After Benz et al. . . 39

10. The Uranium-Thorium Binary System 40

11. The Equilibrium 1273 °K Partial Isotherm of the Th-U-N System Showing Alloys Examined and the Number of Major Phases Identified by X-Ray and Metallographic Examination 41

12. Lattice Parameters of (Th-U)N Across the UN-ThN Pseudobinary 42

13. Results of Experimental Measurements of Electrical Resistivity of Uranium Mononitride by Various Experimenters 45

14. Plot of Electrical Resistivity of Uranium Mononitride as a Function of Pore Volume Fraction with Residual Resistivity Substracted from Total Resistivity 46

15. Electrical Resistivity of ThN as a Function of Temperature 48

16. Thermal Conductivity of Uranium Monitride to 400 °K . . . 50

17. Thermal Conductivity of Uranium Mononitride to 1800 °K . . 51

18. Thermoelectric Power Measurements of UN and ThN 53

19. Thermoelectric Power of ThN as a Function of Temperature 54

FIGURE PAGE

20. Synthesis of Uranium Nitride Powder 59

21. Fabrication of Uranium Nitride Pellets 60

22. Sintering Cycle for Uranium Nitride Pellets 61

23. Typical Microstructure of As-Sintered Uranium Mononitride 62

24. Zone-Melting Apparatus Used to Fabricate (Th-U)N Rods . . 64

25. Photomicrograph of Typical ThN Microstructure as Fabricated from the Zone Melting Process. Magnification: 500X 68

26. Typical Microstructure of ThN after Casting in a Nitrogen Atmosphere 71

27. Schematic Diagram of Guarded Longitudinal Heat Flow Apparatus 80

28. Electrical Resistivity of UN Compared with Previous Experimenters 96

29. Electrical Resistivity of ThN 99

30. Electrical Resistivity of ThN, (Th-U)N, and UN 100

31. Residual Resistivity of (Th-U)N as a Function of Uranium Content 102

32. Extrapolated Values of Electrical Resistivity to High Temperature 104

33. Residual Resistivity of ThN as Function of Temperature as Calculated from Bloch-Gruneisen Equation. These calculations show the deviation from Matthiessen's rule 106

FIGURE PAGE

34. Electrical Resistivity of Thorium Metal 108

35. Thermal Conductivity of ThN 110

36. Thermal Conductivity of (Th-2% U)N 111

37. Thermal Conductivity of (Th-5% U)N 112

38. Total Thermal Conductivity and Lattice Contribution to Thermal Conductivity 117

39. Lattice Component of Thermal Resistivity as Function of Temperature 118

40. Results of Curve Fit to Equation $\lambda = \frac{L\omega T}{\rho}\left[1 - \exp\left(-\frac{T}{\Delta} + 0.2138\right)\right] + \frac{\eta}{T}$ 124

41. Electronic Contribution to Thermal Conductivity of (Th-U)N 127

42. Thermal Conductivity of (Th-2% U)N, Sample Th-16 128

43. Thermal Conductivity of (Th-5% U)N, Sample Th-15 129

44. Lorenz Function as Calculated from Two Component Separation 132

45. Thermal Conductivity of (Th-U)N Extrapolated to High Temperatures 133

46. Weidemann-Franz-Lorenz Ratio for Zone Melted Samples Expressed as Fraction of Sommerfeld Value 135

47. Weidemann-Franz-Lorenz Ratio of Arc Cast Samples Expressed as Fraction of Sommerfeld Value 136

48. Comparison of Thermoelectric Power Data with Previous Experimenters 138

49. Thermoelectric Power of (Th-U)N Alloys Versus Constantan for Arc Cast Samples 139

FIGURES PAGE

50. Thermoelectric Power of (Th-U)N Alloys 141

51. Thermoelectric Power of (Th-U)N Versus Constantan for Zone Cast Alloys 142

52. Thermoelectric Power of Zone Melted (Th-U)N 143

CHAPTER I

INTRODUCTION AND THEORETICAL BACKGROUND

I. BACKGROUND AND PRACTICAL IMPORTANCE OF STUDY

One of the most important physical properties of a nuclear fuel is its thermal conductivity. The thermal conductivity, λ, largely determines the temperature at which the fuel will operate, the maximum obtainable heat flux from a fuel pin, and, consequently, dictates almost the entire design of the reactor. Most current electrical power producing reactors are designed and run using UO_2 as the fuel. This is a severe economic limitation because UO_2 is a poor thermal conductor which results in a maximum linear heat rating per fuel pin of about 0.7 kW/cm. At this heat flux the centerline temperature of the fuel approaches 3000 °K, which is very near the melting temperature of 3125 °K, which is the allowable upper limit of fuel operation. The importance of this can be seen from Equation (1) which relates the heat output, or linear heat rating, of a solid right circular cylinder fuel pin from which the heat flows radially and the heat generation/volume is constant.

$$H = 4\pi \int_{T_1}^{T_2} \lambda dT \ , \qquad (1)$$

where H = linear heat rating

T_1 = surface temperature of fuel

T_2 = center temperature of fuel

λ = thermal conductivity of fuel.

Note that the dimensions of the fuel do not enter into this equation. Thus, the linear heat rating of a fuel pin is determined by the area under a λ versus T curve such as those drawn in Figure 1 for several potential nuclear fuels. Consequently, the operating temperature of the fuel for a given heat rating is determined only by the thermal conductivity and the surface temperature of the fuel. From this, one can see that an increase in λ would result in increased capability for generating heat in a fuel pin, assuming the allowable maximum operating temperature is the same. A fuel with a much higher λ could show a significant reduction in power operating costs and consequently cheaper electrical power.

The search for a fuel with a high thermal conductivity led to an examination of a class of high-melting compounds with metallic characteristics known as refractory hard metals.[1*] These materials are compounds of transition metal atoms with comparatively smaller nonmetal atoms such as carbon, nitrogen, boron, and silicon. These compounds: (1) show metallic luster, (2) have thermal and electrical conductivities near pure metals, (3) have a positive temperature coefficient of electrical resistivity, (4) have high hardness values, (5) have a high modulus of elasticity, (6) have high melting points, and (7) have correspondingly high strengths at elevated temperatures.

The main interest centers around the refractory hard metal alloys resulting from combinations of the elements, uranium, thorium, plutonium, nitrogen, and carbon because of their potential use as fuels for liquid metal fast breeder reactor systems and for space reactors. Their

---

*Denotes reference. See page 148.

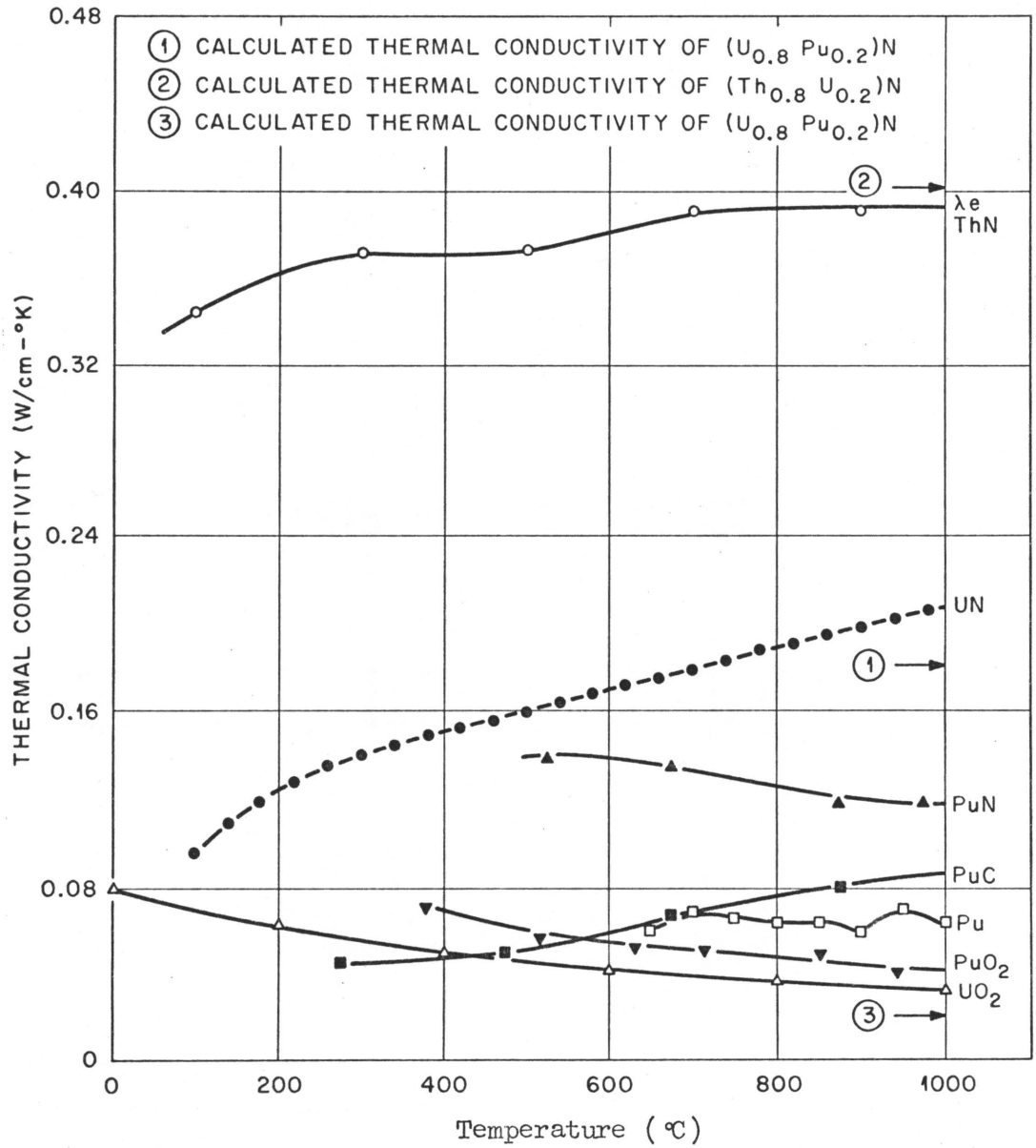

Figure 1. Thermal Conductivities of Some Potential Nuclear Fuels.

attractiveness stems from the following properties: (1) high thermal conductivity, (2) high metal density, (3) high melting point, (4) good compatibility with most cladding materials, and (5) good compatibility with most liquid metals.

Interest in refractory hard metal fuels for both fast breeder and space reactors is increasing as more information becomes known about these systems. Those alloys being investigated most vigorously include uranium nitride (UN), (U-Pu)N alloys, U(N-C) alloys, and (U-Pu) (N-C) alloys. Uranium nitride and U(N-C) alloys are being investigated for liquid metal cooled space reactor systems, while (U-Pu)N alloys and (U-Pu) (N-C) alloys are being investigated for liquid metal fast breeder reactor systems. These alloys afford the potential of operating at linear heat ratings of 2 kW/cm and for the plutonium-bearing fuels of attaining fuel doubling times of less than 10 years.

Unfortunately, none of the materials mentioned above take advantage of the other potentially large source of nuclear fuel, thorium. With this in mind, the investigation of (U-Th)N alloys was initiated.

Because thorium nitride (ThN) and (Th-U)N alloys have high thermal conductivities, they are interesting from the standpoint of using (Th-U)N or (Th-Pu)N as possible reactor fuels. A high thermal conductivity allows the fuel to run cooler for a given heat output from a fuel rod. Lower operating temperatures reduce fission-gas mobility[a] in the fuel which is of prime importance since fuel swelling caused by fission-gas bubbles is the major limitation on fuel performance.

Figure 2 shows linear heat ratings, H, versus fuel centerline temperature, which assumes an average thermal conductivity of

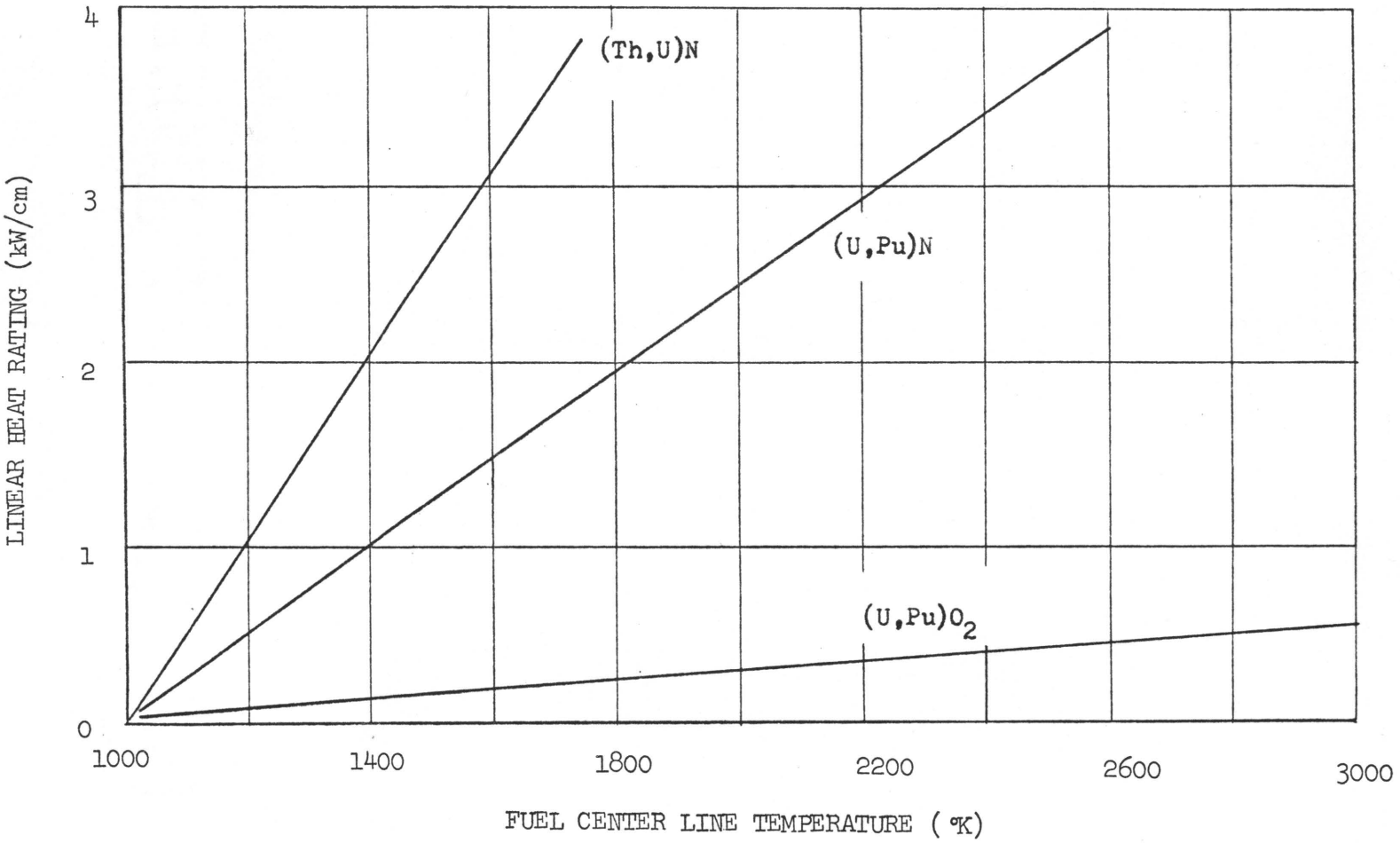

Figure 2. Curves Showing the Relationship Between Operating Fuel Centerline Temperatures and Linear Heat Ratings. These curves assume the fuel is in the shape of a solid right circular cylinder and that the surface temperature of the fuel is at 1000 °K.

0.40 W/cm-°K for (Th-U)N, 0.19 W/cm-°K for (U-Pu)N, and 0.02 W/cm-°K for $(U\text{-}Pu)O_2$. The curve for (Th-U)N can also be used for (Th-Pu)N, as the thermal conductivities should not be much different.

Using the assumed thermal conductivities of (U-Pu)N and (Th-U)N at high temperature, it becomes apparent that if (U-Pu)N alloys have the potential of operating at 1.5 kW/cm, (Th-U)N alloys should be able to operate at nearly 3.0 kW/cm with the same radial temperature distribution. Although high linear heat ratings such as 3.0 kW/cm are precluded in near-term reactors because of the present state of the art of heat removal capabilities, such high linear heat ratings are not necessary for economical operation. The possibility of attaining such high heat ratings shows that the operation of such a reactor would not be limited by the capabilities of the fuel but only by the external capacity for removing heat.

Some calculations performed by J. R. Ritts of the Reactor Division of Oak Ridge National Laboratory illustrate the advantages of a ThN-based fuel in more detail. These calculations were made using fuel pin and reactor designs supplied by the author and using a value of λ_{ThN} shown in Figure 1 calculated from electrical resistivity data of Auskern and Aronson.[3]

A summary of some of the more important results of the calculations is shown in Table 1. Calculations were made for 1000 MW electrical systems utilizing the high thermal conductivities and high fuel densities of the nitrides (40% higher than the oxide). The linear heat ratings assumed produce maximum fuel centerline temperatures no greater than 1875°K, so that current technology should be sufficient to utilize the

TABLE 1

RESULTS OF CALCULATIONS ON PROPOSED REACTOR CONCEPTS USING VARIOUS COMBINATIONS OF NITRIDE FUELS

	Case I	Case II	Case III	Case IV
Fuel	(U-Pu)N	(U-Pu)N	(Th-U)N	(Th-Pu)N
Core Configuration	Square cylinder	Pancake	Square cylinder	Square cylinder
Dimensions, cm	132	193 x 61	155	155
Fuel Pin				
Diameter, cm	1.27	1.27	1.27	1.27
Cladding	Nb–1% Zr	Nb–1% Zr	304 SS	304 SS
Bond	Fe	Fe	Na	Na
Cladding thickness, cm	0.038	0.038	0.056	0.056
Structure	V	V	304 SS	304 SS
Blanket	UN	UN	ThN	UN
Coolant	Natural Li	Na	Na	Na
Conversion Ratio				
Total reactor	1.321	1.400	1.185	1.403
Core	0.705	0.7754	0.887	1.049
Pu Enrichment, %	11.9	17.6	11.2 (^{233}U)	12.3
Doubling Time, year	1.57	4.92	19.4	8.38
Mean Fission Energy, Mev	0.237	0.323	0.1708	0.230
Peak to Average Fission Density				
Radial				
Center	1.246	1.44		
Outside	0.466	0.28		
Axial				
Center	1.276			
Outside	0.512			
Avg. Heat Rating, kW/cm	2.79	2.79	1.64	1.64
Coolant Volume, %	42	42	42	42

proposed fuels. Most of the fuel temperatures, such as those in the (Th-U)N and (Th-Pu)N fuels, would be less than 1600 °K maximum.

In Case I the rather unusual combination of Nb–1% Zr cladding with an iron soft metal bond was used with (U-Pu)N as the fuel. Normally Nb–1% Zr is not considered for cladding materials because of its high neutron absorption cross section. However, by increasing the linear heat rating of the fuel pins and thereby reducing the size of the core, the average neutron energy is increased, which effectively decreases the absorption cross section of the cladding. In addition, a thinner cladding can be used because of the much higher strength of the Nb–1% Zr compared with a stainless steel. Natural lithium was examined as a coolant but a further improvement in reactor performance can be obtained by using sodium as the coolant which would reduce neutron captures with little loss in coolant effectiveness. This calculation was made assuming an annular fuel with 40% of the fuel volume removed from the center to permit the fuel to operate at a maximum temperature of 1875 °K. Another technique to increase the conversion ratio would be to use UO_2 in the blanket region since the ^{14}N neutron cross section is not negligible.

The results of the calculations show a very low requirement for plutonium and a very rapid doubling time both of which represent very economical fuel cycle costs. The smaller diameter core means that the overall reactor size would be significantly reduced resulting in a reduction in plant costs.

In Case II, a (U-Pu)N pancake core was examined because of the desired nuclear safety aspects of the large diameter to thickness ratio

and because the pancake core reduced the coolant demands. Sodium was chosen as the coolant, which eliminated the loss of neutrons from the ^{6}Li capture. This reactor showed a slightly higher conversion ratio but had a more highly enriched core requiring 17.6% Pu. This, however, is still less than the 20% Pu projected for use in the $(U\text{-}Pu)O_2$ reactors. The projected doubling time of 4.92 years is still very attractive.

Two cases were examined for using ThN based fuels, one a liquid metal cooled thermal breeder using (Th-U)N, and the other a liquid metal fast breeder utilizing (Th-Pu)N as fuel. The thermal breeder utilized the Th-^{233}U cycle and had a respectable conversion ratio of 1.185, but because of the lower metal density of (Th-U)N compared with (U-Pu)N, the doubling time for the reactor was 19.4 years. Thorium-uranium nitride has a metal density about the same as $(U\text{-}Pu)O_2$. A conservative average linear heat rating of 1.6 kW/cm was assumed which could be improved on because of the high λ of (Th-U)N compared with (U-Pu)N. The use of vanadium instead of stainless steel in the structure of the reactor would also improve the conversion ratio.

Case IV was a fast breeder reactor using as fuel (Th-Pu)N with UN in the blanket. This reactor resulted in products of both ^{233}U and more plutonium and has the rather unusual property of a conversion ratio in the core greater than 1.0. This would probably require some modification since the reactivity of the core would increase with time producing a potential safety hazard. This could be easily changed, of course, by replacing some of the (Th-Pu)N pins with (U-Pu)N pins probably at the periphery of the core where the heat output from the pins would be smaller. The possibility of producing a core conversion ratio of 1.0

is very significant since it means that the frequency of core reloads would be reduced significantly so that the operating time of the reactor could be increased from the normal average of 80% to 90% or greater. This also means a reduction in the plutonium inventory required. The plutonium inventory would be further reduced by the fact that the equilibrium plutonium content is 12.3%.

Several cost calculations were made on these elements to determine the effect of fabrication costs on fuel cycle costs. The net result in each case varied approximately from 0.12 to 0.03 mills/kW-hr, depending on the assumed plant capacity. These are very attractive fuel cycle costs.

An important consideration in the use of (U-Pu)N fueled reactors is the effect of using annular fuel pellets on the operating temperature of the fuel. Equation (2) shows the relationship between the linear heat rating, H, and the size of the central hole

$$H = \left[\frac{4\pi \int_{Ta}^{Tb} \lambda(T)\, dT}{1 - \frac{2b^2}{a^2 - b^2} \ln \frac{a}{b}} \right], \qquad (2)$$

where, a = outer radius of fuel,

b = radius of central hole.

Thus, H can be increased at a fixed $\int \lambda(T)\, dT$ by increasing the size of the central hole. The increase in linear heat rating, $\frac{Hc}{Ho}$, as a function of the volume of fuel removed by the central holes is shown in Figure 3.

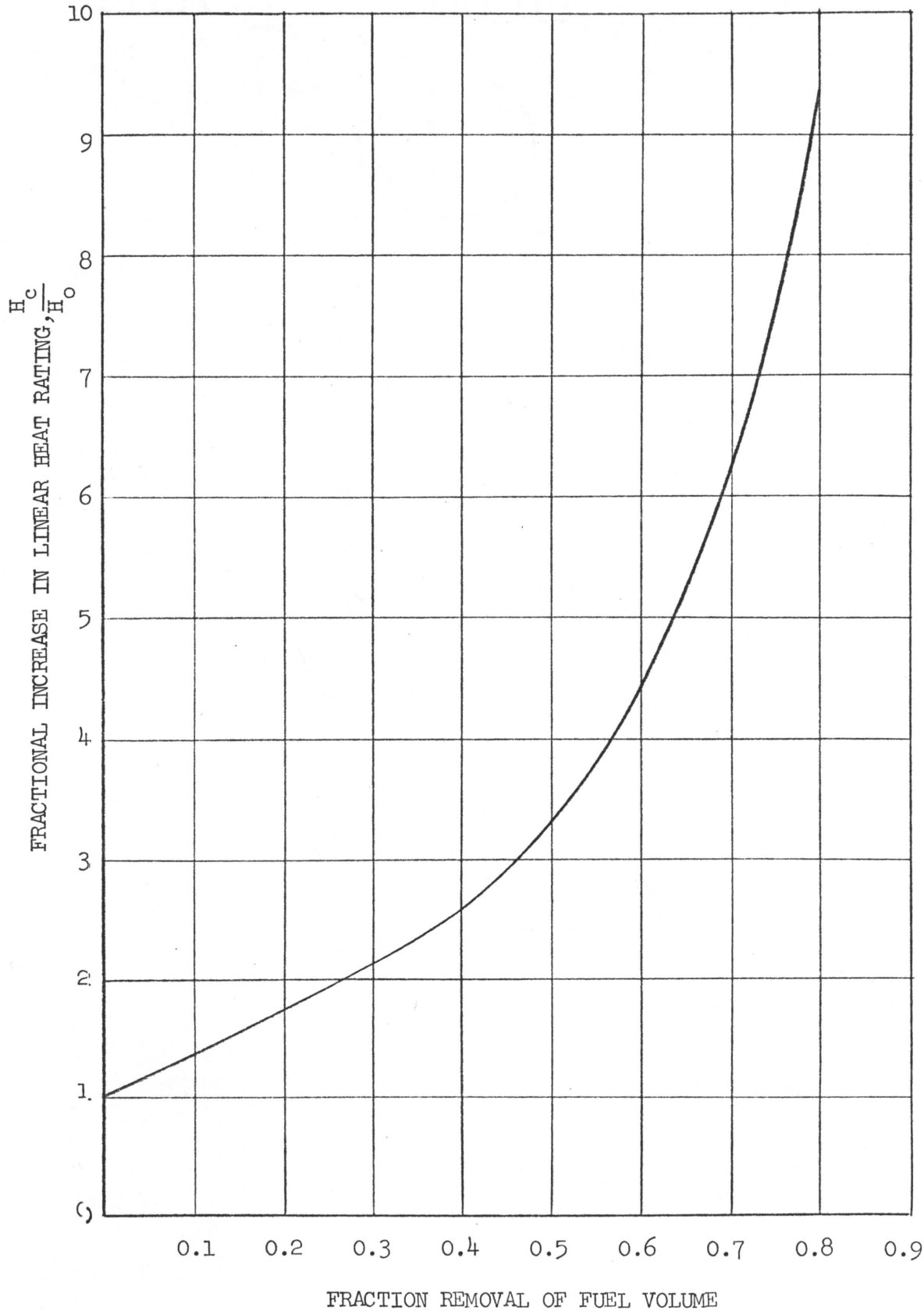

Figure 3. Ratio of Linear Heat Rating with Central Hole, H_c, to Linear Heat Rating of Solid Pellet, H_o, as Function of Volume of Fuel Removed by Hole.

To illustrate the effect of the central hole, the temperature distribution across a UN fuel pin was calculated assuming a λ_{UN} of 0.25 W/cm-°K, a sodium bond and a high thermal conductivity cladding such as Nb–1% Zr. The temperature drops, ΔT, across the fuel pins are

$$\Delta T_{total} = \Delta T_{UN} + \Delta T_{Na} + \Delta T_{cladding} , \qquad (3)$$

where, ΔT_{total} = total temperature drop, °K

ΔT_{UN} = temperature drop across fuel, °K

ΔT_{Na} = temperature drop across Na bond, °K

$\Delta T_{cladding}$ = temperature drop across Nb–1% Zr cladding, °K.

Since the temperature drop across the sodium bond will be small, it is neglected for the following calculations. Thus,

$$\Delta T_{total} = \frac{H \left(\ln \frac{r_a}{r_b} \right)_{cladding}}{2\pi\lambda_{cladding}} + \frac{H}{4\pi\lambda_{UN}} \left(1 - \frac{2b^2}{a^2 - b^2} \ln \frac{a}{b} \right) , \qquad (4)$$

where, r_a = outside radius of cladding,

r_b = inside radius of cladding.

For these calculations a ratio of $\frac{r_a}{r_b} = 1.14$ was assumed which corresponds to a 0.038 cm thick wall on a 0.635 cm diameter fuel pin or a 0.076 cm wall on a 1.27 cm diameter fuel pin.

$$\Delta T_{total} = (1.13 + 10.4\ F)H , \qquad (5)$$

$$\text{where, } F = 1 - \frac{2b^2}{a^2 - b^2} \ln \frac{a}{b} ,$$

$$F = \frac{1}{\left(\frac{Hc}{Ho}\right)} .$$

If a 900 °K cladding temperature is assumed, the maximum temperature, $Tm = 900\,°K + (1.13 + 10.4\,F)H$.

A plot of the maximum fuel temperature as a function of H is shown in Figure 4. Since the maximum temperature varies significantly with F, four curves were plotted for values of F equal to 0.25, 0.50, 0.75, and 1.0. This corresponds to values of $\frac{Hc}{Ho}$ of 4, 2, 1.33, and 1.0. These curves illustrate the effectiveness of using the annular pellets. For instance, using a value of $\frac{Hc}{Ho} = 4$, it is possible to run a fuel pin at 6.5 kW/cm with a central temperature of only 1600 °K. A value of $\frac{Hc}{Ho} = 4$ can be achieved by removing 57% of the fuel volume from the center of the pellets. Thus, it could be concluded that it is possible to run UN fuel pins at 6.5 kW/cm with existing fuels technology.

A fundamental problem with making calculations of reactor operating conditions is that high temperature λ values are very difficult to measure accurately. Because of this, high temperature λ values are often calculated from low temperature λ and electrical resistivity (ρ) measurements and high temperature ρ measurements. These calculations are often more accurate than the high temperature experimental λ measurements if the low temperature data are accurate and if a good fit of the data to existing theories are made. Another problem with predicting λ under reactor conditions is that fission products resulting

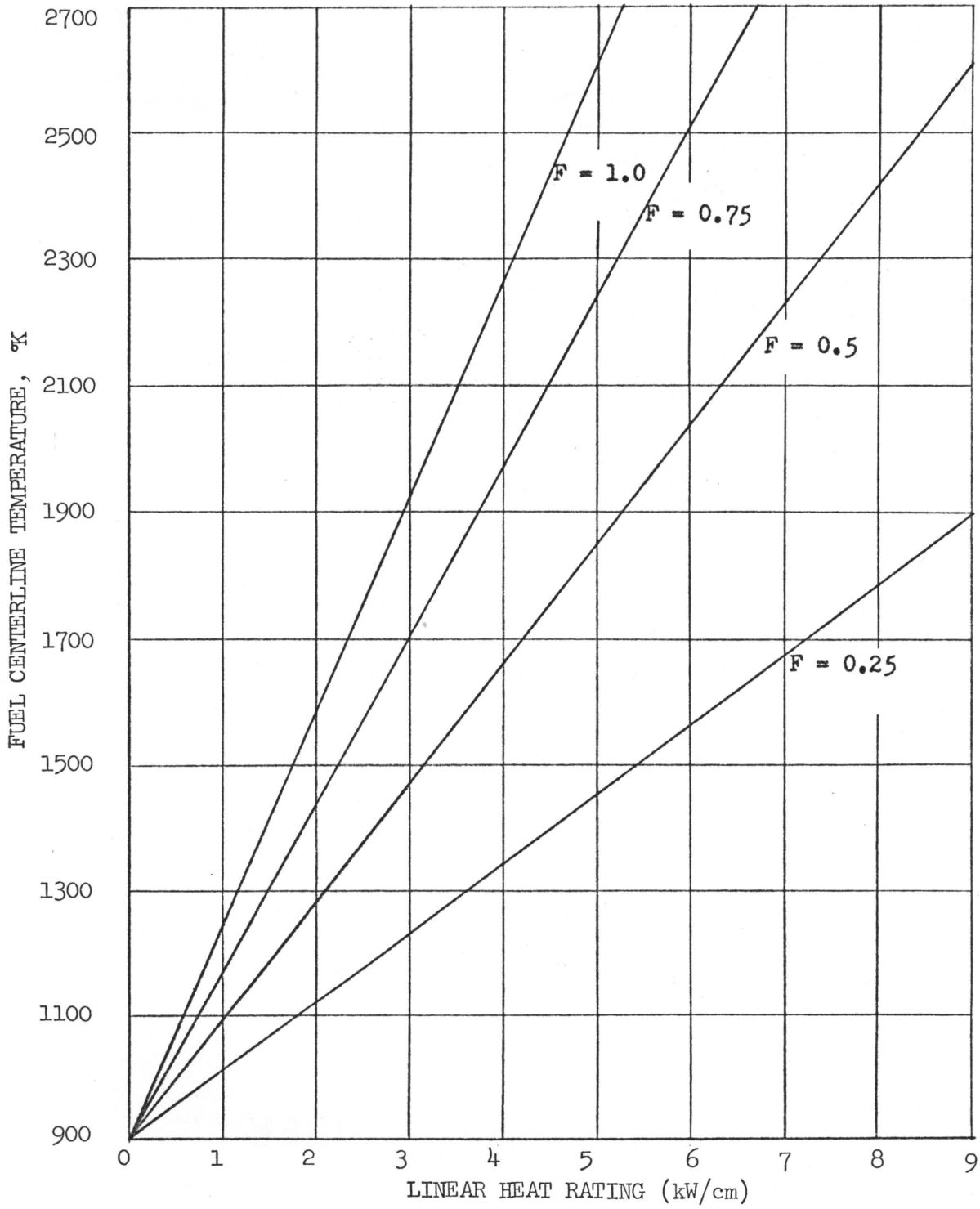

Figure 4. Curves Showing the Effect of Annulus Size in Cylindrical Fuel Pellets on the Maximum Operation Temperature of the Fuel.

from irradiation will cause a reduction in λ. However, the effect of fission products on λ should be small at higher temperatures.

The technique of making good low temperature measurements of λ and ρ was chosen to be a reasonable approach to a systematic examination of (U-Th)N alloys. Thermoelectric power, S, data was obtained in these experiments primarily because they were straightforward to obtain while taking λ measurements. The dissertation goal thus became one of doing a good mathematical analysis of the data to permit calculations of values for λ from ρ at any temperature. The most accurate data separation can be obtained with an "alloy-separation" technique, described later in the text, which had never been tried on ceramic alloys before. The success of this analysis is one of the highlights of this dissertation.

Presented in this dissertation are the following:

(1) A theoretical background of the properties measured (λ, ρ, and S).
(2) Previously determined values of these properties on the materials investigated.
(3) A description of the techniques used for sample preparation.
(4) The measurement techniques used in this investigation.
(5) Results of the study.
(6) A discussion of the results.
(7) Conclusions and recommendations for future study.

Some of the research goals were as follows:

(1) To develop a technique for fabricating (Th-U)N samples with a theoretical density of 90% or greater so that accurate values for λ and ρ could be measured.

(2) to obtain accurate experimental values for λ, ρ, and S from 90 to 400 °K.

(3) To obtain accurate experimental values for $\rho$from 4.2 to 400 °K.

(4) To separate λ into lattice and electronic components. This would permit the calculation of high temperature values of λ in a temperature range where λ measurements are very difficult.

(5) To determine whether (Th-U)N would have an attractive potential as a nuclear fuel.

II. THEORIES OF THERMAL CONDUCTIVITY

The thermal conductivity, λ, is a measure of the rate with which thermal energy can be transferred through a material. In a solid, heat is conducted by quanta of lattice vibrations known as phonons and by electrons. Some materials can conduct heat by photons but this is rarely an important mechanism. Because transport of heat by electrons is often the predominant mechanism, particularly in metals, much can be learned about λ by measuring the electrical conductivity of the metal. In this section some general equations for λ are given; then details of the lattice and electronic thermal conductivities are discussed.

The basic heat flow equation is given by

$$C \frac{\partial T}{\partial t} = \lambda \nabla^2 T \ , \qquad (6)$$

where, C = heat capacity per unit volume, $J/°K\text{-}cm^3$,

T = temperature, °K,

λ = thermal conductivity, W/cm-°K,

t = time, seconds.

The heat capacity, C, is defined as

$$C = C_p D \ ,$$

where, C_p = heat capacity at constant pressure,

D = density of material.

For a solid rod in which all of the heat flows axially through the rod and at steady state, this equation is satisfied[4] by

$$Q = -\lambda \nabla T \tag{7}$$

or,

$$Q = -\lambda \frac{dT}{dx} \ , \tag{8}$$

where, Q, is the flux (i.e., the quantity of thermal energy transmitted across a unit area per unit time). Thus,

$$\lambda = \frac{-Q}{(dT/dx} \tag{9}$$

or,

$$\lambda = \frac{-P}{A(dT/dx} \ , \tag{10}$$

where, P = power,

A = cross-sectional area of the rod.

The values for λ are usually expressed in terms of W/cm-°K.

The form of Equation (7) implies that the transfer of heat is a random diffusion process[4] rather than proceeding directly from one

end of the rod to the other. If the energy were propagated directly, then the rate of energy transfer would be a function only of the temperature difference between the ends of the rod. Such is the case for heat transferred by direct photon radiation.

Thermal conductivity, λ, of electrically conducting solids is assumed to be made up of an electronic component, λ_e, and a lattice component λ_L (ref. 5). Thus,

$$\lambda = \lambda_e + \lambda_L \ . \tag{11}$$

These two contributions are discussed below.

Lattice Thermal Conductivity

Heat is transferred by lattice vibrations which can be described as traveling waves carrying energy. This moving packet of energy is quantized, in analogy to the photon, and is called a phonon. Almost all of the concepts such as the wave-particle duality, which apply to photons, apply equally well to phonons. If nothing interferred with the movement of these particles or waves, phonons would transfer heat nearly instantaneously from hot regions to cold regions of a sample. However, atoms within the solid are in continuous fluctuations so that there are regions of higher and lower density distributed throughout its volume. Because the heat-carrying phonon finds itself being propagated through a medium whose properties vary irregularly from point to point, they are deflected and scattered. The thermal conductivity can be expressed by the equation[4]

$$\lambda = 1/3 \, Cvl \ , \tag{12}$$

where, C = heat capacity per unit volume,

v = velocity,

l = mean free path.

This equation is good for either lattice or electronic conduction with the particles carrying heat being either phonons or electrons. The phonon mean free path is thus limited, and by calculating the mean free path we can roughly determine the thermal resistance. The lattice thermal fluctuations are, in reality, other heat carrying phonons so that what we wish to consider is what happens when two phonons collide.

In an ideal harmonic crystal where the lattice modes are dynamically independent, no interaction occurs. In a real crystal, however, the forces have anharmonic components and the waves interfere with each other. When the phonons interfere, they may combine to form a new wave whose frequency is the sum of the frequencies of the interacting phonons. This obeys the conservation of energy and momentum laws since the energy of a phonon is given by $h\nu$, where ν is the frequency of vibration and h is Planck's constant.

When two phonons combine, the effect is the same as if two phonons have been destroyed and a new one created. By the same token, a single phonon can split up into two new ones. If all phonon-phonon interactions were of this type, so called N type processes (or normal processes), thermal conductivity of a crystal would be nearly infinite. However, Peierls showed that in addition to N processes there exists a thermal resistance resulting from Umklapp processes (U processes), which is the German word for "flopover." These result when two phonons of very short wave length traveling in nearly the same direction combine. In

a normal combination (N process) the resultant wave has an even shorter wavelength (higher frequency) and continues to move in the same direction. However, if the new wavelength is shorter than twice the lattice spacing, the motions of the atoms no longer determine which way the new wave is traveling. In fact, the motion is consistent with a wave of much longer wavelength traveling in the opposite direction. This results in the conclusion that momentum is not conserved in all phonon-phonon interactions.

Umklapp processes reduce the mean free path of phonons quite effectively since they occur at a rate proportional to the absolute temperature. Debye and Peierls both showed that the mean free path of a phonon is proportional to $1/T$ at higher temperatures[4] ($T > \theta$, where θ is the Debye temperature) in agreement with many experimental results. This is because the number of excited phonons is proportional to T, consequently, the mean free path l for each phonon is inversely proportional to the number of phonons with which it can collide, thus $l \alpha 1/T$.

One result of Peierl's theory is that it predicts an exponential increase in thermal conductivity at low temperatures which is experimentally observed. This is because Umklapp processes occur only for interactions of short wavelength phonons, but thermal excitation of high frequency lattice modes is not possible at low temperatures. Consequently, cooling a solid to low temperatures effectively "freezes" out the Umklapp processes, resulting in an exponential increase in the phonon mean free path and hence the thermal conductivity.

An important mechanism for scattering phonons at low temperatures is by inelastic collisions with electrons.[4-7] In materials where a

significant quantity of heat is transferred by electrons, this scattering mechanism may be dominant at low temperatures ($T<<\theta$) where it is proportional to T^{-2}. Interaction between electrons and the lattice vibration at frequency, ν, occurs only if a quantum of energy, $h\nu$, is exchanged between the lattice and conducting electron.

Scattering of phonons also occurs from impurities, dislocations, and atoms with different isotopic numbers (called "isotopic atoms").[4-6] Scattering by impurities and isotopic atoms occur mainly for short wavelength phonons with long wavelengths being little affected. Isotopic atoms and impurities are not important contributions to the thermal resistivity at high temperatures, because the effect is small compared to the Umklapp processes. However, at low temperatures the thermal resistance of impurities and isotopic atoms can be quite significant. Because phonon interaction occurs only for short wavelengths, the low temperature effect must be caused by long wavelength phonons which combine to make short wavelength phonons in N processes and the short wavelength phonons subsequently interact with the impurities and isotopic atoms. According to Ziman,[6] the scattering effect should be proportional to the square of the difference in the isotopic masses and proportional to the inverse fourth power of the phonon wavelength. Scattering by impurity atoms is caused by lattice strain in which case the atomic size difference is more important than the mass difference. In some solids, however, such as beryllium oxide (BeO), where the mass and strain size difference are often both important, the impurity resistivity can be significant at high temperatures.

Scattering of phonons by dislocations is important for short wavelength phonons.[6] While it can be argued that the elastic strain

around a dislocation creates a local change in density which would interact with the phonon, the observed effect on thermal conductivity is larger than calculations based on density changes would lead one to believe. Most of the scattering appears to occur at the core of the dislocation where the arrangement of the atoms is very far from the perfect lattice. Somehow the phonons are so affected by the differences in the relative positions of the atoms at the dislocation core that they are strongly scattered.

Perhaps the easiest way to examine lattice thermal conductivity is to represent it as lattice thermal resistivity, W_L, so that the various mechanisms which make up the resistivity are additive. This is illustrated schematically in Figure 5 (ref. 5), which shows five scattering mechanisms which can contribute to W_L: (1) phonon-electron resistivity, (2) phonon-boundary resistivity, (3) phonon-impurity resistivity, (4) three-phonon Umklapp resistivity, and (5) higher order Umklapp resistivity. At low temperatures W_L gets larger and larger eventually becoming infinite at absolute zero. The phonon-phonon resistance decreases exponentially to zero as Umklapp scattering is frozen out and impurity scattering goes to zero. Phonon-electron and phonon-boundary scattering both increase, becoming infinite at absolute zero so that the lattice thermal resistance goes to infinity and therefore the lattice thermal conductivity approaches zero at 0°K. The summation of these curves produces a minimum in the total W_L, which conversely causes a characteristic peak in λ_L. At high temperature a higher order Umklapp resistance occurs causing a further increase in W_L. The peak in λ_L will be shifted based on the amount of phonon-impurity scattering, which is related to the purity of the material.

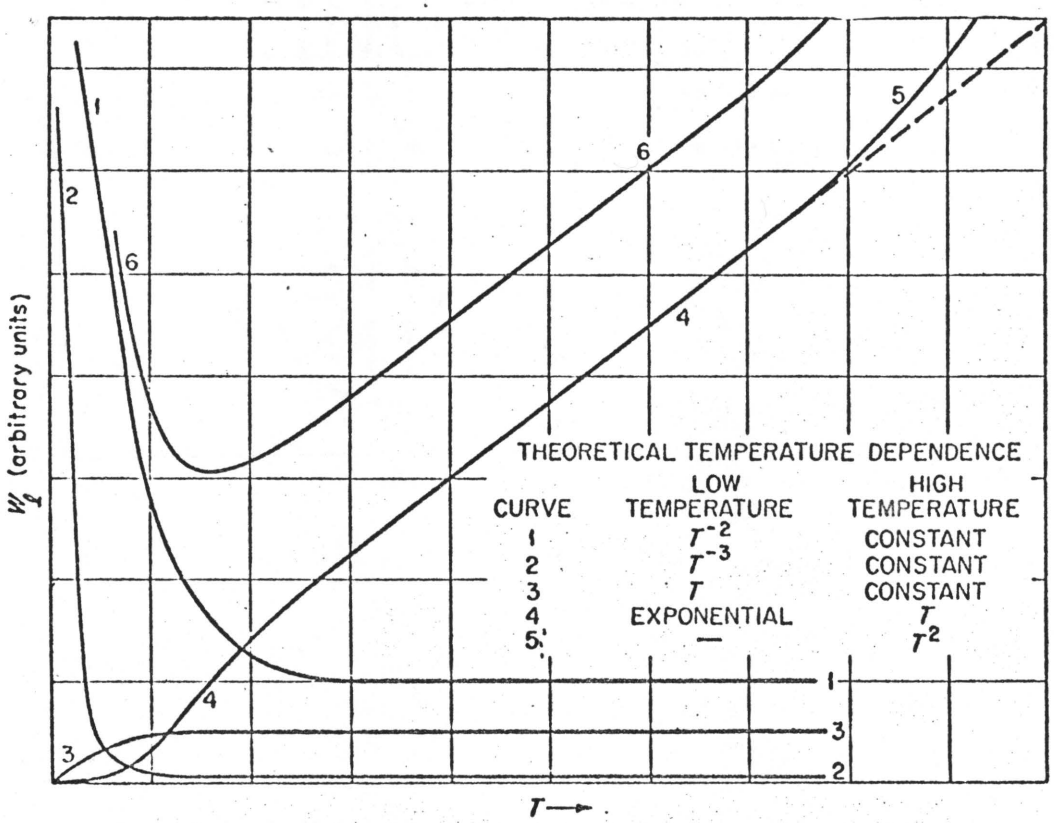

Figure 5. Schematic Representation of the Lattice Thermal Resistivity of a Nonmagnetic Metal. (1) Phonon-electron resistance. (2) Phonon-boundary resistance. (3) Phonon-impurity resistance. (4) Three-phonon Umklapp resistance. (5) Higher order Umklapp resistance. (6) Summation curve.

Source: R. K. Williams and W. Fulkerson, "Separation of the Electrical and Lattice Contribution to the Thermal Conductivity of Metals and Alloys," Proceedings of the Eighth Conference on Thermal Conductivity, October 1968.

Electronic Thermal Conductivity

In some solids, the electronic portion of the thermal conductivity can be extremely important from the standpoint that it may be the dominant mechanism for transporting heat.[4-6] At room temperature most pure metals have λ values 10 to 100 times that of dielectric solids, which leads to the conclusion that the metals must carry most of their heat by electronic conduction.[4,5] Some examples from Kittel[4] are:

Al:	2.26 W/cm-°K
Cu:	3.93 W/cm-°K
Na:	1.38 W/cm-°K
Ag:	4.18 W/cm-°K
NaCl:	0.07 W/cm-°K
KCl:	0.07 W/cm-°K

These solids all have relatively low Debye temperatures (<300 °K) so that the peak in the lattice thermal conductivity occurs at low temperatures. Beryllium oxide which has a high Debye temperature (~1000 °K) still has a high lattice thermal conductivity at room temperature.

In the transport of heat by electrons, higher energy electrons in the hot region of a sample diffuse to the cooler region while the lower energy electrons from the cool portion diffuse to the hot end. The result is a buildup of electrons at the cool end giving rise to the thermoelectric effect;[8] but after steady state has been reached, no net flow of current is observed. Resistance to the flow of electrons occurs because of interference of impurities, boundaries, magnons, phonons, etc.

The electronic portion of the thermal conductivity, λ_e, is usually expressed in terms of a Lorenz function,[4,5,9] L(T)

$$\lambda_e = \frac{L(T)\ T}{\rho} , \tag{13}$$

where, T = temperature,

ρ = electrical resistivity,

which was derived from the empirically observed Wiedemann-Franz-Lorenz law:[5,10]

$$\frac{\lambda \rho}{T} = \text{constant} . \tag{14}$$

This relationship is approximately obeyed by many metals at high temperature. From a theoretical treatment assuming (a) λ_L to be negligible, (b) elastic-electron scattering, and (c) the electron gas is completely degenerate, therefore obeying Fermi-Dirac statistics, Sommerfeld[11] calculated the Lorenz function, L_o, to be

$$\frac{\lambda_e \rho}{T} = L_o = \frac{\pi^2}{3} \left(\frac{k}{e} \right)^2 , \tag{15}$$

where, $L_o = 2.443 \times 10^{-8} \left(\frac{V}{deg} \right)^2$,

k = Boltzmann's constant, and

e = electronic charge.

A degenerate electron gas is one in which the Fermi energy is located in the conduction band many kT away from the top or bottom of the band. In the case of overlapping bands such as in UN, this requires

that the Fermi energy be far away from any band edge. Equation (15) is the first term in the series solution of the Boltzmann transport equation for elastic electron scattering in a one-band metal. Although the series is usually truncated after the first term, it is possible that higher order terms should be considered. Most authors who discuss their data with respect to the two components usually separate the electronic thermal conductivity from λ by assuming L to be the Sommerfeld value. This is not really satisfactory, however, because L should vary significantly from L_o at low temperatures and does not always equal L_o even at the high temperature limit.[5]

Even in the simple, degenerate single band models, the actual value of the Lorenz function is expected to deviate from the Sommerfeld value because (a) L_o is only the first term in the solution to the Boltzmann transport equation and (b) because the electron-phonon scattering process which produces most of the electrical resistivity is inherently an inelastic process. The elastic scattering formula for L carried to the third term is as follows

$$L = \frac{1}{e^2T^2}\left\{\frac{\pi^2}{3}(kT)^2 - \left[\frac{\pi^2}{3}(kT)^2\frac{\sigma'}{\sigma}\right]^2 + \frac{8\pi^4}{45}(kT)^4\frac{\sigma''}{\sigma}\right\}_{E=\delta}, \qquad (16)$$

where, σ = electronic conductivity,

σ' = first derivative of electronic conductivity with respect to energy,

σ'' = second derivative of electronic conductivity with respect to energy,

δ = Fermi energy,

if the higher derivative terms such as $\sigma'''(E)$ and $\sigma' \sigma''$ are ignored. The value of the electrical conductivity is given by $\sigma(E)$ if the Fermi level, δ, is at E and E is the energy of the conduction electrons. The second term is related to the thermoelectric power, S, since

$$S = \left[\frac{\pi^2}{3} \frac{k^2 T}{e} \frac{\sigma'(E)}{\sigma(E)}\right]_{E = \delta} . \tag{17}$$

Thus the first two terms in the equation are

$$L = L_o - S^2 . \tag{18}$$

The third term in Equation (16) is the most difficult to calculate and as yet no good calculation of this term has been accomplished. In a pure, defect-free solid the inelastic scattering in the electron-phonon collision causes L to deviate significantly from L_o (Figure 6), particularly at low temperatures where the phonon energies are significant with respect to kT. This is because the Sommerfeld value for L is calculated assuming the electron gas to be completely degenerate and the electron-phonon scattering to be elastic. At high temperatures where the energy given up by a phonon in an electron-phonon collision is small relative to the energy of the electron, the assumption of elastic scattering is a good approximation in spite of the fact that all electron-phonon interactions are inherently inelastic. At low temperatures where the energy given up by a phonon to an electron is significant with respect to the energy of the electron, the assumption that the interaction is elastic is no longer valid. The Lorenz function should go to zero at 0°K since the product of λ and ρ

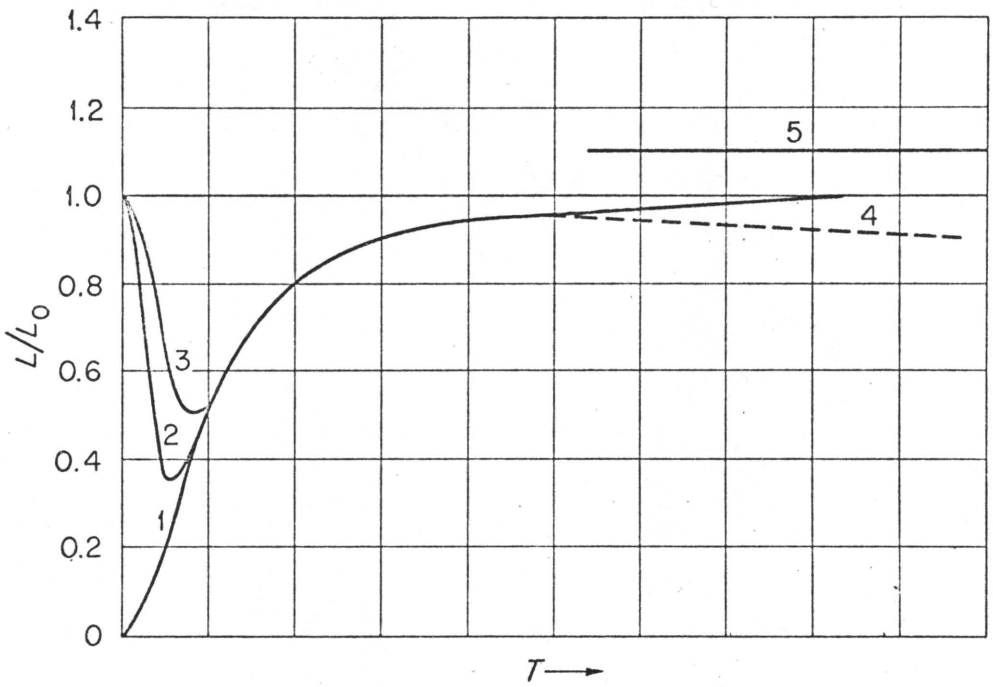

Figure 6. Schematic Representation of the Lorenz Function Showing Deviations from L_o. (1) Pure, defect-free metal with no electron-electron scattering. (2)(3) Effects of increasing impurity content. (4) Effect of electron-electron inelastic scattering at high temperatures. (5) Effect of ambipolar enhancement.

Source: R. K. Williams and W. Fulkerson, "Separation of the Electronic and Lattice Contribution to the Thermal Conductivity of Metals and Alloys," Proceedings of the Eighth Conference on Thermal Conductivity, October 1968.

goes to zero at 0°K faster than T because near 0°K λ is proportional to T^{-2} and ρ is proportional to T^{5}. In real crystals, of course, L approaches L_o at low temperatures because impurity scattering is still present and this scattering is elastic.

For the case of materials where several bands overlap at the Fermi surface, other phenomena may cause deviations from L_o. Some possibilities summarized by Williams and Fulkerson[5] are (1) ambipolar energy transport, (2) the presence of a narrow, high density of states band which overlaps the conduction band near the Fermi surface, and (3) inelastic electron-electron scattering. Ambipolar energy transport, originally postulated for band-gap semiconductors, can occur if more than one of the overlapping bands contribute significantly to the electrical and thermal conductivity. Gallo[12] made calculations based on a simplified two-band model which predicts that the increase in value of L is small at low temperatures and approaches a constant value at high temperatures. For ambipolar effects to be significant, three conditions must be met: (1) the electrical conductivities of the two bands must be nearly equal, (2) the thermoelectric power of the two bands must be large and opposite in sign, and (3) the temperature must be high. In the second case where a narrow, high density of states overlaps the conduction band, slow convergence of the series solution to the Boltzmann equation can cause deviations in L. Inelastic scattering of electrons should result in a negative nearly linear deviation of L from L_o at high temperatures.[5]

Examination of the various possible contributions to L shows that theoretical calculations of L would be unreliable. Consequently, values for L are generally calculated from experimental data of λ and ρ.

III. THEORIES OF ELECTRICAL RESISTIVITY

The electrical resistivity of a material is generally separated into components by[5,13,14]

$$\rho = \rho_P + \rho_i + \rho_m \ , \tag{19}$$

where ρ_P, ρ_i, and ρ_m correspond to the resistivities due to the scattering of electrons by phonons, impurities, and spin disorder (magnons). Equation (19) is a good assumption at medium and high temperatures where a relaxation time can be assumed for lattice scattering (i.e., that the electron-phonon scattering is elastic). As long as the impurity content is small, ρ_i is approximately independent of temperature; this is a statement of Matthiessen's rule.[5] Thus only the terms ρ_P and ρ_m vary with temperature.

Impurity scattering is effectively elastic at all temperatures as negligible energy is transferred at any interaction. In the low temperature region, however, where electron-phonon interactions cannot be assumed to be elastic, a departure from Matthiessen's rule is observed. Also, departures from Matthiessen's rule are observed in multivalent metals. These may be described by a two-band model since each conduction band depends in a different way on scattering and Matthiessen's rule applies differently to each band.[15] The total conductivity may then show a deviation. Some experimental observations indicate that departures depend on the type of impurity atoms or other defects present as well as their quantities; this is particularly true with transition-metal and rare-earth impurities. Matthiessen's rule is

to be taken as a first approximation only and is suspect where $\rho_i \sim \rho_P$. Deviations from Matthiessen's rule are generally found to be positive such that ρ_i will be greater than the residual resistivity, ρ_o.

Since ρ_i is assumed constant with temperature, it is usually separated from the total electrical resistivity by extrapolating ρ measurements to 0°K because ρ_P and ρ_m go to zero as $T \rightarrow 0$. The extrapolated value is known as the residual resistivity and is assumed equal to ρ_i. The ratio of $\frac{\rho_{298}}{\rho_i}$ is known as the resistivity ratio and is an index of material perfection. The ratio may range from a low on the order of 2 to as high as $\sim 10^5$ depending on the purity of the material.

An electron will only be scattered by the lattice vibrating at frequency, ν, if a quantum of energy, $h\nu$, is exchanged between the lattice vibrations and the conduction electron. It follows that as absolute zero is approached, the resistance due to thermal vibrations must vanish since both electrons and lattice are settling into their lowest energy states. Thus, there will be no resistance arising from the zero-point vibrations of the lattice.

In the temperature range much less than the Debye temperature, θ, where low angle phonon-electron scattering occurs, ρ_P is particularly sensitive to the exact details of the scattering mechanism.[5] Consequently, use cannot be made of the relaxation time for solution to the Boltzmann transport equation because of the inelasticity of the scattering process. Near 0°K, ρ_P varies as T^5, this results from a T^3 term calculated assuming a Debye spectrum, which says that the number of scatterers is proportional to T^3, and a T^2 term which results from low angle scattering. The angle of scatter is of the order $\frac{T}{\theta}$ and

ρ_P is a function of the square of the scattered angle. The temperature dependence changes from T^5 dependence at very low temperatures to a T dependence at high temperatures.

The lattice or phonon contribution to ρ is frequently assumed to be given by the Bloch-Gruneisen relation[4,13,14,16,17]

$$\rho_P = \rho_\theta \, 4.22 \left(\frac{T}{\theta}\right)^5 J_5\left(\frac{\theta}{T}\right) , \tag{20}$$

where,

$$J_5(x) = \int_0^x \frac{z^5 \, dz}{(e^z - 1)(1 - e^{-z})} , \tag{21}$$

which gives $\rho \propto T$ for $T >> \theta$

$\rho \propto T^5$ for $T << \theta$.

The constant ρ_θ is the phonon component of ρ (T) at θ and can be evaluated by $\rho_\theta = \frac{B\theta}{1.054}$, where B is $\frac{d\rho}{dT}$ at high temperatures.

The third contribution to the resistivity, ρ_m, comes from spin disorder scattering of electrons, which is important if the material is antiferromagnetic at low temperatures as is UN (ref. 17). At absolute zero, the atoms and electrons occupy their ground states, allowing a conduction electron to pass through the lattice without interacting with the magnetic moments of the atoms. As the temperature is raised, thermal energy is added such that spins are uncoupled. Because at low temperatures the spin coupling covers long distances (infinite at 0°K), the uncoupled spin will propagate through the lattice. The propagation of this energy can be described as a wave and is termed

a "spin wave" or "magnon." These spin waves represent packets of disorder in an otherwise magnetically ordered lattice and electrons may interact with these spin waves. The density of spin waves increases with increasing temperature, effectively increasing the disorder of the lattice until the Neél temperature, T_n, is reached. Above the Neél temperature, the lattice is disordered with respect to spin and material becomes paramagnetic. Consequently, the contribution of ρ_m to ρ increases with temperature up to the Neél temperature and is almost constant above this temperature. The tests performed for this work were primarily in the higher temperature region above the T_n for UN.

IV. THEORIES OF THERMOELECTRIC POWER

The presence of an electric field in a sample subjected to a temperature gradient arises from the buildup of electrons on the cooler end of the sample with fewer electrons on the hot end.[8] The higher energy electrons at the hotter end diffuse down the temperature gradient transporting energy, while the lower energy electrons diffuse from the cool to the hot end. The strength of the resulting electric field is given by

$$\epsilon = S \nabla T \ , \tag{22}$$

where, S is the absolute thermoelectric power (also known as the absolute Seebeck coefficient).

It is difficult in practice to measure this directly because the same temperature gradients exist in the measuring apparatus as exists in the sample. Ziman[7] idealizes this to a circuit of two metals,

A and B, whose junctions are at temperatures T_1 and T_2, and we break into metal B at some intermediate temperature, T_o (see Figure 7). The voltage across this point will then be given by an integral around the circuit:

$$\epsilon_{AB} = \int \vec{E} \cdot \vec{dr} \tag{23}$$

$$\epsilon_{AB} = \int S \frac{dT}{\vec{dr}} \vec{dr} \tag{24}$$

$$\epsilon_{AB} = -\int_{T_o}^{T_1} S_B \, dT - \int_{T_1}^{T_2} S_A \, dT - \int_{T_2}^{T_o} S_B \, dT \tag{25}$$

$$\epsilon_{AB} = \int_{T_1}^{T_2} (S_B - S_A) \, dT \tag{26}$$

For most experiments it is convenient to calculate the absolute value of S by taking relative S measurements using a material for which the absolute value of S versus T is known. The two materials generally used as standards are lead (up to 400 °K) and platinum (up to 1300 °K).

Making comparisons of S for a material would not be too meaningful if it were not possible to obtain absolute S measurements on at least one material. Absolute S measurements can be made by using either of two techniques:[8] (1) thermoelectric power measurements using a superconductor below the transition temperature, and (2) calorimetric measurements of the Thompson heat at the junctions. Superconducting materials below their transition temperature have values for S = 0. Thus by making up the circuit in Figure 7 with one of the arms being in the superconducting state, it is possible to directly measure the

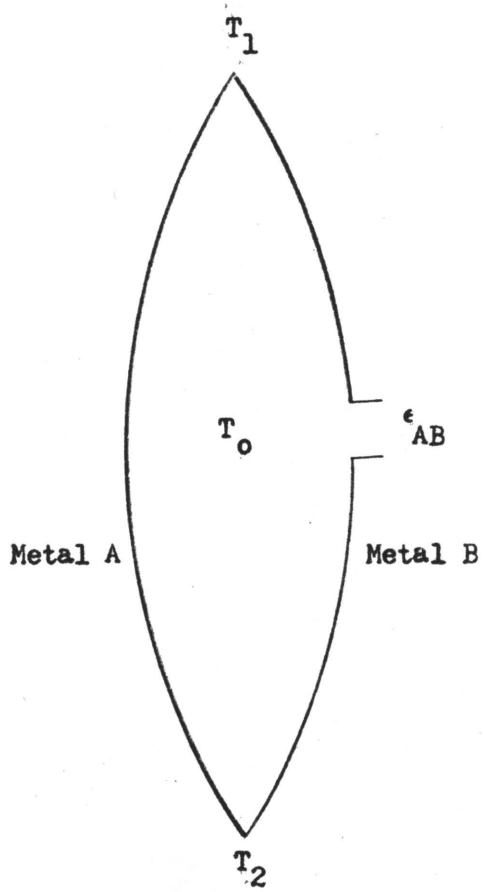

Figure 7. Schematic Diagram of Two Metals with Junctions at Two Different Temperatures T_1 and T_2 to Illustrate Thermoelectric Effect.

thermoelectric property of the conductor of interest. The limitation to this method, of course, is that it is valid only at very low temperatures where materials can be made superconducting. To determine high temperature absolute values of S experimentally, the relationship developed by Thompson relating the Thompson heat, μ, to S is used. The Thompson relation is

$$\mu = \frac{T\, dS}{dT} , \tag{27}$$

which reduces to

$$S(T) = \int_0^T \frac{\mu}{T}\, dT , \tag{28}$$

since S(0) is zero from the third law of thermodynamics. The Thompson heat is determined calorimetrically from the relation by passing an electric current through a conductor. The net heat produced in a conductor per unit volume per second ($\dot{Q}$) is given by

$$\dot{Q} = \frac{J_x^2}{\sigma} - \mu J_x \frac{dT}{dx} , \tag{29}$$

where, J_x = current density,

σ = electrical conductivity,

$\frac{dT}{dx}$ = temperature gradient.

The second term in Equation (29) is a thermoelectric heat whose sign depends on the direction of the current and the temperature gradient. Thus accurate calorimetric measurements allow one to calculate a value for S absolutely.

CHAPTER II

REVIEW OF EXPERIMENTAL MEASUREMENTS

I. PROPERTIES OF THE URANIUM-THORIUM-NITROGEN SYSTEM

The author could find very little information on the ternary system of uranium-thorium-nitrogen except as it exists in the three binary systems which make up the ternary system. The three binary phase systems are shown in Figures 8–10 (refs. 18–20). Since the U-Th phase diagram is not important in this study except as it may affect fabrication parameters, it will not be discussed further. A more thorough background of the UN system is summarized in the author's Master's Thesis.[2] Consequently, background information will be restricted to information on ThN and that information which is available on the (Th-U)N system.

Venard and Spruiell[21] studied part of the U-Th-N phase diagram and together with existing literature, they established the partial phase diagram shown in Figure 11. Using x-ray diffraction techniques and metallography, they[22] showed that ThN and UN exhibit complete solid solubility and that the lattice parameters appeared to follow Vegard's law (see Figure 12). The small amount of scatter in the data could have easily been caused through the rather large quantity (1800 ppm) of oxygen present. The terminal point of the three-phase region occurs at 50.5 atomic percent Th, 3 atomic percent U, and 46.5 atomic percent N which corresponds to the compound $(Th_{0.944}, U_{0.056})N_{0.869}$.

Some of the more important properties which are known about ThN are tabulated in Table 2.

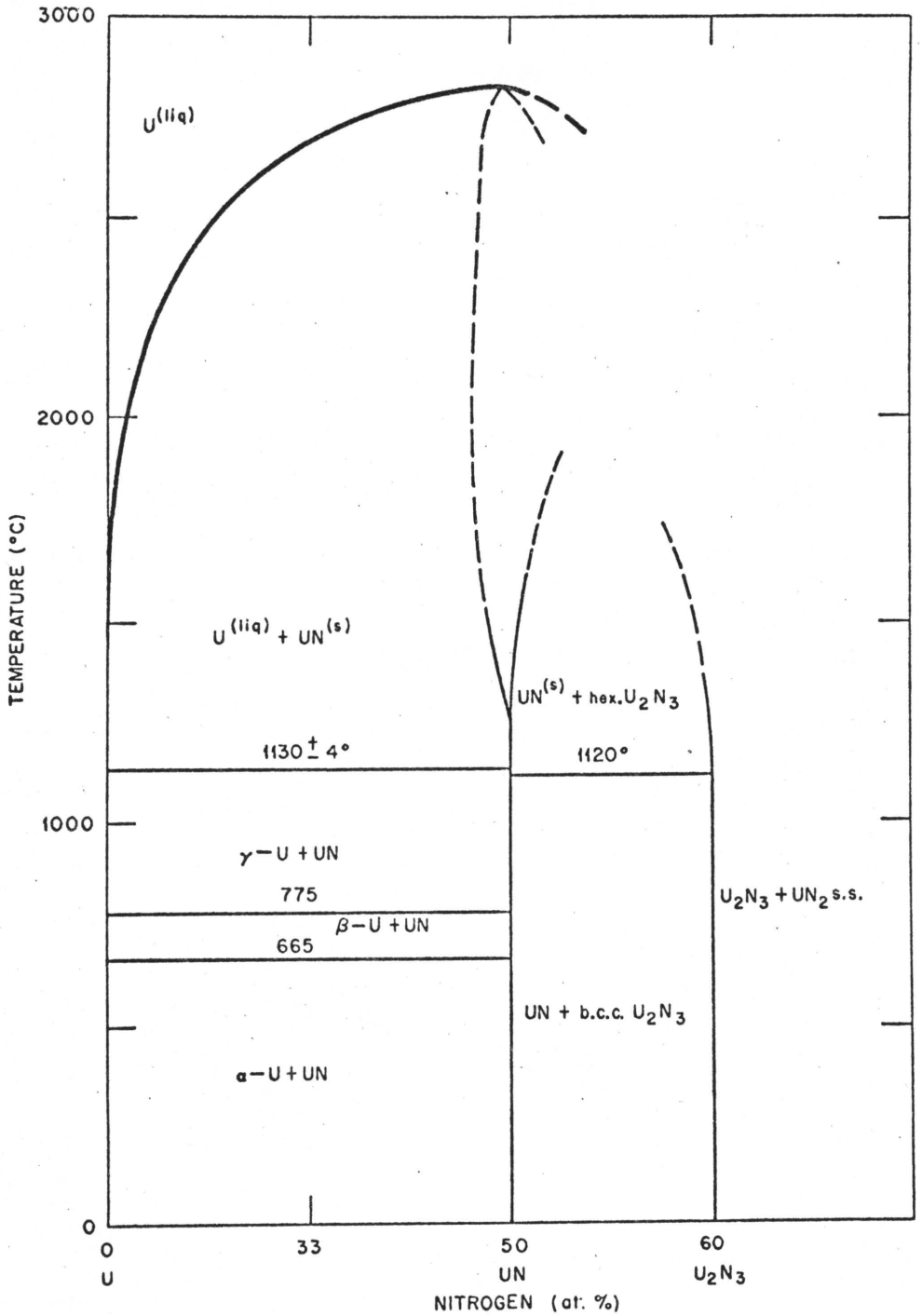

Figure 8. The Uranium-Nitrogen Binary System After Benz and Bowman.

Source: R. Benz and M. G. Bowman, "Some Phase Equilibria in the Uranium-Nitrogen System," Journal of the American Chemistry Society, 88(2): 264-268, 1966.

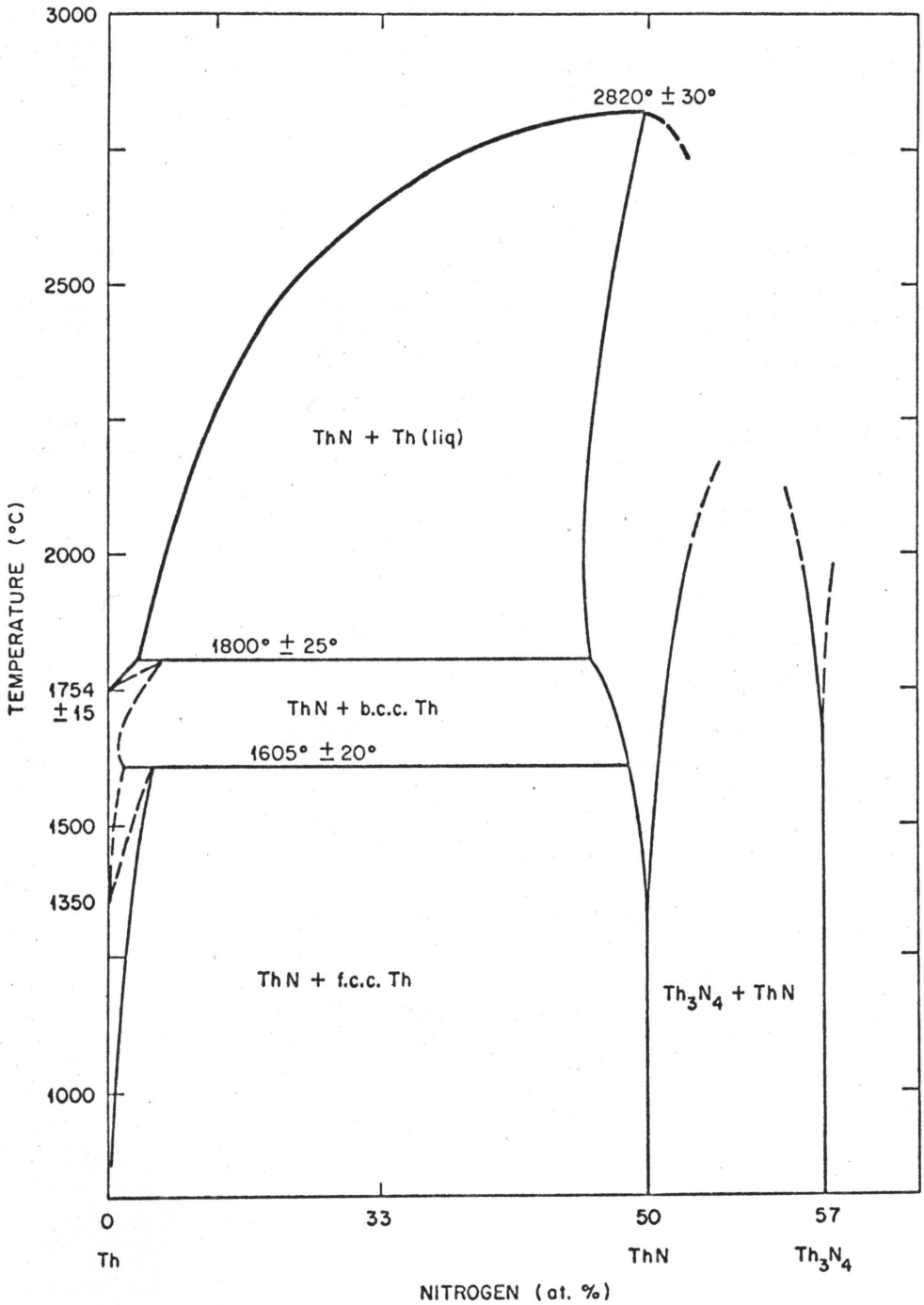

Figure 9. The Thorium-Nitrogen Binary System After Benz et al.

Source: R. Benz, C. G. Hoffman, and G. N. Rupert, "Some Phase Equilibria in the Thorium-Nitrogen System," Journal of the American Chemistry Society, 89(2): 191–197, 1967.

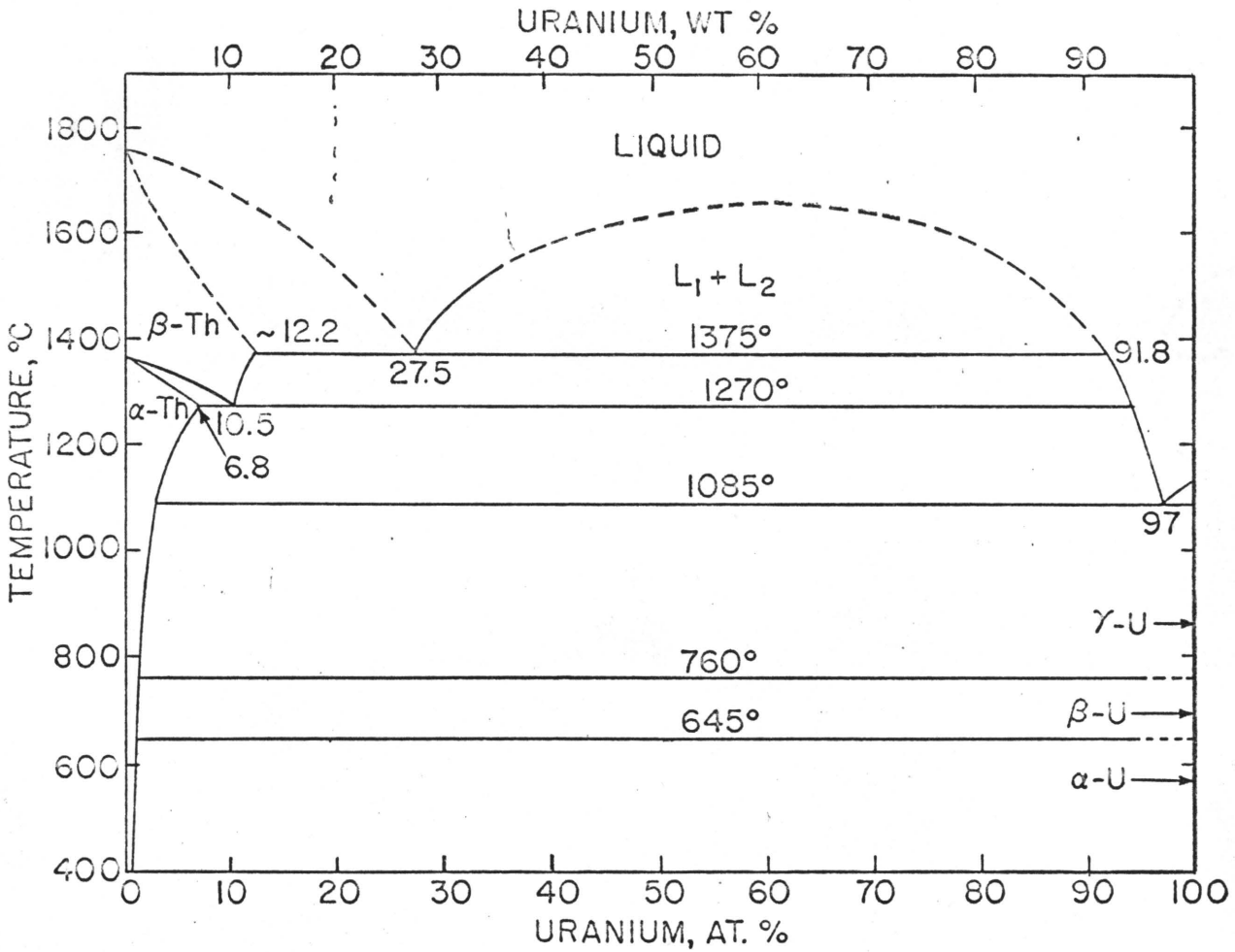

Figure 10. The Uranium-Thorium Binary System.

Source: O. N. Carlson and E. R. Stevens, A Compilation of Thorium Binary Phase Diagrams, IS-1752, January 1968.

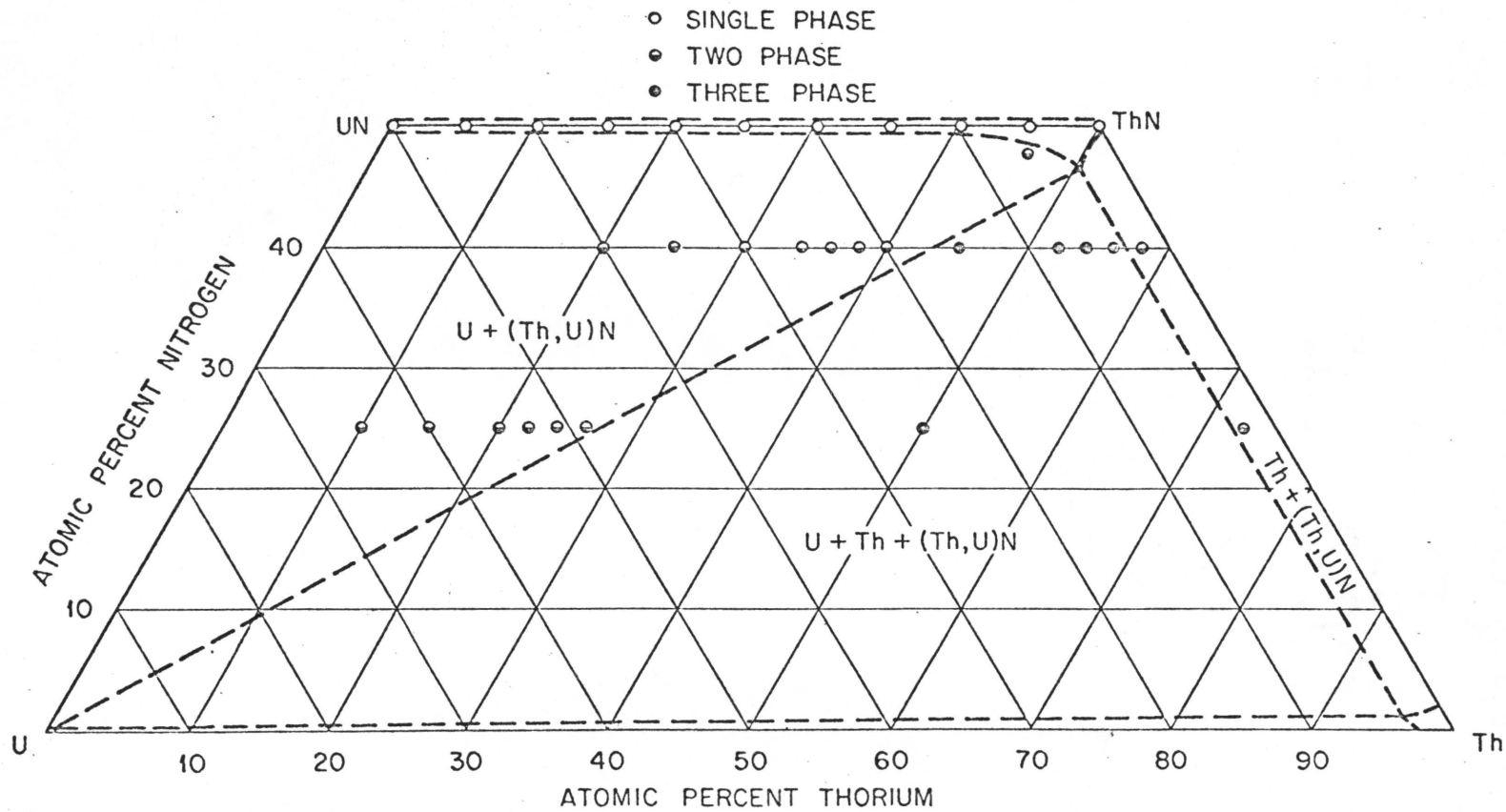

Figure 11. The Equilibrium 1273 °K Partial Isotherm of the Th-U-N System Showing Alloys Examined and the Number of Major Phases Identified by X-Ray and Metallographic Examination.

Source: J. T. Venard and J. E. Spruiell, "Phase Relations in the Th-U-N Ternary System at 1000 °C," Journal of Nuclear Material, 27: 257-263, 1968.

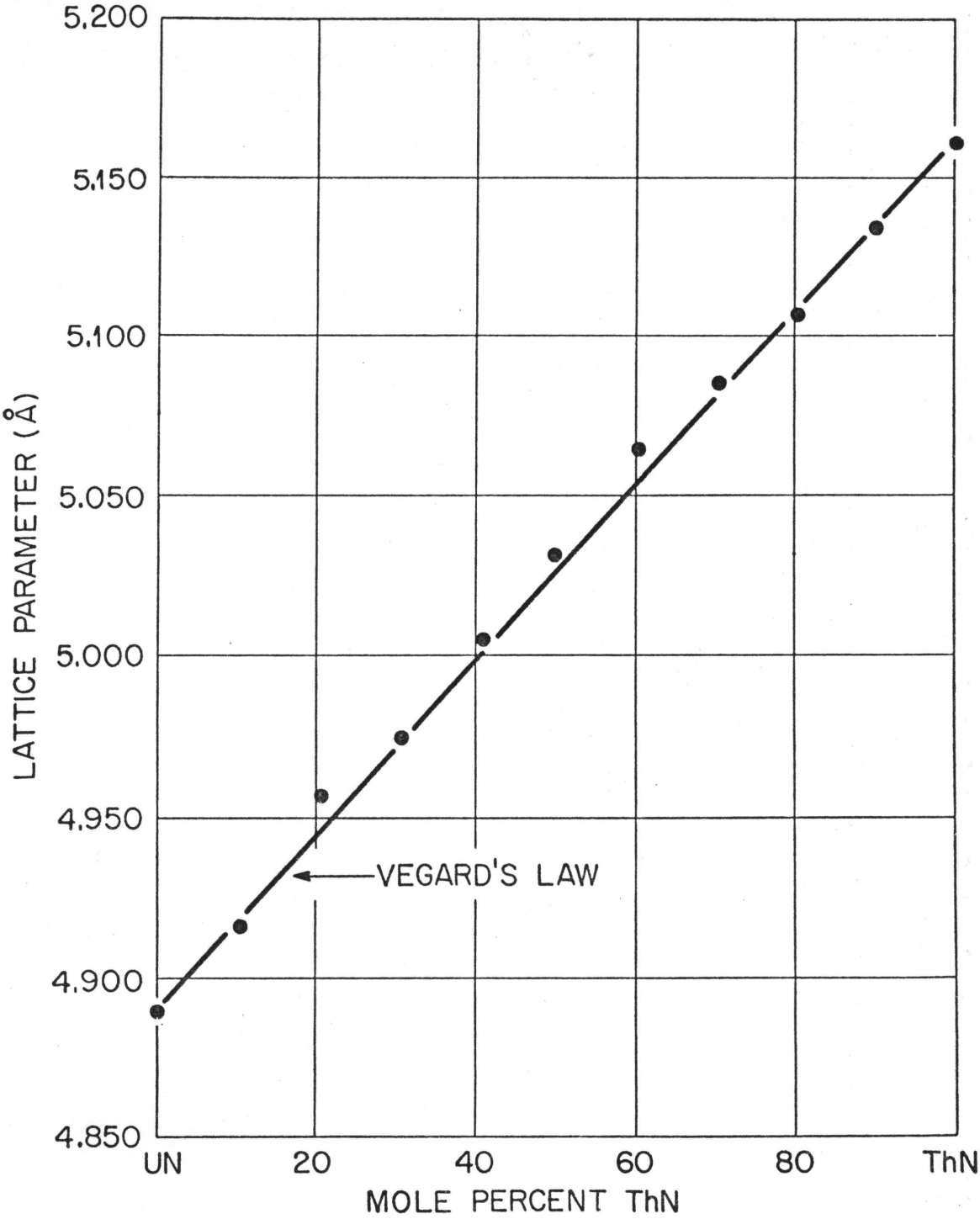

Figure 12. Lattice Parameters of (Th-U)N Across the UN-ThN Pseudobinary.

Source: J. T. Venard, J. E. Spruiell, and O. B. Cavin, "Lattice Parameters Across the UN-ThN Pseudobinary," Journal of Nuclear Material, 24: 245-246, 1967.

TABLE 2

SUMMARY OF SOME PROPERTIES OF INTEREST IN ThN

Property	Value	Reference*
Crystal Structure	Face-Centered Cubic	23,24
Lattice Parameter	5.1619 Å	23,24,26, 27,28
Melting Temperature	3090 °K (0.6 atm N_2)	22,25,26, 29
Decomposition Pressure	$\exp\left(8.086 - \frac{33.224}{T} + 0.958 \times 10^{-17}\ T^5\right)$ atm	25
$\Delta G^\circ_{f_{273}}$	-51.1 kcal/mole	23
ΔH°_{298}	-90.6 kcal/mole	30
ΔS°_{298}	-23.5 cal/mole-°K	30
Density[a]	11.88 g/cm^3	24
Thermal Coefficient of Expansion	7.39×10^{-6}/°K	27

*See page 148.

[a]Calculated from lattice parameter of Venard and Spruiell.

II. ELECTRICAL RESISTIVITY

In the UN-ThN system electrical resistivity measurements have been made previously on only UN (refs. 17, 32–36) and ThN (refs. 23, 24, 38). In addition, electrical resistivity measurements have been made on the ThN-ThC system by Auskern and Aronson[23,24] and on UN-PuN by Van Craeynest et al.[33] Only the data on ThN and UN will be discussed.

The UN ρ data[17,32–37] is presented in Figure 13. Measurements on cold pressed and sintered samples and arc cast samples were corrected to theoretical density using

$$\rho_{TD} = \rho_{meas}\left[\frac{1 - P}{1 + \beta P}\right] , \qquad (30)$$

where, ρ_{TD} = electrical resistivity of theoretically dense material,

ρ_{meas} = electrical resistivity as measured,

P = fraction of volume as porosity,

β = constant.

A value of $\beta = 0.5$ was used and all second phase oxide assumed to be equivalent to porosity (this is indicated in Figure 14 by horizontal lines shifting the data to the right). This correction, though approximate, is consistent as is illustrated in Figure 14. Below 87% theoretical density, however, this correction does not appear valid.

Most of the reported work below room temperature is that of Moore et al.[17] with the lone exception being that of Omichi and Kikuchi.[37] In the temperature range of 0 to 150°K, the values reported for UN are

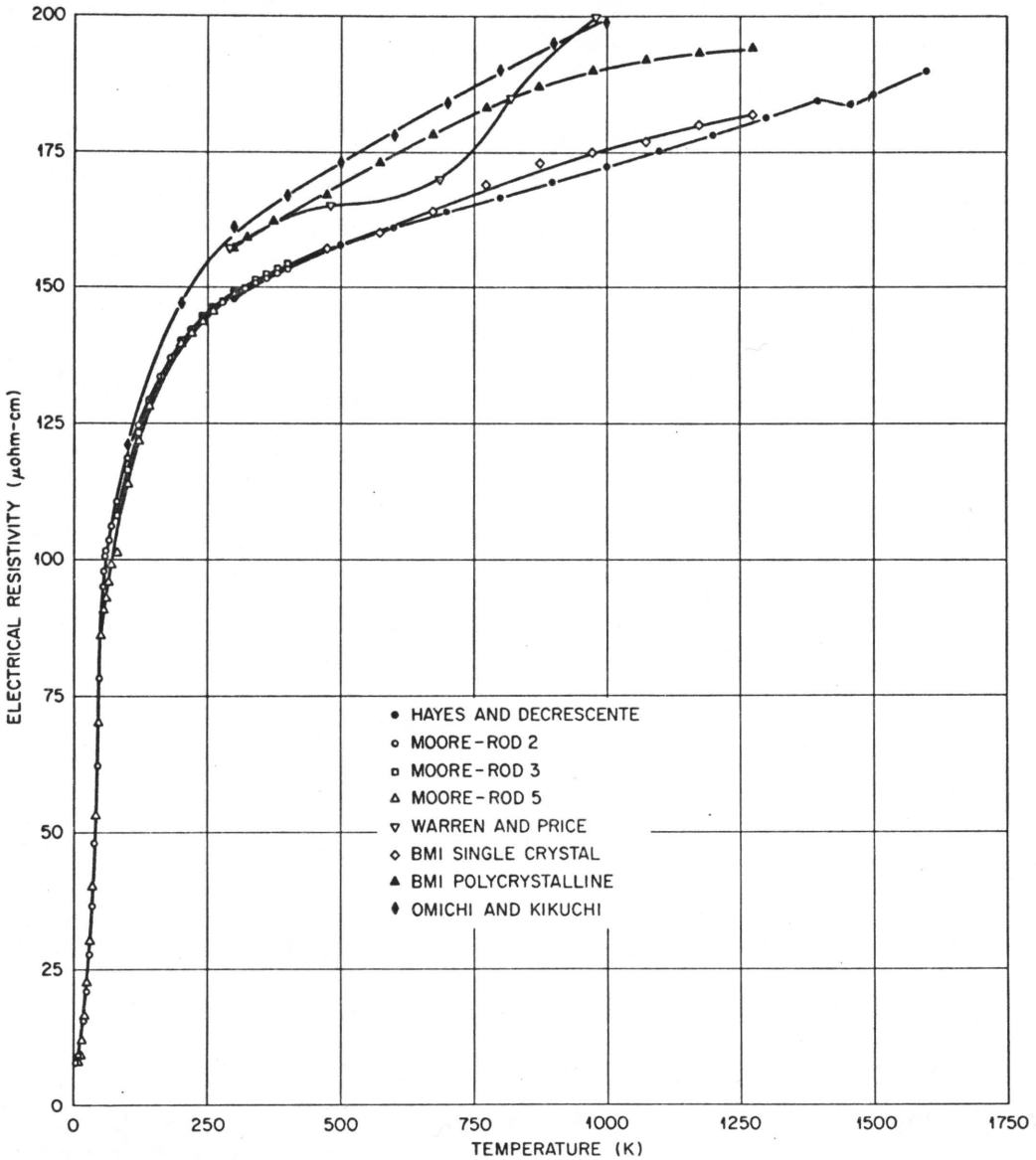

Figure 13. Results of Experimental Measurements of Electrical Resistivity of Uranium Mononitride by Various Experimenters.

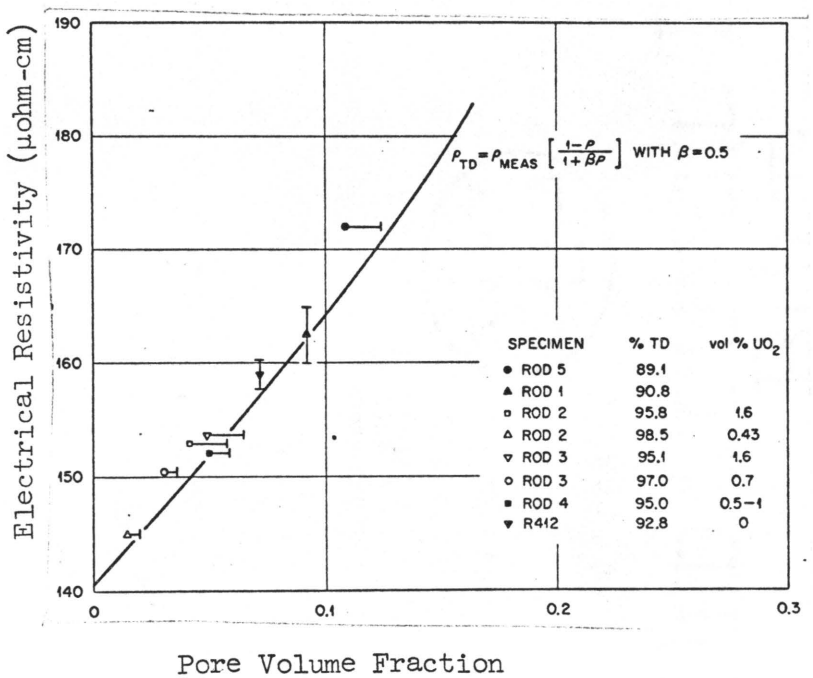

Figure 14. Plot of Electrical Resistivity of Uranium Mononitride as a Function of Pore Volume Fraction with Residual Resistivity Subtracted from Total Resistivity.

Source: J. P. Moore, W. Fulkerson, and D. L. McElroy, "Thermal Conductivity, Electrical Resistivity, and Seebeck Coefficient of Uranium Mononitride," Journal of the American Ceramic Society, 53(2): February 1970.

consistent, but above 150 °K there is a large spread in the reported data among different experimenters. The values reported by Hayes and DeCrescente[32] and those of Battelle Memorial Institute[34,35] single crystals appear to be most consistent with the low temperature data reported by Moore et al.[17] An unusual dip occurs in the data by Hayes and DeCrescente at about 1400-1450 °K. This dip is probably due to experimental error since it is difficult to explain on the basis of theory unless an unreported phase change in UN has occurred at that temperature.

The electrical resistivity of ThN as measured by Auskern and Aronson[38] is shown in Figure 15. The resistivity at room temperature was 20 μohm-cm, about the same as thorium metal, with a residual resistivity of 3 μohm-cm in their samples. The curve drawn through the data is that calculated from the Bloch-Gruneisen equation adjusted for the residual resistivity.

The resistivity of the Th_3N_4 phase is much higher, lying in the range between semiconductors and insulators.[38] Room temperature values were reported to be between 10^{11} and 10^{14} μohm-cm with the value being very sensitive to heat treatment. Consequently, it is imperative in sample preparation to prevent the formation of Th_3N_4 in the structures as it will have a significant effect on ρ and probably on λ.

III. THERMAL CONDUCTIVITY

The only thermal conductivity data which could be found in the ThN-UN system are for UN (refs. 17, 32, 34, 35). Moore et al.[17] have made the most recent and most consistent measurements on UN; their

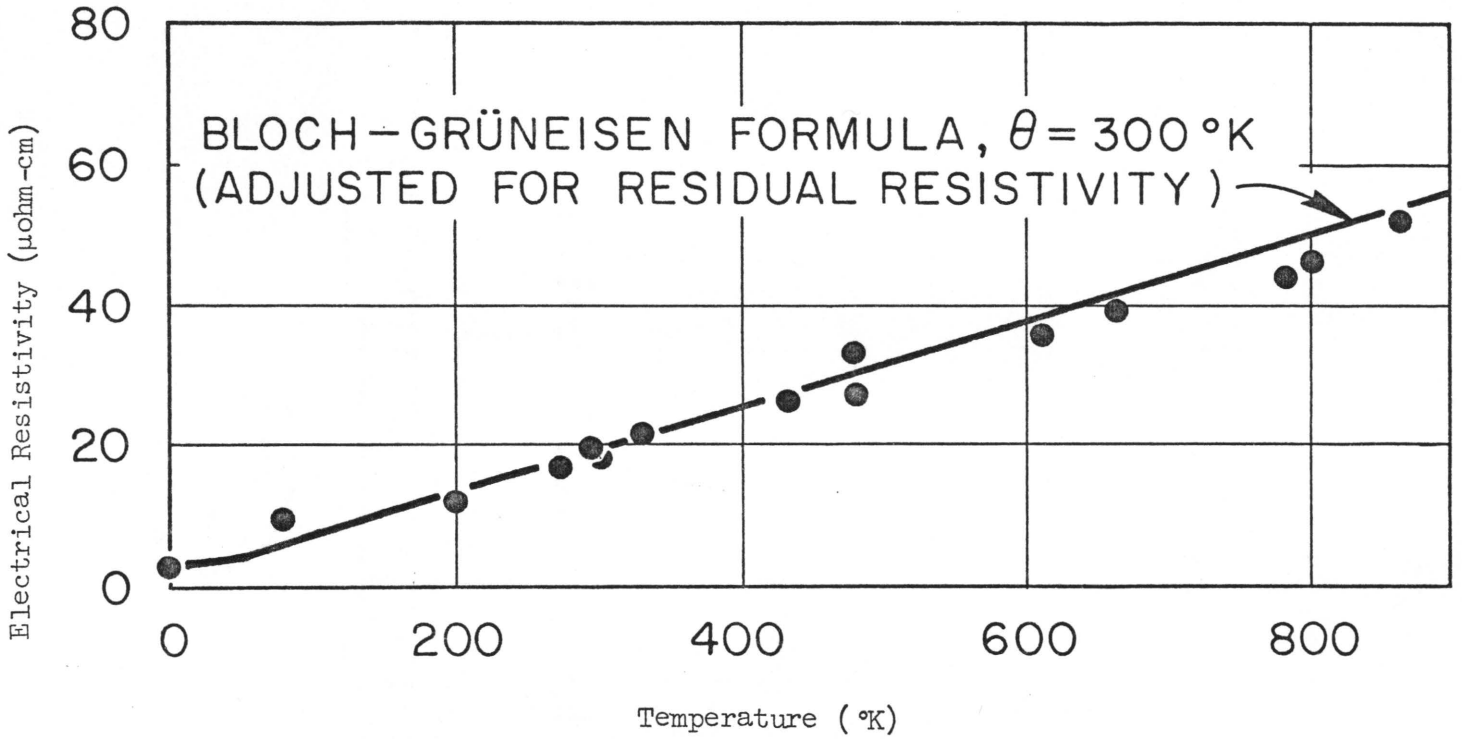

Figure 15. Electrical Resistivity of ThN as a Function of Temperature.

Source: A. B. Auskern and S. Aronson, "Electrical Properties of Thorium Nitrides," Journal of Physics and Chemistry of Solids, 28: 1069–1071, 1967.

data are compared graphically with those of other investigators in Figures 16 and 17.

The measurements made by Hayes and DeCrescente[32] were taken on a large UN sample using a radial heat flow apparatus. A heater in the center of a UN cylinder established a thermal gradient with heat flowing from the center to the periphery. Thermocouples stationed radially from the center provided temperature measurements from which values for λ were calculated. The data showed considerable scatter and are probably less accurate than the data from the longitudinal heat flow apparatus used by Moore et al.[17]

Most of the λ values[39] reported on UN are within $\pm 17\%$ at room temperature and within $\pm 13\%$ at 1000 °K of the data and extrapolated curve of Moore et al.[17] These include five λ (refs. 17, 23, 25–27) and two thermal diffusivity experiments[40,41] used to calculate λ values. The exceptions which fall outside the range are the very early results of Taylor and McMurtry,[42] which are too high; the data of Pascard,[43] which appear to high at low temperatures and have the wrong temperature dependence; and the data of Nasu and Kikuchi,[44] which is too low particularly at high temperatures. The most recent data of Takahasi et al.[30] appear to have been carefully taken and fall only about 10% below that of Moore et al.[17] Unfortunately, the authors had no ρ measurements on their specimens. The best λ values are thought to be those of Radosevich and Williams[45] below 100 °K, Moore et al. between 100 and 400 °K, the extrapolated values of Moore et al. to 1000 °K, and the smoothed results of Hayes and DeCrescente at high temperature.

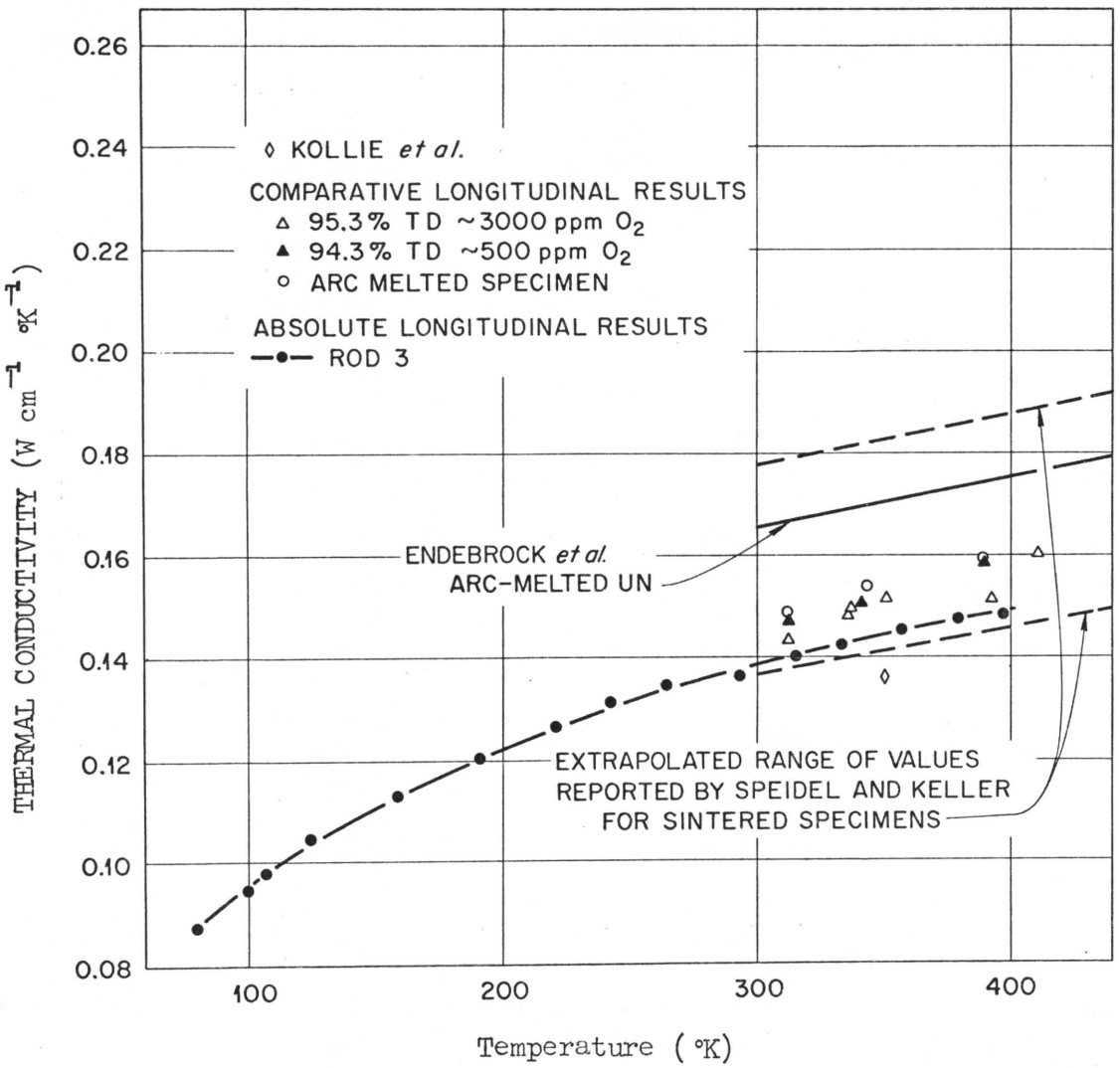

Figure 16. Thermal Conductivity of Uranium Mononitride to 400°K.

Source: J. P. Moore, W. Fulkerson, and D. L. McElroy, "Thermal Conductivity, Electrical Resistivity, and Seebeck Coefficient of Uranium Mononitride," Journal of the American Ceramic Society, 53(2): February 1970.

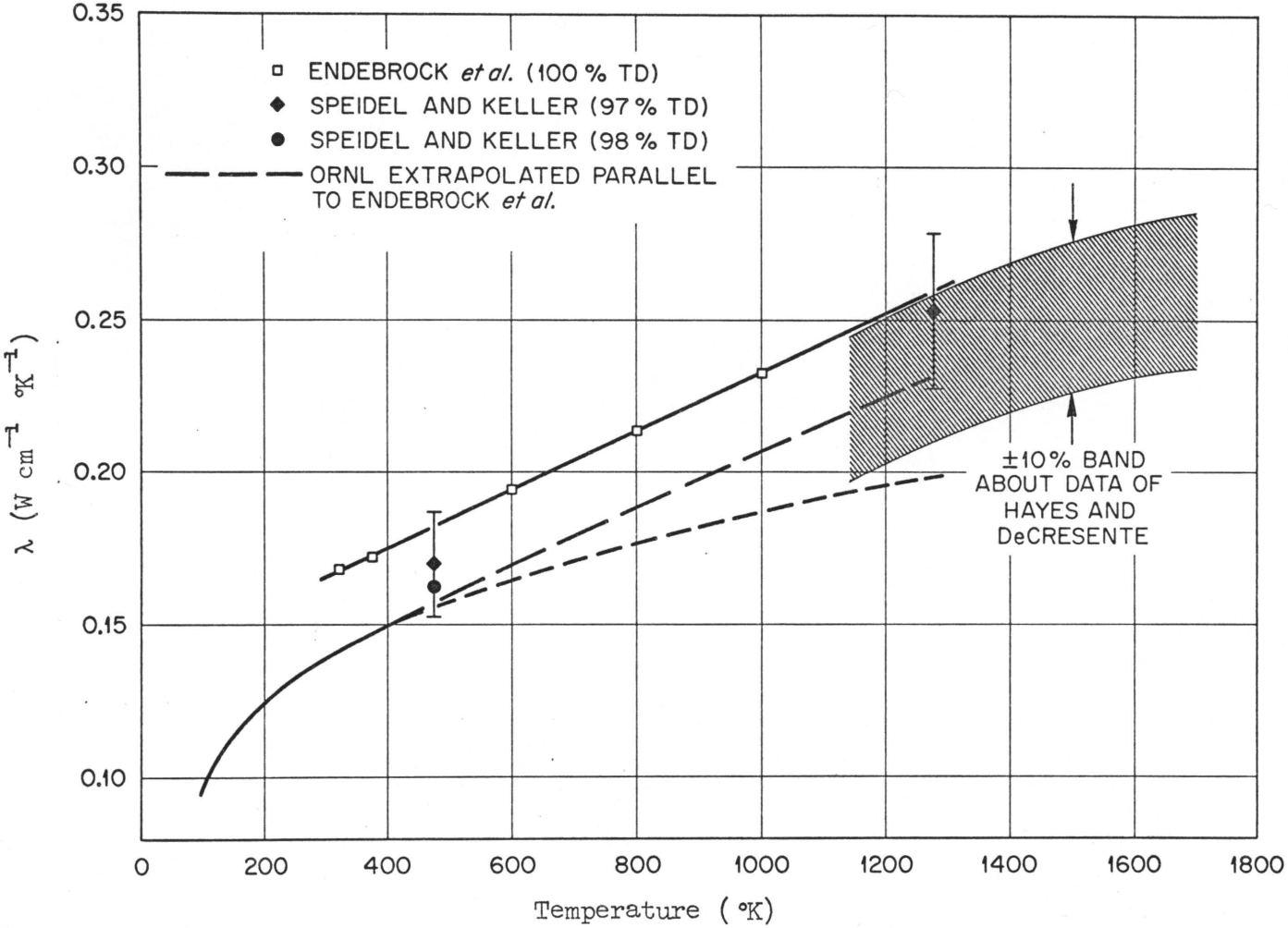

Figure 17. Thermal Conductivity of Uranium Mononitride to 1800 °K.

Source: J. P. Moore, W. Fulkerson, and D. L. McElroy, "Thermal Conductivity, Electrical Resistivity, and Seebeck Coefficient of Uranium Mononitride," Journal of the American Ceramic Society, 53(2): February 1970.

IV. THERMOELECTRIC POWER

The absolute Seebeck coefficient, S, of UN was reported by Moore et al.;[17] by Costa et al.;[39] and by Warren and Price.[35] A plot of the absolute Seebeck coefficient as a function of temperature is shown in Figure 18. The values for S are positive and much larger than one expects to find for most metals. The data of Moore et al.[17] (accurate to ±1.2%) show S decreasing with temperature with a rapid decrease below T_n, 55 °K, a minimum at about 34 °K, and a rise to a small peak at about 10 °K.

In the discussion of their data, Moore et al.[17] suggest that the decrease in S below T_n is related to a reduction of the diffusion component through magnetic scattering. They suggest the increase of S below 34 °K and the local maximum is caused by magnon drag.

Unlike UN, the absolute Seebeck coefficient of ThN (ref. 38) is small and negative and decreases with temperature (Figure 19). From their data and using Hall Coefficient measurements, Auskern and Aronson estimated the Fermi energy of ThN to be 6 ev. They also calculated the effective electron mass to be 0.7 times the true electron mass.

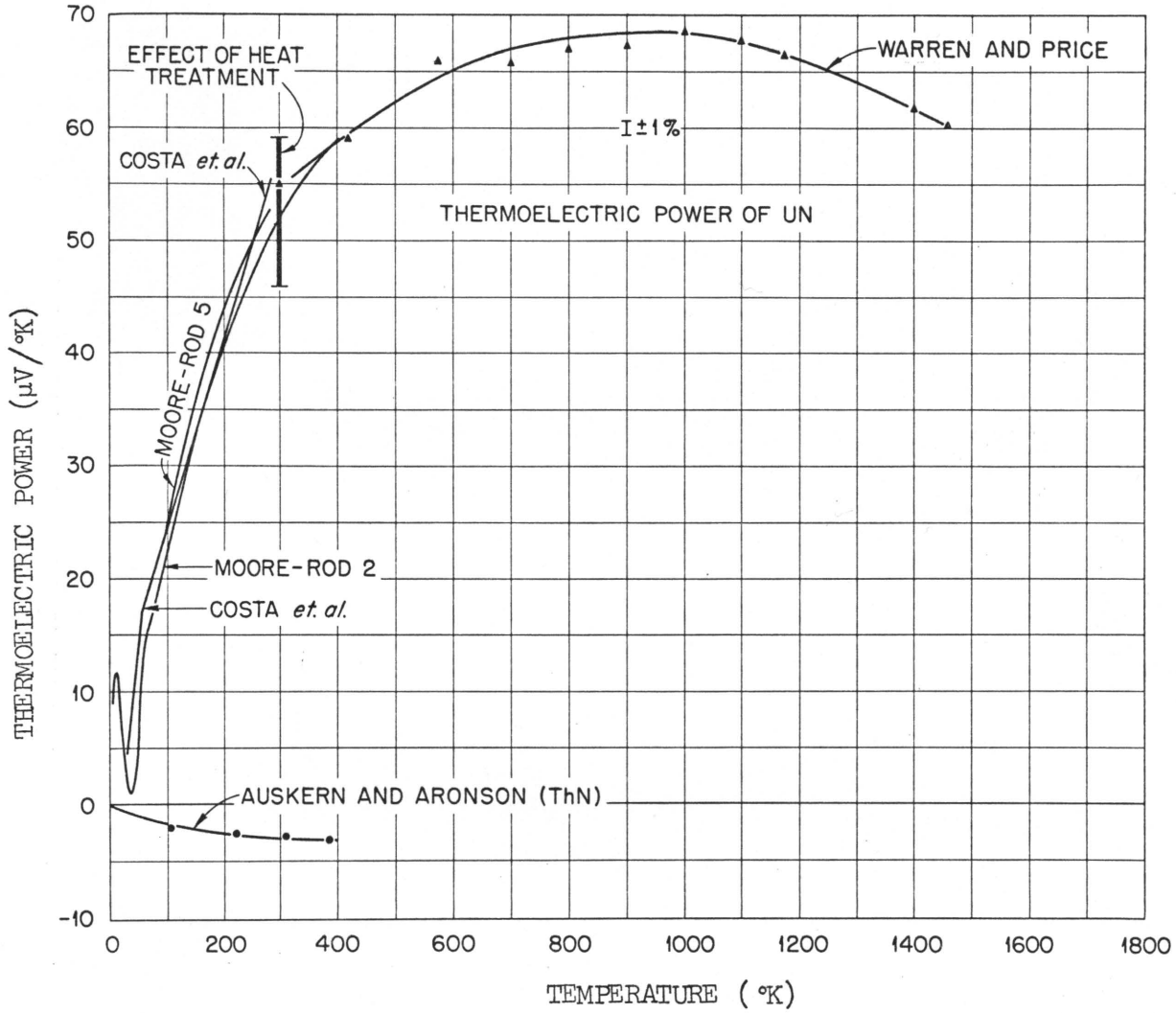

Figure 18. Thermoelectric Power Measurements of UN and ThN.

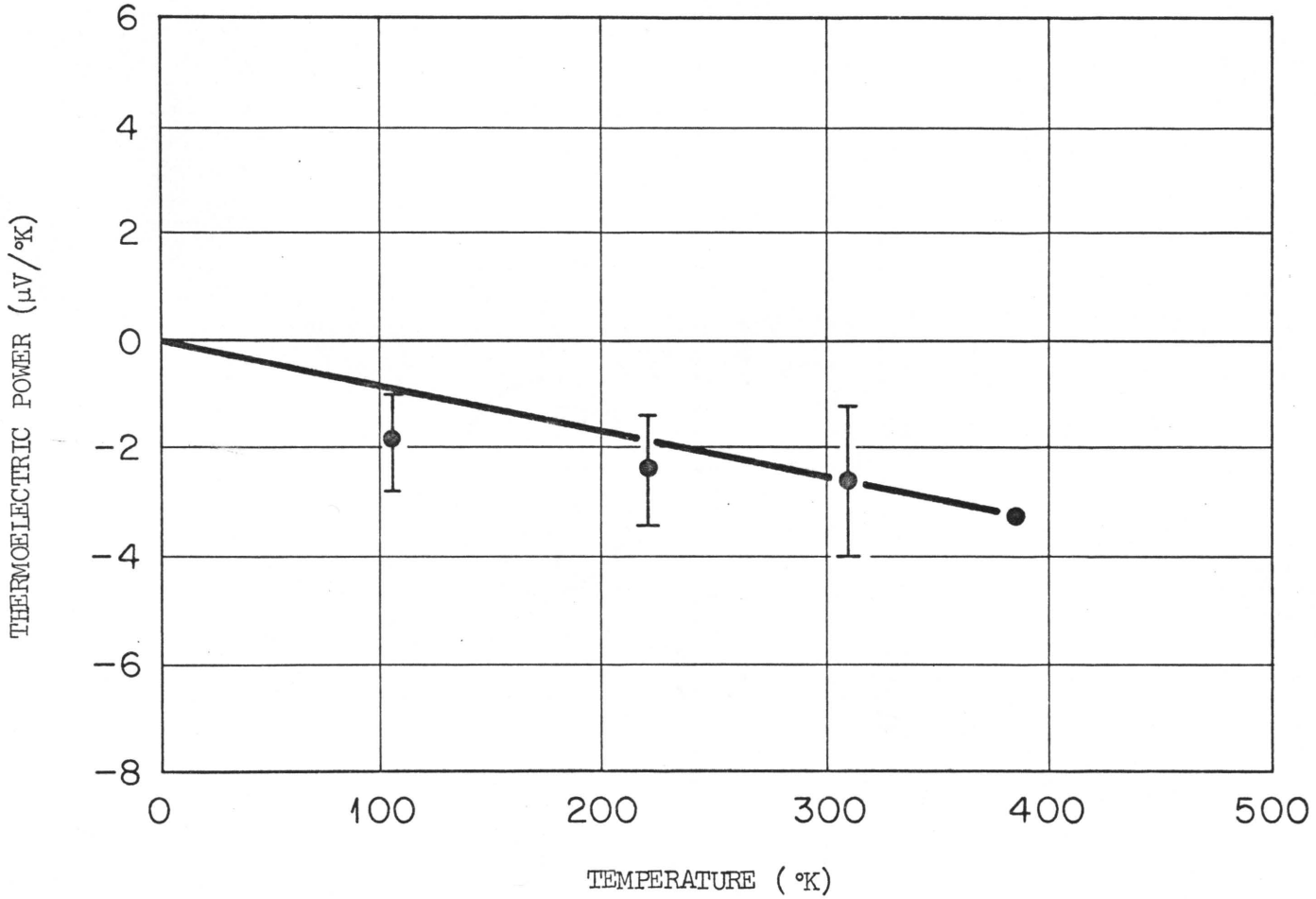

Figure 19. Thermoelectric Power of ThN as a Function of Temperature.

Source: A. B. Auskern and S. Aronson, "Electrical Properties of Thorium Nitrides," Journal of Physics and Chemistry of Solids, 28: 1069-1071, 1967.

CHAPTER III

EXPERIMENTAL DETAILS

I. SAMPLE PREPARATION

The samples used to obtain the data reported in this dissertation were fabricated using three different fabrication schemes. The samples prepared are shown in chronological order in Table 3. Wet chemical analyses of each of the specimens is shown in Table 4. Spectrographic analyses of trace elements in some of the samples are shown in Table 5.

Uranium Nitride Fabrication

The first sample, UN-3, prepared by cold pressing and sintering, was obtained from J. P. Moore,[17] who had previously made low temperature ρ and S measurements from 4.2 to 400 °K and λ measurements from 80 to 400 °K. The sample was fabricated by R. A. Potter of the Metals and Ceramics Division of Oak Ridge National Laboratory, Oak Ridge, Tennessee, using the synthesis, fabrication, and sintering steps shown in Figures 20-22. The microstructure of the specimen is shown in Figure 23. This UN sample was a 97.0% theoretically dense rectangular bar whose final dimensions were 0.5705 × 0.5573 × 5.715 cm.

Thorium Nitride and (Thorium-Uranium) Nitride Fabrication

Thorium nitride and (Th-U)N samples were made by arc casting, cold pressing and sintering, and zone melting. As will be discussed, arc casting and cold pressing and sintering techniques produced samples which were not satisfactory for obtaining λ and ρ data. Consequently,

TABLE 3

TECHNIQUES OF SAMPLE PREPARATION

Sample	Nominal Composition	Fabrication Technique
UN-3	UN	Cold Press and Sinter
AC-6	ThN	Arc Cast
AC-1	(Th-1% U)N	Arc Cast
AC-15	(Th-2% U)N	Arc Cast
AC-5	(Th-5% U)N	Arc Cast
Th-13	ThN	Induction Zone Heating
Th-16	(Th-2% U)N	Induction Zone Heating
Th-15	(Th-5% U)N	Induction Zone Heating
Th-20	ThN	Induction Zone Heating
Th-21	(Th-5% U)N	Induction Zone Heating

TABLE 4

CHEMICAL ANALYSIS OF SAMPLES

Sample Number	Nominal Composition	Chemical Analyses, wt %				
		Th	U	N	O	C
UN-3	UN		94.72	5.364	0.043 0.10	0.072
AC-6	ThN	93.7	0.0135			
AC-1	(Th–1% U)N	93.5	1.0			
AC-15	(Th–2% U)N	92.4	1.96	5.36	0.21	0.038
AC-5	(Th–5% U)N	88.0	4.22			
Th-13	ThN	91.7	0.001	5.46 5.50	0.22 0.24	0.032
Th-16	(Th–2% U)N	88.2	2.10	5.50	0.18	0.040
Th-15	(Th–5% U)N	88.4	4.66	5.58 5.61	0.18 0.093	0.034
Th-20	ThN	92.3	2.12	5.58 5.56		0.027
Th-21	(Th–5% U)N	89.2 89.2	4.68 4.57	5.60 5.57	0.108 0.108	0.085

TABLE 5

RESULTS OF SPECTROGRAPHIC ANALYSIS OF SPECIMENS

	Weight Fraction in Parts Per Million		
Element	Th-13	Th-15	Th-16
Ag	1	< 0.2	< 0.2
Al	3	2	0.5
As	< 0.1	< 0.1	< 0.1
B	0.05	0.5	5
Ca	2	2	5
Cd	< 0.3	< 0.3	< 0.3
Co	< 0.1	< 0.1	< 0.1
Cr	1	0.7	0.7
Cu	0.5	0.7	0.7
Fe	2	5	2
Hf	2	< 1	< 1
K	2	5	5
Mg	0.5	0.3	1
Mo	< 1	< 1T	< 1T
Na	5	10	10
Ni	1	10	5
P	0.3	3	0.3
Si	15	30	~200
Ta	2	2	0.7
Th	M	M	M
Ti	0.7	0.2	0.7
Tb	0.3	< 0.2	< 0.2
U	< 1	> >1000	>1000
W	< 1	3	8
Zn	< 1	< 1	< 1
Zr	50	7	20
S	10	7	10
Y	1	< 0.2	< 0.2
La	20	< 0.2	< 0.2
Lc	20	0.2	0.5
Pn	3	< 0.2	< 0.2
Nd	10	< 0.5	< 0.5
Gd	3	< 0.5	< 0.5
Dy	0.7	< 0.5	< 0.5
Ho	0.2	< 0.2	< 0.2
Sm	< 0.5	< 0.5	< 0.5
Eu	< 0.5	< 0.5	< 0.5

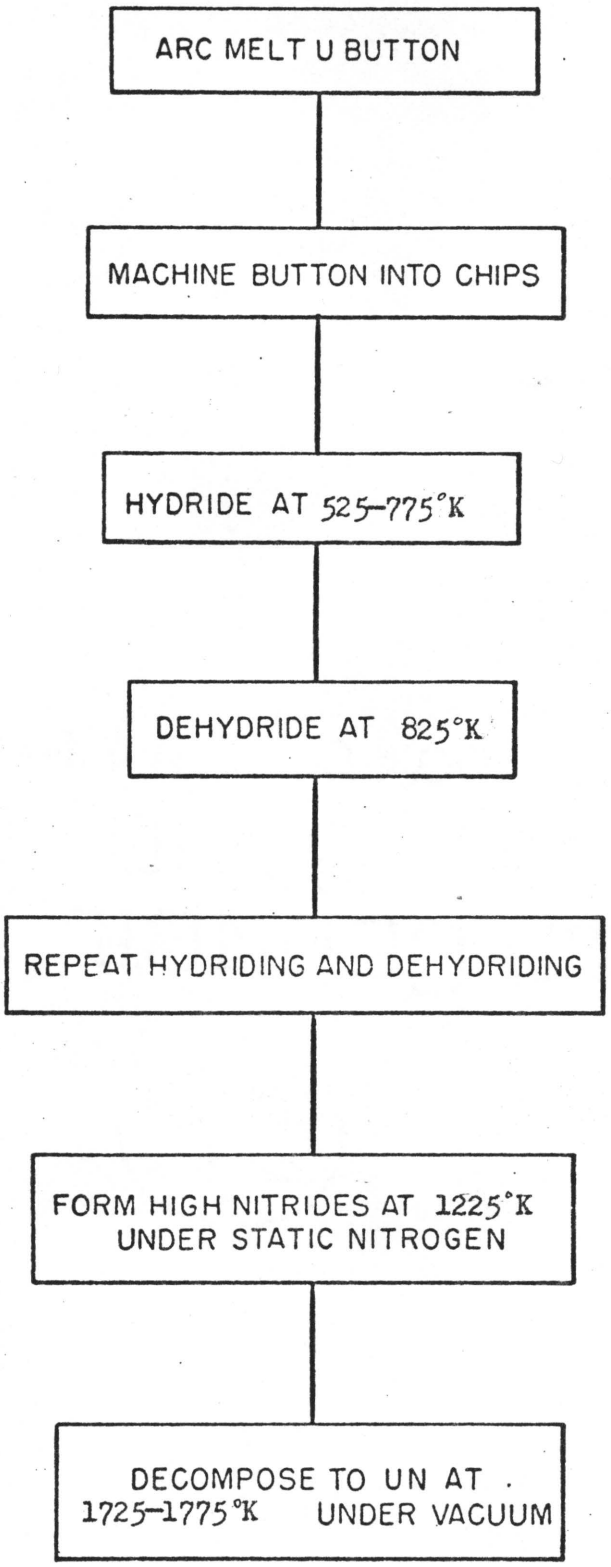

Figure 20. Synthesis of Uranium Nitride Powder.

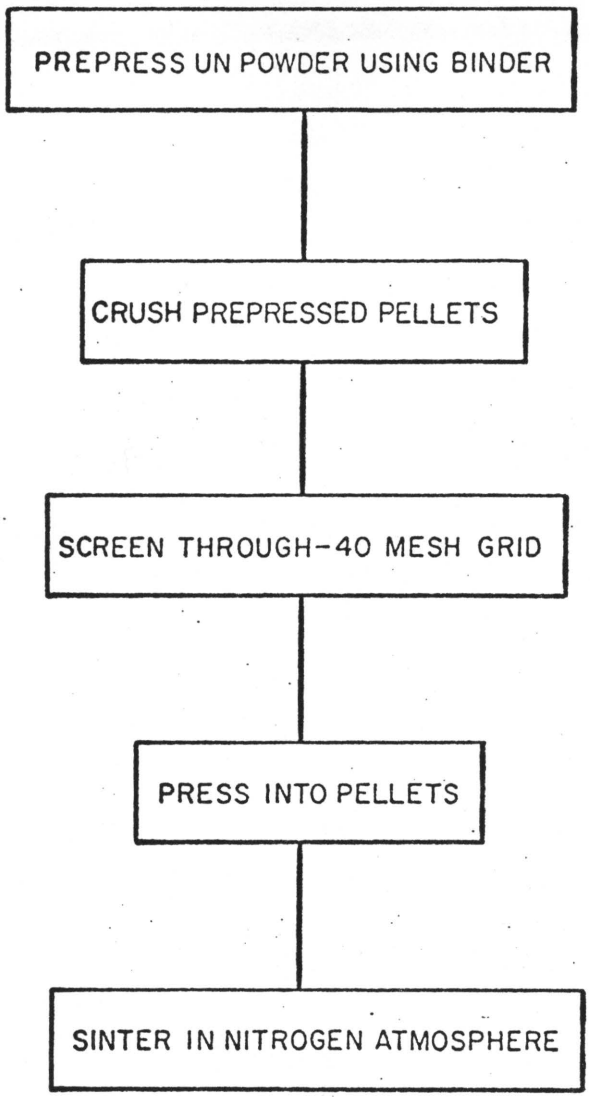

Figure 21. Fabrication of Uranium Nitride Pellets.

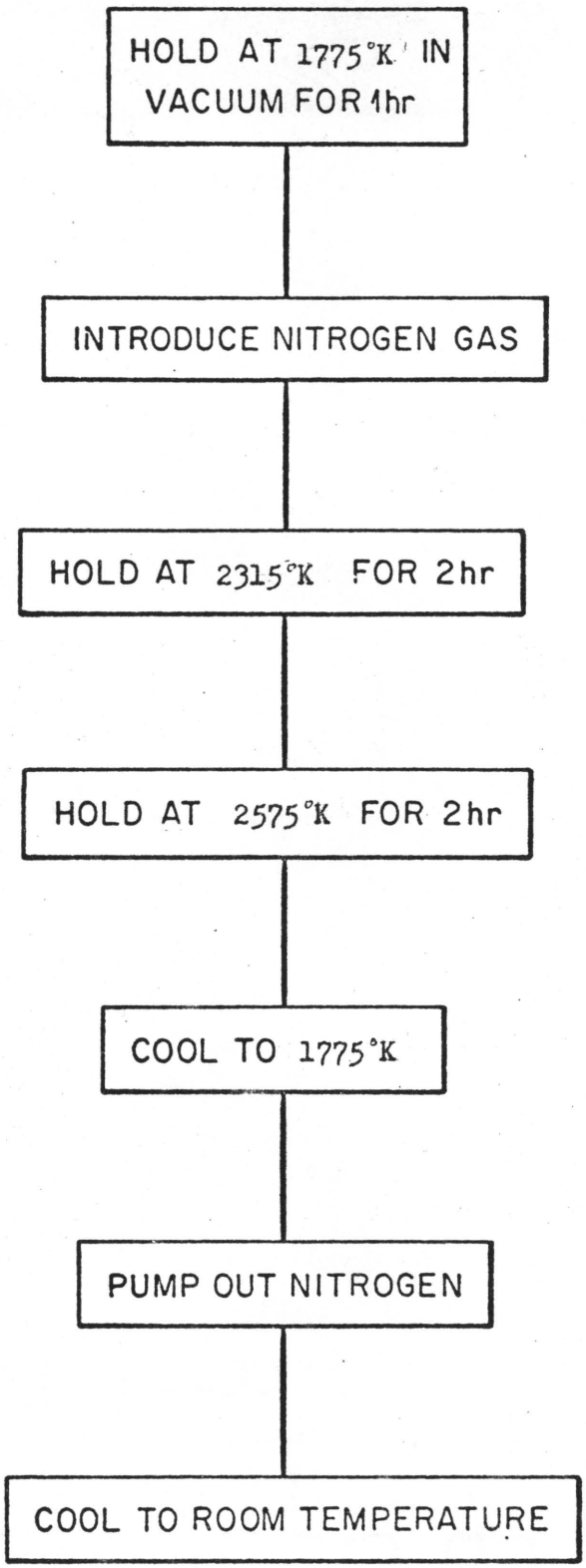

Figure 22. Sintering Cycle for Uranium Nitride Pellets.

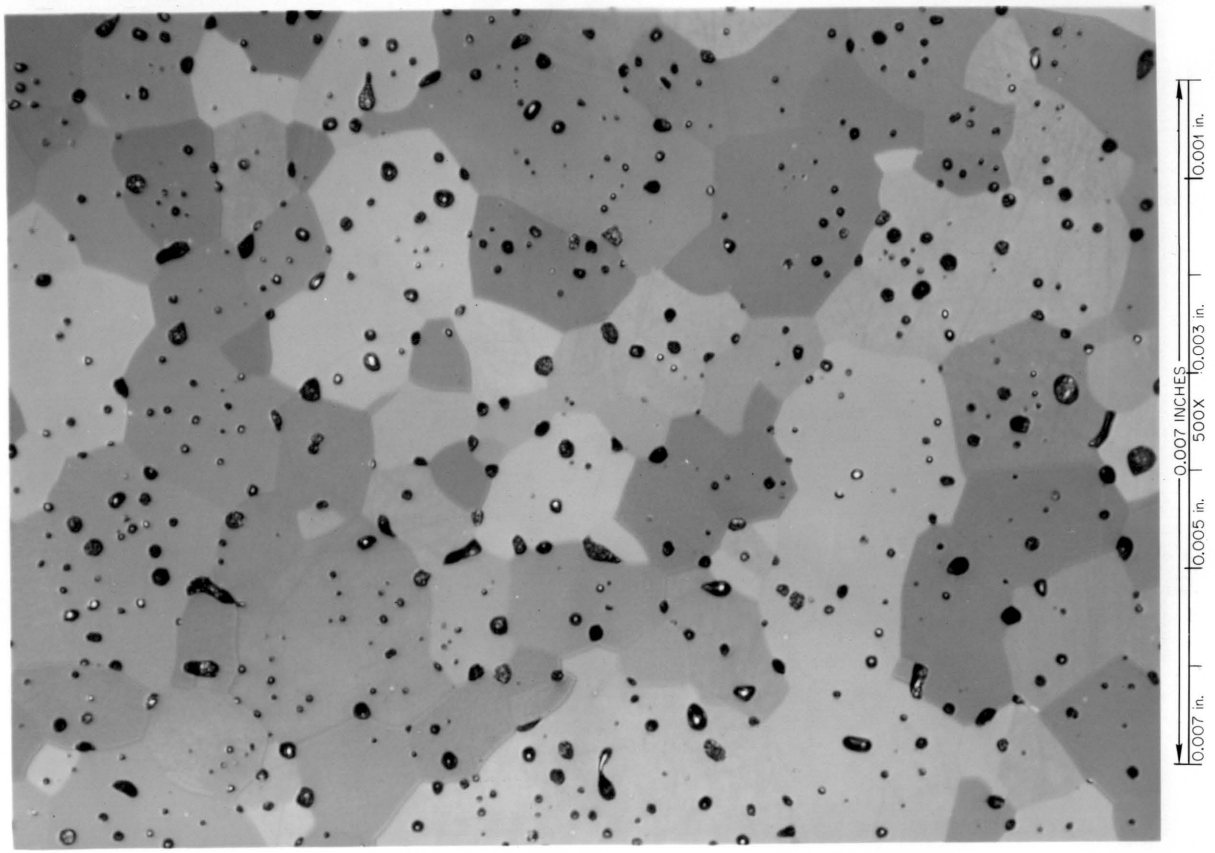

Figure 23. Typical Microstructure of As-Sintered Uranium Mononitride.

a great deal of effort was expended to develop a zone melting process which was finally used to obtain good samples for this study.

The zone melting process consisted of the following steps.

(1) Casting a Th-U alloy of the desired composition.

(2) Swaging the casting into a rod approximately 0.6 cm diameter.

(3) Cutting the swaged rod into usable lengths of approximately 20 cm long.

(4) Zone melting a 7 to 10 cm length of the metal alloy rods in a nitrogen atmosphere.

(5) Cutting the nitrided portion of the rod from the rest of the rod.

(6) Centerless grinding the rod to obtain a smooth uniform outer surface and diameter.

(7) Annealing the machined rods in a nitrogen atmosphere at 2725 °K for 6 hr to eliminate any residual free metal.

The metal alloys were cast into billets using the high-purity thorium and uranium. The uranium and thorium metals were drop cast in a water cooled copper mold using a tungsten electrode in argon. The chamber was pumped down to a vacuum of 10^{-8} atmosphere and back-filled three times prior to striking the arc. Prior to melting a sample, a zirconium button was melted to further reduce any oxygen present. This resulted in a casting atmosphere of approximately 1 ppm of oxygen or less. The rods were cast into billets 7 to 10 cm long and approximately 2.5 cm in diameter.

After swaging and cutting the rods to length, the rods were placed in the zone melting furnace (see Figure 24). The design of the moving components and the induction heating coil was done largely by Ji Young Chang while he worked at Oak Ridge National Laboratory. The moving

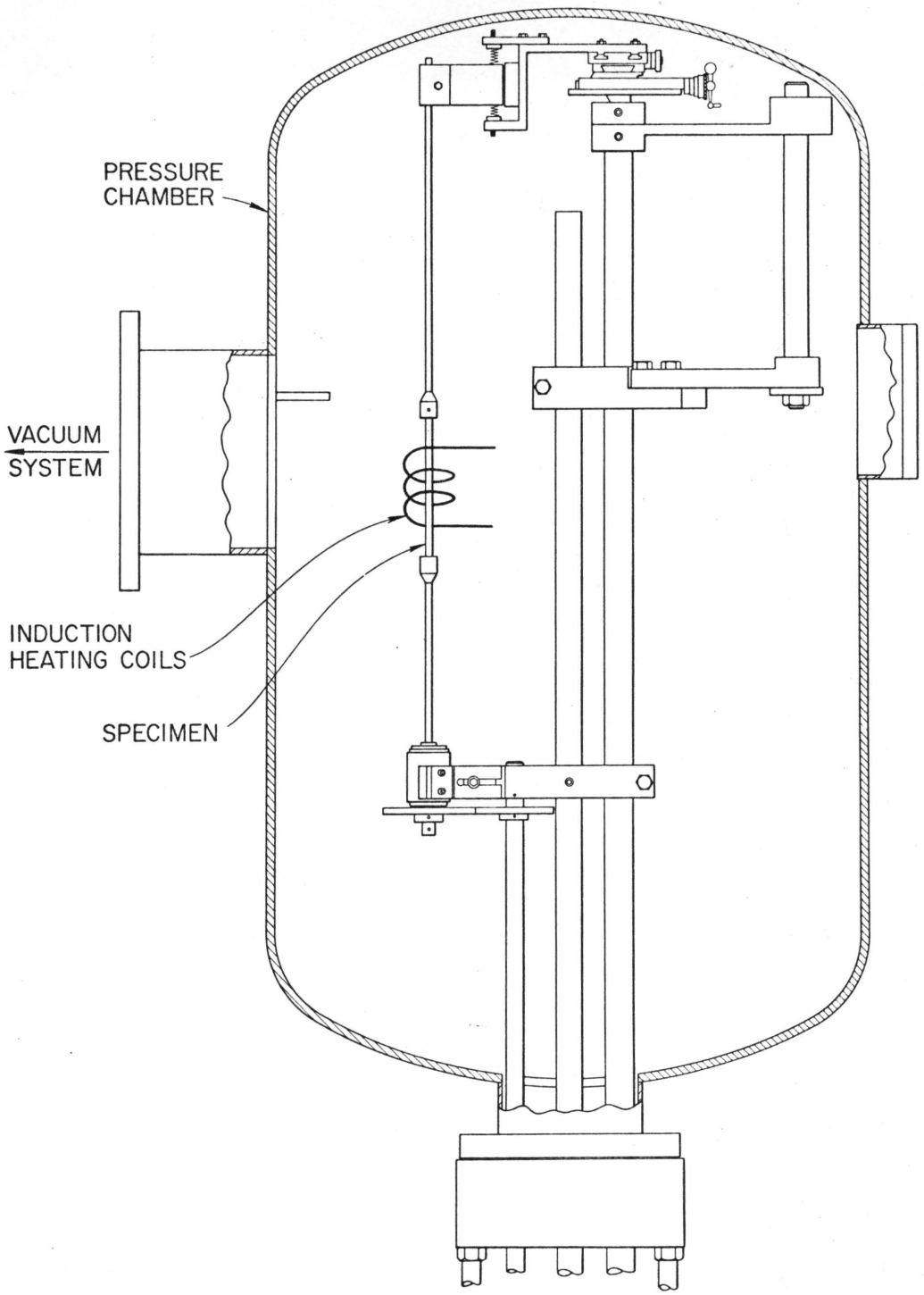

Figure 24. Zone-Melting Apparatus Used to Fabricate (Th-U)N Rods.

components of the furnace were fabricated in the machine shop at Oak Ridge National Laboratory and installed and tested by the author.

After all of the components were determined to be working satisfactorily, two test runs were made on tungsten rods to determine if sufficient power was available to attain temperature. After these test runs, a sample of thorium was placed in the furnace and melted in a nitrogen pressure of 1.3 atmosphere which was obtained by pumping to a pressure of 10^{-7} atmosphere or lower and backfilling with nitrogen gas. By the ninth run on thorium, greater than 99% of the thorium had been successfully converted to ThN. This conversion takes place in a small molten "zone" of thorium, which holds its shape by surface tension. Nitrogen diffuses very rapidly through this molten thorium converting it to ThN. Because the nitrogen is coming from the gaseous state, the nitrogen activity must be higher on the outside than at the interior of the sample, which causes the solid nitride to form at the outer surface first. The forming of this outside skin of nitride serves to strengthen the molten rod, but it also hinders the diffusion of nitrogen to the center of the rod. Consequently, several passes were made on the rod increasing the temperature of the rod on each pass until the sample was very near the melting temperature of ThN. Typically, the first pass was made at a pyrometer reading of 2675-2725 °K. The zone was moved at a rate of 2.5 cm/hr. Previous experiments by Ji Young Chang in the same furnace but without the moving components showed a temperature correction for the sight glass and non-black body conditions to be approximately 400 °K. Thus, on the last pass the ThN sample was very near the melting temperature of 3095 °K. The (Th-U)N

alloys were made using the same technique and temperature calculated for ThN.

Several attempts were made to make UN, the last attempt being successful. Converting uranium to UN turned out to be significantly more difficult than converting thorium and Th-U alloys to their respective nitrides. The difficulty arises because uranium melts at a much lower temperature and has a much slower diffusion rate of nitrogen[46] than does ThN. Another complication is the very large volume change associated with converting uranium to UN in which the uranium atom density decreases 29%. Converting thorium to ThN, however, reduces the thorium atom density only 4.6%. A fourth complication is the formation of U_2N_3 in the low temperature ranges. The first pass must be made at a temperature low enough so that the molten uranium rod will not lose enough surface tension strength so that it breaks in two, yet high enough in temperature so that the nitrogen will diffuse through the outer skin of nitride formed and high enough so that most of that skin is not U_2N_3. The problem with the U_2N_3 is that if it reconverts to UN later in the process it will undergo a very large volume change thereby shrinking and breaking the outer skin.

After the zone melting step, the nitrided portion of the rod was cut off and centerless ground. The centerless grinding was done by taking off about 0.0025 to 0.005 cm each pass through the grinder. The rods were machined until they "cleaned up," (i.e., until there were no chips or indentations in the diameter of the rod).

The last step in the fabrication of the samples was to anneal the rods at 2625 °K for 6 hr in a nitrogen atmosphere to eliminate any free

metal which still remained in the sample and to homogenize the distribution of the thorium and uranium atoms in the (U-Th)N matrix. Experiments by Venard and Spruiell showed that long time, high temperature heat treatments will eliminate these inhomogeneities. Because of the possibility of nitriding the sample to Th_3N_4 during the thermal cycle, the path outlined below was followed.

(1) Heat ThN sample to 1775 °K in vacuum of 10^{-10} atm.

(2) Introduce 0.5 atm N_2 gas.

(3) Hold at 1775 °K in N_2 for 2 hr.

(4) Raise temperature to 2725 °K; hold for 2 hr.

(5) Cool to 2575 °K.

(6) Reduce nitrogen pressure to 2.6×10^{-3} atm.

(7) Cool to 1775 °K.

(8) Pump out to 10^{-10} atm.

(9) Cool to room temperature.

The rational behind step 3 is to transform the free thorium metal near the periphery of the sample to ThN at a temperature in which the metal is still solid. This prevents reaction between the tungsten container and thorium metal which becomes molten above 2118 °K.

After heat treatment the samples were radiographed using 1000 Kev x rays to determine whether any residual porosity was left from the fabrication process. Several x rays were made of each sample using different film exposures and rotating the sample between each x ray taken. The x rays showed considerable casting porosity in the arc cast samples but only a small amount of porosity near the ends of the zone melted samples. A photomicrograph of a typical as-fabricated structure is shown in Figure 25.

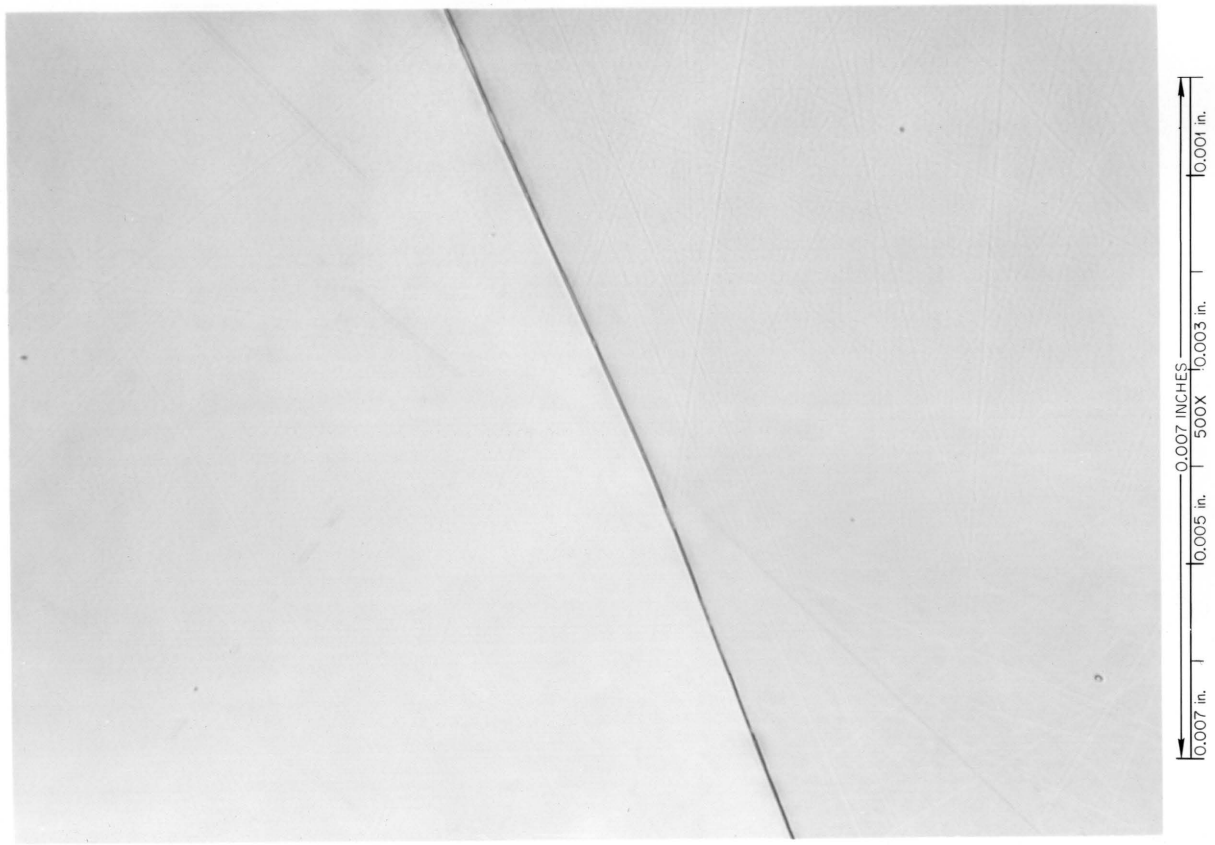

Figure 25. Photomicrograph of Typical ThN Microstructure as Fabricated from the Zone Melting Process. Magnification: 500X.

The procedure for making UN directly from uranium metal shows real promise for making relatively cheap samples for research work and possibly for use in space reactors. An even more promising extension of this technique would be to use it to convert U-Pu alloys to (U-Pu)N for use as fuel in liquid metal fast breeder reactors. The UN product produced from this zone melting technique was nearly theoretically dense with large grains (approximately 0.3 cm diameter). Further development should produce samples with even larger grains or possibly single crystals. The large grains enhance the irradiation behavior of UN by elimination of the grain boundary trapping sites for fission gas bubbles. Irradiation tests by the author on some UN single crystals showed a factor of 50 reduction in fuel swelling would be realized on other nitride systems such as (U-Pu)N, (U-Th)N, and (Th-Pu)N.

Samples AC-6, AC-1, and AC-5 were prepared by arc casting thorium and thorium-uranium alloys in a beehive furnace containing nitrogen atmosphere using a tungsten electrode. This resulted in a casting which contained about 97% of the ceramic alloy and about 3% residual metal. This technique was satisfactory for producing thorium and (Th-U)N alloys containing up to about 5% uranium. At the uranium rich end of the phase diagram, however, the casting resulted in about 20% free metal. This quantity of metal could not be converted to UN because of the slow nitrogen diffusion rate in UN and because the large volume change in going from uranium with a density of 19.05 gm/cm^3 to UN with a uranium density of 13.52 gm/cm^3 resulted in extensive cracking and porosity formation.

Arc casting of (Th-U)N alloys was begun by melting high purity uranium and thorium into a homogeneous alloy in the same manner

described previously for casting uranium and thorium in preparation for the zone casting step. The thorium uranium alloy was then melted and kept molten for three to four minutes. After cooling, the sample was brought to atmospheric pressure, turned over, and melted again. Each sample was melted a total of three times after which the alloy was assumed to be homogeneous. It is apparent from the phase diagram (Figure 10), however, that the alloy could not be homogeneous on a microscopic or submicroscopic scale. The metal ingots were then recast in a nitrogen atmosphere of approximately 1000 mm Hg pressure to form the nitride. The samples were turned over and recast again to provide a more homogeneous distribution of nitrogen. However, as the samples took up nitrogen, the melting point of the casting began to increase and the sample could not be kept uniformly molten. When the casting was turned over to nitride the other side of the rod, the sample did not become molten throughout the sample. This resulted in an undesirable residual casting porosity.

After casting, the samples were found to be radioactively hot, presumably from daughter products from the decay of thorium which apparently adhered to the surface of the samples giving off a low energy beta. These decayed very rapidly and after 24 hr the samples could be easily handled from a radiation hazard standpoint.

The microstructure of a typical as-cast sample is shown in Figure 26. The sample was primarily the nitride phase with about 3% free metal at the grain boundaries. The samples were stored in vacuum pump oil prior to machining to prevent oxidation. Samples left exposed to air completely converted to the oxide in about two days. No other liquid was found to be suitable to prevent sample oxidation.

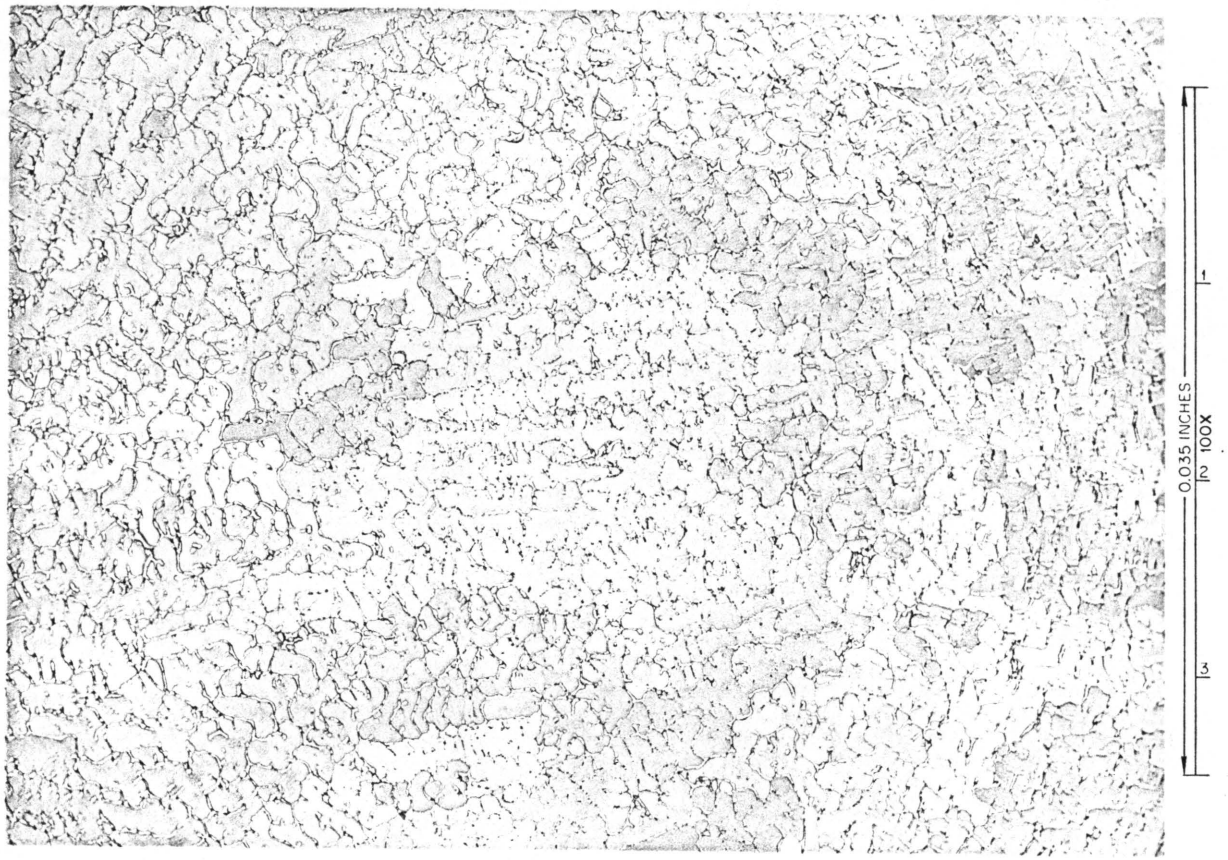

Figure 26. Typical Microstructure of ThN after Casting in a Nitrogen Atmosphere.

After casting, the samples were machined in the Oak Ridge National Laboratory "hot shop." Because of the presence of the small amount of free metal, the samples could be machined quite easily. This was a big advantage in the handling of this ceramic material. It was possible to take a 0.025 cm interrupted cut on the lathe without breaking the sample. The samples were machined into right circular cylinders ranging from 0.5 to 6 cm in length with a 0.125 cm diameter hole drilled down the center to aid in the heat treatment that followed.

After machining, the samples were heat treated in a tungsten mesh furnace to 2625°K in nitrogen at 0.5 atm. The purpose of the heat treatment was to eliminate the residual metal still contained in the samples.

After heat treating, metallography typically showed large grains of up to 0.3 cm diameter with no second phases present like that shown in Figure 25. However, the samples also contained a large amount of nonuniform residual porosity which made a porosity correction very difficult and consequently introduced a large source of error into the calculated thermal and electrical conductivities. A very long and time consuming effort was expended in trying to correct for this porosity by using an eddy current technique to measure electrical resistivity independent of any porosity correction. However, the results we obtained for λ and ρ using this technique were inconsistent with existing theories on thermal conductivity. The thermoelectric power data we obtained from measurements on the samples were good, however, since no porosity correction is required in the measurement of this property.

Because of the problem of nonuniform porosity in the cast samples, samples were made by cold pressing and sintering ThN powder. A

three-month effort by the Ceramics Laboratory at Oak Ridge National Laboratory to make rods produced samples only 80% theoretically dense. No means was discovered for increasing the density so this technique was eventually discarded. As was pointed out previously, samples which have densities below 88% of theoretical, cannot be accurately corrected for porosity to obtain a thermal conductivity of the theoretically dense material. In addition, a physical blending of ThN and UN powders produced a two-phase ceramic material rather than a homogeneous mixture as we had hoped. This meant that for each composition to be studied it was necessary to hydride and nitride a previously cast alloy of that composition. The cost of such an operation for a range of alloys was prohibitive so this approach was dropped.

II. MEASUREMENT TECHNIQUES

Four pieces of equipment formed the basis for most of the experimental measurements: (1) an electrical resistivity knife edge, (2) an electrical resistivity apparatus, (3) a guarded longitundinal heat flow apparatus, and (4) a PDP-8 computer-operated-data-acquisition system (CODAS).

Electrical Resistivity Knife Edge

In order to accurately measure the room temperature electrical resistivity of a sample, the voltage drop on the sample between two "knife edges" of known separation was measured. With these data, the distances between adjacent thermoelements on the sample could be accurately calculated.

Two electrical resistivity knife edges were used in these experiments: (1) a knife edge already in use by the Physical Properties

Group at Oak Ridge National Laboratory, and (2) a knife edge built and assembled into an argon atmosphere glove box especially for these tests. The knife edge measurements are used to accurately determine the room temperature electrical resistivity of the samples. Once an accurate resistivity measurement is made at room temperature, thermocouple distances can be measured electrically much more accurately than they can be measured optically.

In order to measure the resistance of a sample using the knife edges, a current is passed through the sample by removable electrodes from a direct current power supply (Electronic Research Associated Model 36-12M with $\pm$0.05% load and line regulation and $\pm$0.005% rms ripple). The voltage drop along the sample was taken where two razor blades contacted the sample. The razor blades (or knife edges) are separated with a machined quartz block which has parallel sides. The distance between the razor blade knife edges was determined using two techniques. First the distance was determined using a shadowgraph accurate to 0.01% and second a standard sample with a known ρ and a low $\frac{d\rho}{dT}$ was used to check the distance electrically. The two techniques agreed to within 0.01%. Quartz is used because its low thermal coefficient of expansion prevents any significant change in the knife edge separation with slight variations in room temperature. A thermocouple is attached to the sample being measured so that the temperature of the sample can be precisely determined. A Rubicon 6-Dial potentiometer with a certified uncertainty of $\pm$0.01% + 0.01 μV was used to measure the potential across the knife edges, the thermocouple emf, and the potential drop across a standard 0.01 ohm resistor in series with the sample for current determinations. Occasionally the PDP 8 computer was substituted for the 6-Dial potentiometer with no significant loss of accuracy.

The knife edges installed in the argon glove box was identical to the knife edge already in use except that the data were taken on a Leeds and Northrup Type K-5 potentiometer and the current supplied by a Kepco Model KS18-10(M) power supply. Lines from the sample went to a micarta tie down board with nylon screws inside the glove box. From the tie down board wires went through the glove box wall to an ice bath reference junction where they join copper wires.

Values for electrical resistivity were calculated from the equation

$$\rho = \frac{RA}{l} , \tag{31}$$

where, R = resistance between voltage taps,

A = cross sectional area,

l = distance between voltage taps.

This becomes

$$\rho = \frac{EA}{Il} , \tag{32}$$

where, E = voltage drop between probes,

I = current through the sample.

The current is calculated from the voltage drop across a standard 0.01 ohm resistor in series with the sample. The voltage drop is obtained by reading the voltage drop in one direction, reversing the current, and rapidly reading the voltage drop in the other direction. Reading the voltage drop in both directions eliminates the thermoelectric power effect which shows up in the samples due to Peltier heating. The

magnitude of this effect is proportional to the thermoelectric power of the sample with respect to the knife edge material and to the heat generated where the current leads are attached. This heat is given by

$$Q = (S_{spec} - S_{current\ leads})TI \ , \qquad (33)$$

where, Q = heat generated,

S_{spec} = thermoelectric power of specimen,

$S_{current\ leads}$ = thermoelectric power of current leads,

T = temperature,

I = current.

In the case of UN where the absolute thermoelectric power is large and positive, this effect can be quite substantial. Consequently, it is important to take the data upon reversing very rapidly. For this reason the PDP-8 computer to be described below, is a useful tool for ρ measurements. Within seconds after reversing the current on UN the voltage drop begins changing significantly. In the case of ThN which has a very small thermoelectric power at room temperature, this effect is less important. The current leads used for both UN and ThN were copper.

Electrical Resistivity Apparatus

Electrical resistivity and thermoelectric power data for temperatures greater than 300 °K were obtained with the specimens positioned in an evacuated alumina tube that was heated in a tubular furnace capable of reaching 2000 °K. An auxiliary heater was wound around the outside of the tube to establish a temperature gradient along the rod specimen for thermoelectric power measurements. For the

ρ measurements, a standard four-probe technique was used. Measurements of ρ and S were made in pressures ranging from 10^{-10} to 10^{-9} atm to prevent oxidation of the samples.

The current leads were brought into the ends of the specimen. Two thermocouples were welded to the sample with the positive and the negative thermoelements serving as voltage taps. Tungsten versus W-26% Re thermocouples were used because of their compatibility with UN and ThN. Tungsten was used for the positive leg instead of W-5% Re to permit a more accurate calculation of the thermoelectric power.

The current source for the electrical resistivity measurements was a direct current power supply (Electronic Research Associated Model 36-12M with $\pm$ 0.05% load and line regulation and $\pm$0.005% rms ripple). For some of the initial data, a Rubicon 6-Dial potentiometer with a certified uncertainty of $\pm$0.01% and 0.01μV was used to measure the potential drop along the specimen, the thermocouple electromotive force, and the potential drop across a standard 0.01 ohm resistor for current determinations. For most of the data, however, the PDP-8 computer system was used because it could take the data much more rapidly and as accurately as the 6-Dial potentiometer. Because of the large Peltier heating effect in UN on reversing the current, the CODAS system was actually more accurate at high temperature. Details of the CODAS system are described in a later section.

Thermoelectric power data were obtained on the UN sample by supplying power to the auxiliary heater and establishing a temperature gradient on the sample. After the sample reached thermal equilibrium, usually requiring about 2 hr, voltage drops, ΔE, and the associated temperature differences, ΔT, were measured. Three thermal gradients

were applied for each average temperature and linearly interpolated to obtain the slope which is the value of S.

$$S = \left(\frac{\Delta E}{\Delta T}\right)_T , \tag{34}$$

Each data point was taken such that the average temperature of each of the three points was within 0.5 °K.

A calibration curve of the tungsten versus W–26% Re thermocouples was run early in the resistivity tests because of the relatively large differences observed between the W/W–26% Re thermocouples and a Pt–10% Rh/Pt thermocouple placed near a tungsten end clamp in the ρ measurements. The calibration test was run by making a common junction of platinum, Pt–10% Rh, tungsten, and W–26% Re wires by wrapping them tightly together with platinum wire. These were then insulated with Al_2O_3 and inserted into a 2 in. long niobium rod with a hole drilled to a depth of 1 1/2 in. to hold the thermocouples. The purpose of the niobium rod was to even out the temperature distribution. The Pt–10% Rh/Pt wire used in this test had been previously calibrated at Oak Ridge National Laboratory. The calibration showed the temperatures of the W/W–26% Re thermocouples to be incorrect by as much as 12 °K. This temperature calibration was used to correct the data.

Guarded Longitudinal Heat Flow Apparatus

The guarded longitudinal heat flow apparatus was used to measure λ, ρ, and S from 80 to 400 °K. The apparatus was immersed in baths of liquid nitrogen and ice and water which provided the heat sinks for the flow of heat.

The guarded longitudinal heat flow apparatus shown in Figure 27 was a modification of an apparatus described by Moore et al.[47] It consisted of a cylindrical rod specimen attached to a removable copper base mounted in a vacuum chamber. The free end of the specimen had a radial heater attached to it with an epoxy resin. The electrical power dissipated in the heater and the measured temperature gradient along the rod were used to calculate λ, assuming longitudinal heat flow. Radiation and conduction losses were minimized by surrounding the specimen with a temperature controlled guard cylinder which is surrounded with a copper sleeve. Radiation exchange between the guard cylinder and the specimen was minimized by placing spun Al_2O_3, a loose, fibrous insulating material, in the annulus between the specimen and guard cylinder. The guard cylinder was attached to the removable copper base with eight screws to provide good thermal contact between the guard cylinder and base. Indium foil was placed where the sample was attached to the removable copper base, where the guard cylinder was attached to the removable copper base, and between the removable copper base and the copper base plates.

The assembly contained three resistance heaters: one wrapped around the free end of the specimen (H_1), a second wrapped around the guard cylinder (H_2), and a base heater (H_3). The specimen heater (H_1) was used to generate the ΔT on the sample for the λ and S measurements. The heater was made by wrapping varnish-coated 0.013 cm diameter Nichrome wire onto masking tape wrapped around a glass rod. Varnish-coated 0.013 cm diameter copper wire was attached for current input leads. A Chromel-constantan thermocouple was placed at the point where the heater current leads came off the sample. The heater and thermocouple were

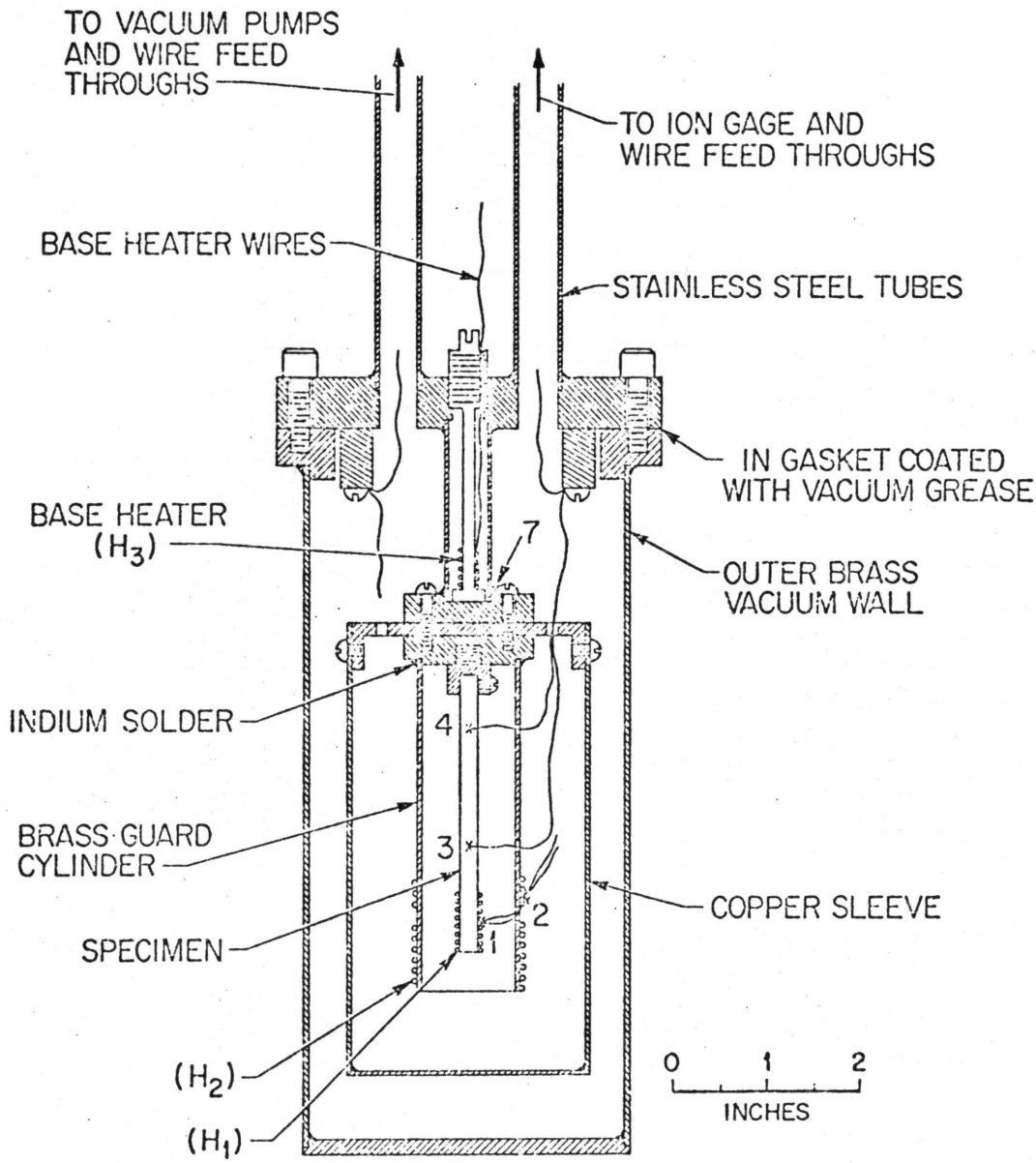

Figure 27. Schematic Diagram of Guarded Longitudinal Heat Flow Apparatus.

Source: J. P. Moore, D. L. McElroy, and R. S. Graves, "Thermal Conductivity and Electrical Resistivity of High-Purity Copper from 78 to 400 °K," Canadian Journal of Physics, 45: 3849–3865, 1967.

epoxied together using a thermally conducting, electrically insulating epoxy. Ideally, potential taps should have been soldered onto the current leads midway between the specimen and guard cylinder but, because of the experimental difficulty in handling the system in a glove box, no potential taps were made. However, a correction was applied for the resistance of the copper lead wire coming from the assembly. To further reduce the error in measuring power, the resistance of H_1 was made very large (90 to 110 ohms) compared to the lead resistance (<0.2 ohms). Consequently, the above correction was small compared to the total resistance of the heater.

The heat losses were reduced by maintaining the same temperature gradient on the guard cylinder that existed on the sample. This was done by minimizing the monitored temperature differential between the sample heater where the copper lead wires come off and the point on the guard cylinder where the current input leads were placed in good thermal contact. Power was supplied to the guard cylinder heater proportionate to the temperature difference between the guard cylinder and the specimen heater.

The base heater, H_3, consisted of constantan wire wound on a brass rod. Heater H_3 provides the means for raising the temperature of the sample above the ambient temperature by supplying power from a manually controlled variac. By immersing the entire assembly in Figure 27 in a dewar filled with either liquid nitrogen or an ice-and-water mixture, data were obtained at temperatures between 77.7 and 400 °K.

Thermocouples were attached at five positions on the assembly. Thermocouple 1 was attached to the heater where the lead wires leave the heater region. The wires from Thermocouple 1 pass through the

guard cylinder, and are in thermal contact but electrically insulated at this point. The temperature of this ground point was measured with Thermocouple 2. Thermocouples 3 and 4 were used to measure the temperature gradient in the specimen. They were attached to the specimen by spot welding the individual thermocouple wires in place, and then adding a drop of electrically insulating epoxy to improve the mechanical strength of the thermocouple attachment. The distance between Thermocouples 3 and 4 was determined electrically by passing a direct current through the sample, measuring the voltage drop, and comparing the voltage drop with the knife edge measurements. Thermocouple 1 was used to control the power to heater H_3 to maintain the desired temperature of the specimen.

All wires in the system were connected to a Teflon terminal ring with nylon screws. The Chromel-P and constantan thermoelements extended from this Teflon ring to an ice-bath reference junction where they joined copper wires. These copper wires were attached to a thermal-free switch and a Leeds and Northrup Type K-5 potentiometer. In addition, the outputs were wired into the PDP-8 computer. The wires from the measurement and control circuitry entered the chamber through stainless steel tubes and were in thermal contact with the flange. One of the stainless steel tubes used for admission of the thermocouple wire served as a connection to a vacuum system capable of 10^{-10} atm.

For measuring electrical resistivity, a 0.013 cm diameter, varnish-coated copper current lead was wrapped around the end of the specimen and tack welded to it. It was further fixed in place with an electrically conducting epoxy. The specimen heater was epoxied to the sample over the current lead, which gave the current lead additional strength.

The current lead was then placed in thermal contact with the guard cylinder at the same place as the heater wires and thermocouple. The current was determined by measuring the voltage drop across a standard 0.01 ohm resistor. The calibration of the resistor showed its resistance to be 0.010015 ohms at 295 °K.

A direct current was supplied to the specimen heater using a constant voltage control from a Kepco Model KS18-10(M) power supply. The voltage, E, was determined by measuring the voltage drop across a Leeds and Northrup No. 7592D-C volt box and the current, I, was measured by reading the voltage drop across a standard 0.01 ohm resistor with Leeds and Northrup Type K-5 potentiometer. The Chromel-P versus constantan thermocouples were read on the K-5 potentiometer with the copper-to-Chromel and copper-to-constantan junctions immersed in an ice-water mixture in a dewar flask.

The thermal conductivity was then calculated from the equation

$$\lambda = \frac{P}{A\left(\frac{dT}{dx}\right)} \quad , \tag{35}$$

where, P = power supplied to specimen heater, EI,

A = cross sectional area of sample, and

$\left(\frac{dT}{dx}\right)$ = temperature gradient.

For the experimental data, this equation becomes

$$\lambda = \frac{EIl}{A(\Delta T)} \quad , \tag{36}$$

where, E = voltage drop across specimen heater,

I = current through specimen heater,

l = distance between specimen thermocouples, and

T = temperature difference measured between specimen thermocouples.

The thermoelectric power was calculated from the voltage drops between the two constantan thermoelements using the equation

$$S = \frac{\Delta E}{\Delta T_c} , \tag{37}$$

where, ΔE = voltage drop between constantan legs of the thermocouples, and

ΔT_c = temperature difference between constantan legs of thermocouples.

It is important to note that ΔT_c in Equation (37) is different than ΔT in Equation (36) unless the constantan and Chromel legs happen to be spaced exactly the same distance apart. Assuming the temperature gradient to be linear, the temperature as read on the thermocouple, ΔT, can be corrected to ΔT_c by

$$\Delta T_c = \Delta T \left(\frac{2 R_{const}}{R_{const} + R_{Chromel}} \right) , \tag{38}$$

where, R_{const} = resistance measured between constantan legs, and

$R_{Chromel}$ = resistance measured between Chromel legs.

Prior to running the thermal conductivity experiments with power to the specimen heater, a set of isothermal corrections were experimentally obtained as a function of temperature by reading the specimen thermocouples

and voltage drops with no power to the specimen heater to compensate for thermocouple calibration. The temperatures and voltage drops are always nonzero even with no power being lost because of such things as composition differences in thermocouple wires, heat leakage into the system from H_3, the heater controlling the temperature, and heat leakage due to imperfectly matching the specimen and guard cylinder temperature gradients. The isothermal data were obtained at four temperatures with the chamber in both the liquid nitrogen bath and ice-and-water bath. Generally, the correction was larger in the liquid nitrogen bath than in the ice-and-water bath because the temperature gradients along the thermocouple wires were greater in liquid nitrogen.

The ice-and-water bath in which the thermal conductivity apparatus was immersed was made with finely crushed ice with a small propeller used to continuously stir the mixture, thereby preventing the formation of a temperature gradient in the bath due to warmer water layers forming near the bottom. It was not necessary to stir the liquid nitrogen bath but the contents had to be emptied from the dewar containment at least once a day to eliminate the buildup of liquid oxygen and CO_2, which tend to change the Bath temperature.

Calibration of Equipment

Prior to making measurements on the (Th-U)N samples of interest, the longitudinal heat flow equipment was checked out with the modifications described previously. Thermal conductivity and electrical resistivity measurements were made on a Nb–10% W sample previously measured by Moore.[48] A tabulated comparison of the results is shown in Table 6. The agreement between data was well within the experimental error of $\pm 2.1\%$.

TABLE 6

COMPARISON OF THERMAL CONDUCTIVITY OF Nb–10% W AS MEASURED ON EQUIPMENT USED IN STUDY WITH PREVIOUS MEASUREMENTS BY MOORE

Temperature (°K)	λ (W cm^{-1} $°K^{-1}$)	Deviation from Smoothed Values[a] (%)
Original Modified Equipment		
97.98	0.3483	+0.17
137.448	0.3854	+0.63
298.404	0.4648	−0.36
New Thermal Conductivity Apparatus		
140.5	0.3814	−0.9
194.5	0.4142	−1.1 (9 °K ΔT)
201.2	0.4274	+1.3 (3 °K ΔT)
270.7	0.4529	−0.5

[a]Compared with λ measurements by J. P. Moore, personal communication, September 1969.

After the tests were run on the arc cast samples, a new longitudinal heat flow apparatus was set up because of the work load of the original apparatus. Equipment which had been previously ordered was assembled and a "debugging" session ensued to reproduce the results obtained on Moore's apparatus. After we were satisfied that the equipment was operating satisfactorily, the Nb–10% W sample was reinstrumented and data points taken again. The data obtained and the agreement with the curve generated by Moore is shown in Table 6.

CODAS System and Circuitry

Using CODAS (Computer-Operated-Data-Acquisition System),[49] it was possible to speed up the actual data taking process by a factor of about 1000. The voltage signals from two thermocouples and the voltage drop signal were placed in series opposition with a suppression voltage from a Dial-A-Volt zener diode reference supply and the resulting differential signals connected to amplifiers. The amplification circuits were coupled to a multiplexer analog-to-digital converter in the PDP-8 computer, which digitized the signals. Knowing the signal amplification and suppression voltages from a calibration procedure, a computer program was written to read T_1, T_2, E_+, then reverse the current and read T_1, T_2, and E_-. The program would then average the temperatures $\bar{T}$ and voltage drops for the two current directions and then print out $\bar{T}_1$, $\bar{T}_2$, $\bar{T}$, and ρ. Twenty signals of each reading were obtained for a total of 120 readings. The time to read all of the signals was about six seconds with another four seconds used to calculate and print out the data. The readibility of the signals was 0.01% for a full scale deflection of the amplifiers. To maintain this sensitivity,

the input current to the sample and the bias voltage were maintained such that near full scale deflection was achieved.

For further details of CODAS, its accuracy, and capabilities, the reader is referred to reference 49.

Prior to making measurements with CODAS, some time was spent to determine the accuracy of CODAS for taking measurements compared with taking the data from the 6-Dial potentiometer. Two techniques were used to make the comparison. First, a Dial-A-Volt zener diode was used to supply an 85 μV signal. This signal when read on the potentiometer with the amplifiers and line load behind it was 82.43 μV. This signal was also read using CODAS. The second comparison was made by passing a direct current through a copper sample so that a voltage drop of about 85 μV occurred between the razor-blade knife edges. Electrical resistivity values were calculated from both the 6-Dial data and CODAS. The results of these two calibration tests are shown in Table 7.

These tests showed that the values we calculated using CODAS can be as good as the calibration of the computer. If proper care is taken, the use of CODAS should not increase the error relative to using the 6-Dial by more than 0.1%.

The signals from the guarded longitudinal heat flow were connected into PDP-8 computer and λ, ρ, and S data were taken. One advantage of using this technique is that it is easy to determine when thermal equilibrium has been attained. The PDP-8 was programmed to take data at selected time intervals and when the temperatures and calculated conductivities stabilized, the data were recorded and the temperature changed to the next desired temperature. While this method reduced the time required to take data, it was a relatively unproven technique so

TABLE 7

COMPARISON OF VOLTAGE READINGS FROM 6-DIAL POTENTIOMETER WITH CODAS

	Value Calculated		Difference (%)
	6-Dial	CODAS	
Zener signal, μV	82.43	82.42	0.01
ρ_{Cu}, μohm-cm	1.7237	1.7233	0.02

the more standard, reliable technique of reading the data from the potentiometer was used. It should be noted, however, that the data points taken using the computer were within 0.2% of the data taken from the K-5 potentiometer. To the author's knowledge, this represents the first time thermal conductivity data have been taken using the PDP-8 computer to read the signals.

Because the use of the PDP-8 computer was not the central point of the dissertation, it was not used to obtain data that were not repeated on the K-5 potentiometer. This was to eliminate any question as to the accuracy of the data which might arise because of the use of the computer system.

Error Analysis

A detailed error analysis for λ, ρ, and S for the guarded longitudinal heat flow apparatus has been presented by Moore et al.[47] Using this as a guide, an error analysis of the particular sample configuration used in these tests is summarized in Table 8. The relative error for λ, ρ, and S may be expressed as errors as follows:

$$\text{For } \lambda: \quad \left|\frac{\Delta\lambda}{\lambda}\right| = \left|\frac{\Delta E}{E}\right| + \left|\frac{\Delta I}{I}\right| + \left|\frac{\Delta A}{A}\right| + \left|\frac{\Delta l}{l}\right| + \left|\frac{\Delta(\Delta T)}{T}\right|$$

$$\text{For } \rho: \quad \left|\frac{\Delta\rho}{\rho}\right| = \left|\frac{\Delta E}{E}\right| + \left|\frac{\Delta I}{I}\right| + \left|\frac{\Delta A}{A}\right| + \left|\frac{\Delta l}{l}\right|$$

$$\text{For S:} \quad \left|\frac{\Delta S}{S}\right| = \left|\frac{\Delta V}{V}\right| + \left|\frac{\Delta(\Delta T)}{T}\right|$$

These equations are used to determine the total determinate absolute error. The "most probable error," β, was defined by Moore et al.[17] as

TABLE 8

SUMMARY OF MEASUREMENT ERRORS FOR (Th-U)N ALLOYS IN THE GUARDED THERMAL CONDUCTIVITY RIG

Error	ρ	S	λ
Temperature Measurement			
Uncertainty of measurement temperature	+0.1 °K	+0.1 °K	+0.1 °K
Uncertainty of ΔT measurement (%)		±2.0	±2.0
Dimensional Measurement (%)			
Distance between thermocouples	<±0.36		<±0.36
Area	±0.08		±0.08
Power Measurement (%)			
Measurement of E and I	±0.1		<±0.17
Power loss down leads			<±0.2
Uncertainty in Voltage Between Similar Legs of Specimen Thermocouples	±0.1	±0.5	
Total Determinate Error (%)	± 0.64	± 2.5	±2.81
Most Probable Error (%)	±0.40	±2.06	±2.05

$$\beta = (\Sigma\, e_i^2)^{1/2} , \qquad (39)$$

where, e_i = error of individual measurements.

Errors in the electrical resistivity apparatus should be the same as those listed in Table 8. For the knife edge measurements the most probable errors should be $\pm 0.16\%$ and 0.1°K.

Several months after having completed the experimental work, J. P. Moore[50] discovered an additional potential source of error related to positioning of thermocouple wires on the samples being measured for thermal conductivity. The possible source of induced error results from the fact that the thermocouple leads of Chromel-P and constantan are not welded exactly colinear on the sample in spite of all attempts to make them as colinear as possible. Since the wires will only rarely be exactly colinear an emf is introduced into the thermocouple readings because of the emf resulting from the thermoelectric power of the sample in a temperature gradient. The severity of the error is related to the displacement from colinearity of the thermocouple wires, the distance between the thermocouples, and the thermoelectric power of the sample with respect to the thermocouple. In the case of ThN where S is nearly zero this error is negligible. For the worst case, assuming both sets of thermocouples to be non-colinear within two wire diameters and a value for S of 10 μV/°K, the error could be as high as 1%. Since we do not know how non-colinear any particular thermocouple is, the exact error cannot be determined. The error can be assumed to be 1% or less.

The error bands on the figures are denoted by the symbol (I).

CHAPTER IV

RESULTS AND DISCUSSION

Data were obtained on the (Th-U)N system as shown in Table 9. The actual composition of the samples studied are summarized in Tables 4 and 5 of Chapter III. Details of the measurement results are presented in the following discussion.

I. HIGH-TEMPERATURE ELECTRICAL RESISTIVITY

Electrical resistivity values were taken on a pressed and sintered UN rod with a square cross section as described previously. Several values of ρ, λ, and S had previously been measured on this sample by Moore et al.[17] at temperatures below 400 °K. However, no high-temperature measurements had been made, so ρ and S measurements were made extending the measured values from 300 to 1700 °K.

Difficulty was encountered in instrumenting the sample because most metals will react with UN at high temperatures. Since tungsten and rhenium are compatible, tungsten versus W-26% Re thermocouple wire was selected. Several attempts were made to weld the thermocouple wires to the sample but the welds had almost no strength and the joint failed to hold. The thermocouples were finally attached by electrical discharge machining two holes 0.020 in. long by 0.010 in. wide in the UN sample. The thermocouples were forced into the holes and then strapped in place with more tungsten wire held against the Al_2O_3 thermocouple insulation.

TABLE 9

SUMMARY OF DATA TAKEN ON (Th-U)N SYSTEM

Measurement	Temperature Range, °K	Samples
ρ	4.2	All Samples
	80–400	ThN (Th–2% U)N (Th–5% U)N
	300–1300	ThN
	300–1600	UN
λ	80–400	ThN (Th–2% U)N (Th–5% U)N
S	80–300	ThN (Th–2% U)N (Th–5% U)N
	300–1700	UN

The initial ρ data obtained on the 6-Dial potentiometer are shown in Table A1, Appendix A. The data were obtained by reading the thermal emfs, current, and a voltage drop, manually reversing the current by throwing a switch, then reading the voltage drop again as rapidly as possible. After reversing the current, Peltier heating caused the temperature distribution and therefore the voltage drop to change relatively rapidly for a few minutes. Because the thermoelectric power in UN is so large (50-60 μV/°K), it often took a long time to attain equilibrium. The problem increased in severity with temperature such that at 900°K it required about 6 hr to obtain the resistivity at one temperature. In addition, small movements of the thermocouple wires caused additional inaccuracies in the measurements. Because of these difficulties it became apparent that a considerable reduction in time and an increase in accuracy could be realized by taking the data with the CODAS system.

A summary of the UN ρ values taken with CODAS is tabulated in Table A2, Appendix A. The values listed in this table are a summary of three runs, the first two of which were terminated early when one of the thermocouple legs came loose. Typically 10 sets of data were taken before changing the temperature. All of the CODAS values taken from the three different runs lie within ±0.25% of the value obtained from the 6-Dial potentiometer.

Smoothed values of ρ for UN are given in Table B1, Appendix B, and plotted in Figure 28. Only those ρ values from 295 to 1700°K are from this work but measurements that Moore et al.[17] made on this rod below 295°K are shown for comparison. The curves in Figure 28 are the same as that shown in Figure 8, except that the values just

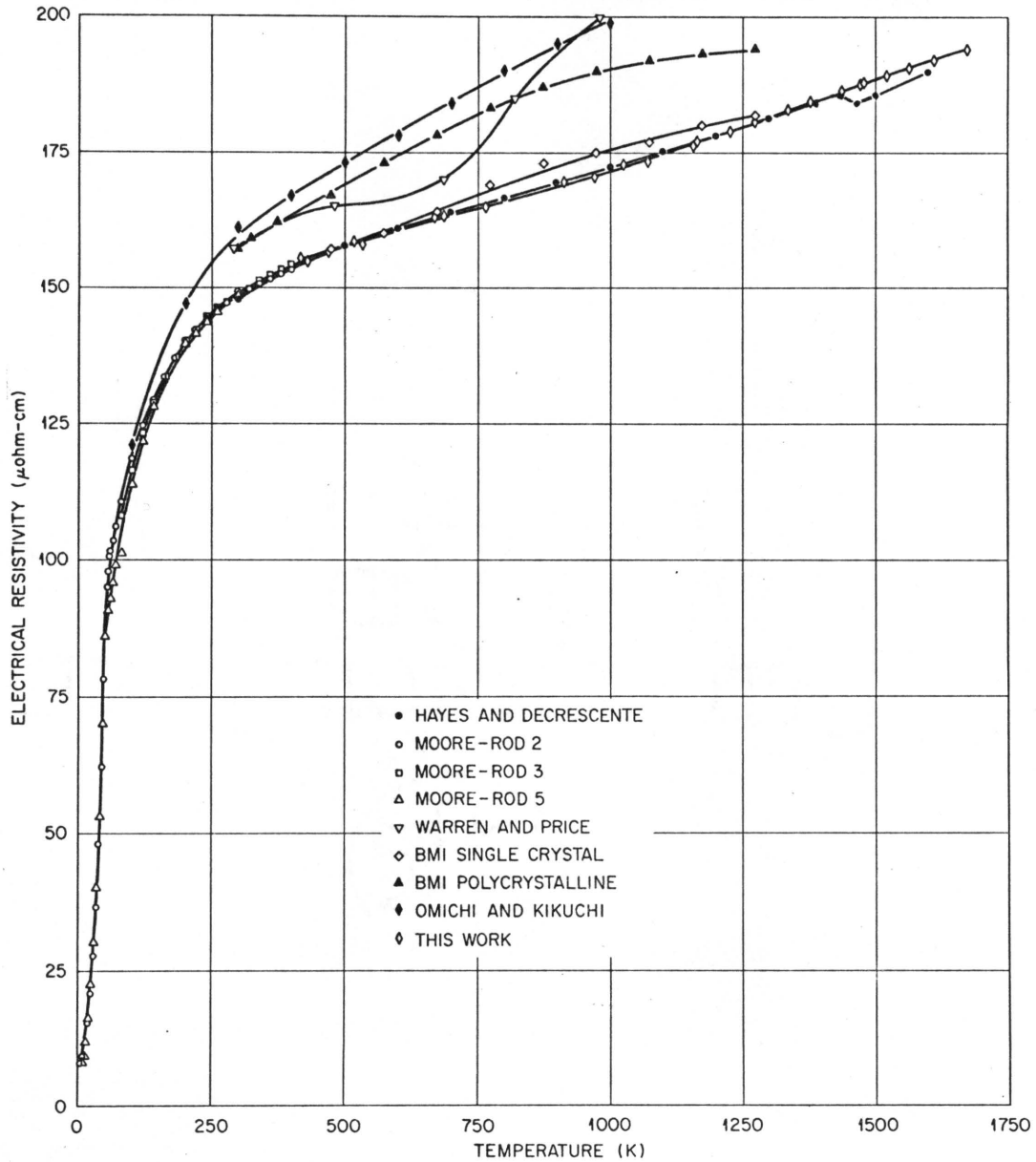

Figure 28. Electrical Resistivity of UN Compared with Previous Experimenters.

described have been added to compare the results with previous experimenters.

The results of the test shows excellent agreement with the data obtained by Hayes and DeCrescente.[32] The two sets of data agree within experimental error except for the dip in the data at 1450 °K reported by Hayes and DeCrescente. The data reported in this work show no such dip and since no phase change is known to occur at this temperature the dip in the curve is thought to result from experimental error in their measurements.

The data reported by Battelle Memorial Institute[35] on single crystals also shows reasonable agreement with this work. Battelle Memorial Institute also reported results[34] on polycrystalline pressed and sintered material which had ρ values reported to be larger by about 10%. The high values could result from oxygen contamination, erroneous measurements of the sample density, or an error in making the ρ measurements. The data reported by Warren and Price[36] are high and have a very unusual and unexpected shape which is probably incorrect. Omichi and Kikuchi[37] report data which becomes linear at about the same temperature (300 °K) observed by most experimenters, but their reported ρ values are very high and have a slope greater than any other reported data. The linear behavior of the curves at high temperatures results from electron-phonon interactions as would be predicted by theory in the absence of any phase changes.

High temperature ρ measurements were made on the ThN sample from 298 to 1300 °K in the electrical resistivity apparatus. The sample was instrumented by the author but the actual data taking and reporting of the data was done by T. G. Kollie.[51] The smoothed data as reported

by Kollie is presented in Table B2, Appendix B. The data are plotted in Figure 29. The slope for the data between 298 and 1273 °K was 0.0592 μohm-cm/°K. This compares with a value for UN of 0.0307 μohm-cm/°K. The high temperature ρ data agree with the low temperature ρ data at room temperature where data were taken with both systems to within 0.9%. The slight discrepancy of the data is largely attributed to the fact that Kollie's sample was exposed to a vacuum for four months prior to running the sample and an occasional oxidizing atmosphere for short periods of time.

II. LOW-TEMPERATURE ELECTRICAL RESISTIVITY

Electrical resistivity data were obtained on the zone melted ThN and (Th-U)N alloys from 4.2 to 400 °K. The first data point was a knife edge measurement in the glove box to establish ρ at room temperature. Data points at 4.2 °K were calculated from a ratio of resistance measurements made at room temperature and at liquid helium temperatures and from the knife edge ρ data. The samples were then instrumented for the longitudinal heat flow apparatus where ρ data were obtained along with λ and S data. After the samples were instrumented, the knife edge data were used to measure electrically the distance between the voltage taps and thermoelements. Electrical resistivity was then obtained from 77 to 400 °K. The results (Figure 30 and Tables A3-A6, Appendix A) show the ρ versus T curves to increase in slope from nearly zero at 0 °K to a constant value at about 100 °K. In the temperature range 100 to 400 °K the slopes appear to remain constant. Smoothed values are tabulated in Tables B2 and B3, Appendix B.

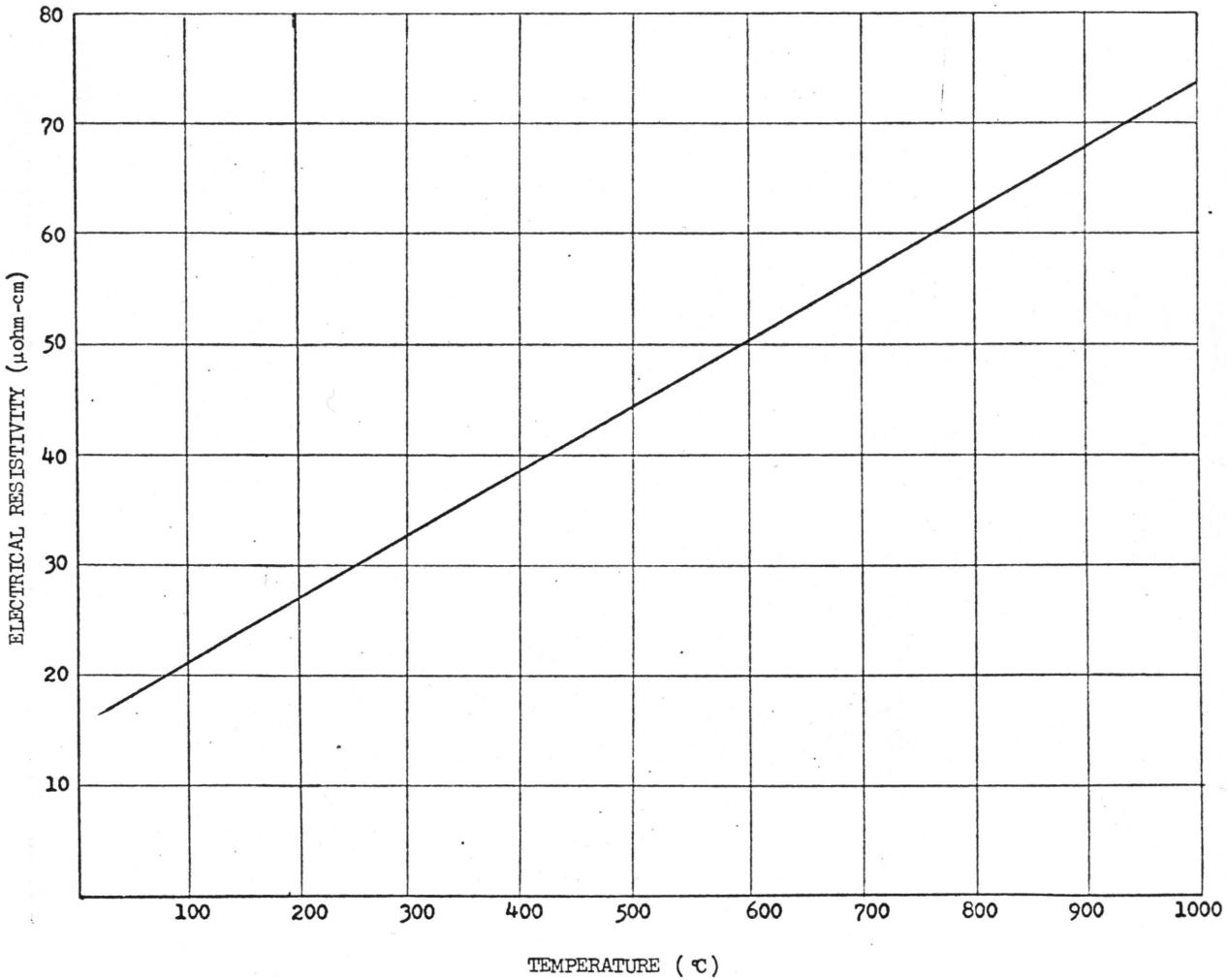

Figure 29. Electrical Resistivity of ThN.

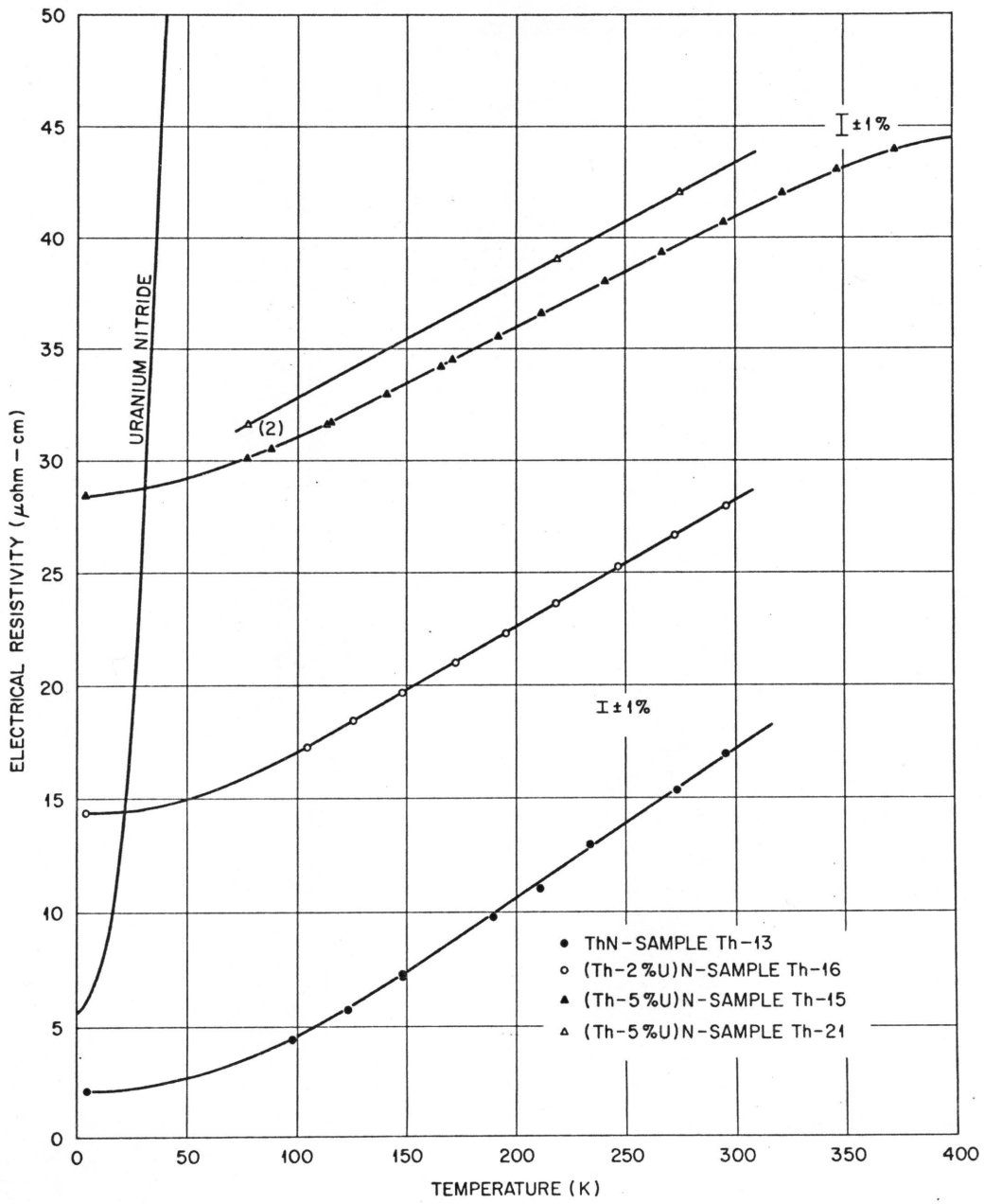

Figure 30. Electrical Resistivity of ThN, (Th-U)N, and UN.

The slopes of the (Th-U)N ρ data are very small at low temperatures compared with the UN curve. The large slope in the UN curve is due primarily to magnetic thermal disordering of antiferromagnetic UN on heating. On the other hand, ThN is diamagnetic and therefore has no magnetic scattering. It is apparent, however, that the small additions of UN to ThN in this study was sufficient to cause a large change in the residual resistivity. However, larger UN additions to ThN cannot continue to show the large resistivity changes observed at the thorium rich end of the diagram. Otherwise, a linear extrapolation of the UN additions would predict a residual resistivity of 520 μohm-cm for UN, while the actual observed residual resistivity of UN is only 6 μohm-cm. This suggests that the residual resistivity of (Th-U)N will show a maximum at some point on the phase diagram. A plot of ρ_o as a function of UN content in ThN is shown in Figure 31.

The ThN sample used in this test showed a residual resistivity of 2.109 μohm-cm at 4.2 °K. This compares with a residual resistivity of 3 μohm-cm reported by Auskern and Aronson.[37] This gives a resistivity ratio ($R_{300}/R_{4.2}$) of 8.08 for the ThN sample used in these experiments compared to a resistivity ratio of approximately 7 for Auskern and Aronson.

Fulkerson et al.[52] have shown that the residual resistivity, ρ_o, of UN can be changed from about 6 μohm-cm to 1 μohm-cm by varying the heat treatment of the samples tested. In addition, UN shows a very rapid increase in ρ as the antiferromagnetic order is lost up to the Neél temperature (50-60 °K). Fulkerson et al.[52] showed the Neél temperature to vary as a function of heat treatment. The magnitude of the ρ minimum at the Neél temperature also appeared to vary as a function

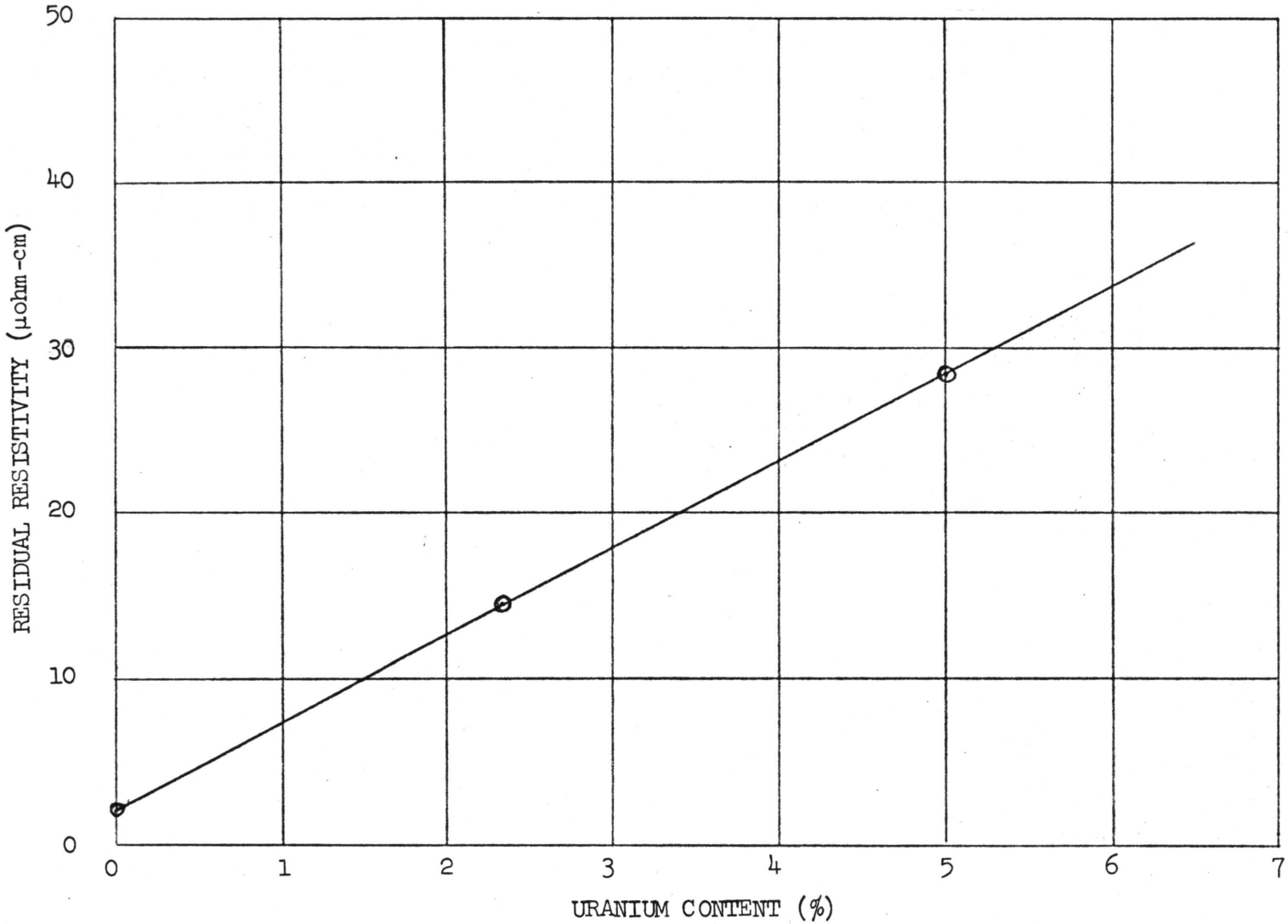

Figure 31. Residual Resistivity of (Th-U)N as a Function of Uranium Content.

of heat treatment in their measurements. Above the Neél temperature, ρ continues to increase but with $\frac{d\rho}{dT}$ getting smaller with temperature. At a temperature of about 300 °K the slope was approximately constant. From 300 to 1700 °K a constant slope of 0.0307 μohm-cm/ °K was measured. Although no data on ThN were taken between 4.2 and 80 °K, no anomolous behavior is expected to cause results other than a smooth line between the points in this region. The equations of the linear portions of the curves are as follows:

ThN:	$\rho = -2.122 + 0.063571\ T$	(100–300 °K)
	$\rho = -0.347 + 0.058144\ T$	(300–1700 °K)
(Th–2% U)N:	$\rho = 11.385 + 0.055646\ T$	(100–300 °K)
(Th–5% U)N:	$\rho = 25.946 + 0.049625\ T$	(100–300 °K)
(Th–5% U)N:	$\rho = 27.494 + 0.052377\ T$	(100–300 °K)
UN:	$\rho = 142.336 + 0.030727\ T$	(300–1700 °K)

The addition of the uranium to ThN increases the intercept of the ρ versus T relationship but decreases the slope. This is consistent with the high intercept and low slope of paramagnetic UN. Because the slopes appear to be constant, equations were used to extrapolate the values of ρ to 2000 °K as shown in Figure 32 and Table B4, Appendix B. At 300 °K, the two ThN ρ values differ by about 0.9% with the ρ value taken from the low temperature data considered to be the better value. This is because of the long time sample exposure to vacuum, discussed previously.

From the equations presented above, values for the phonon contribution ρ_P were calculated from the Bloch-Gruneisen relation Equation (20) and

$$\rho_\theta = \frac{B\theta}{1.054} \quad . \tag{40}$$

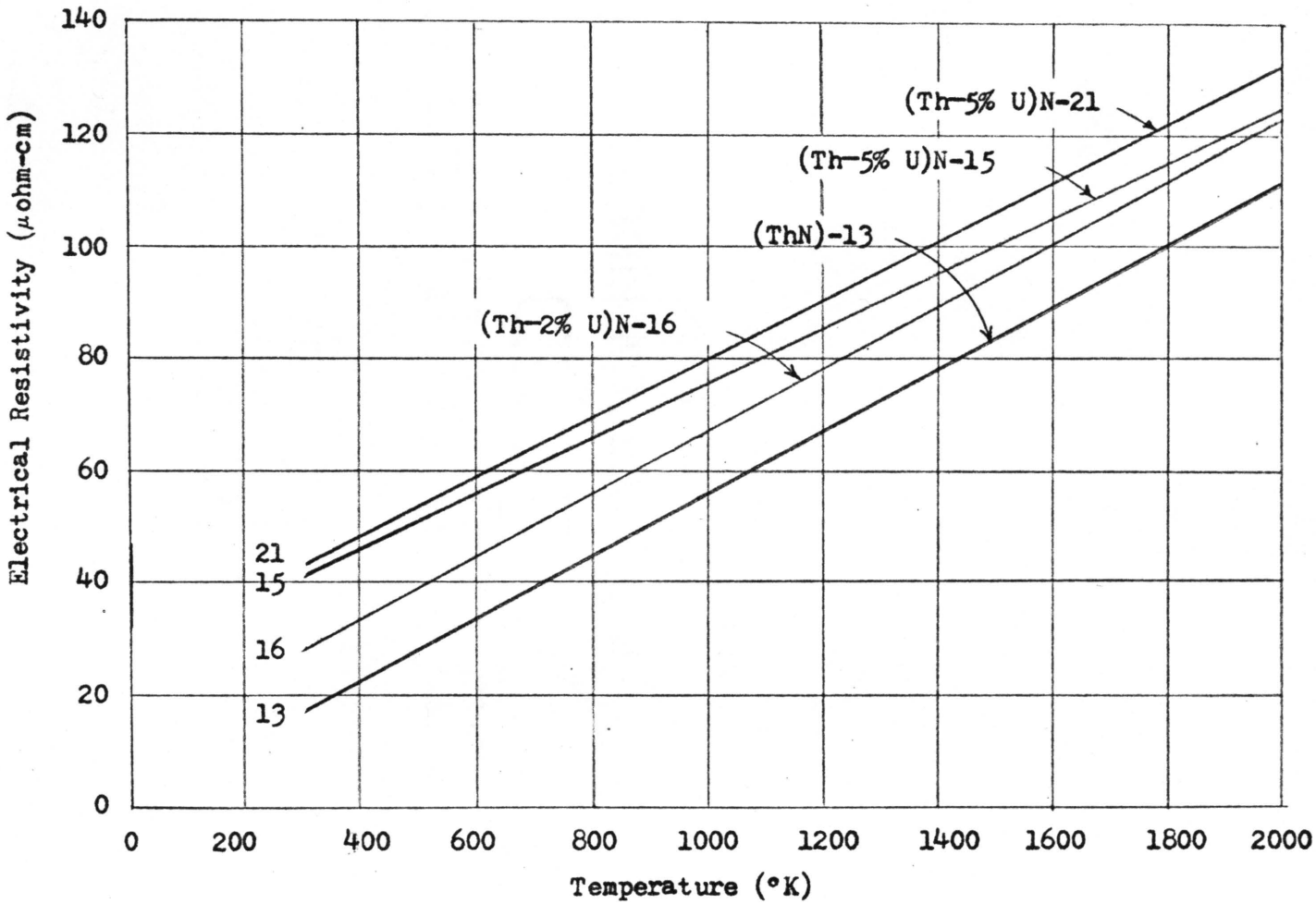

Figure 32. Extrapolated Values of Electrical Resistivity to High Temperature.

A value of 286 °K was used for θ based on the low temperature specific heat data of de Novion.[53] The results of the Bloch-Gruneisen calculations tabulated in Table B5, Appendix B, are compared with the experimental results of $\rho - \rho_o$. All of the calculations from the Bloch-Gruneisen equation are high compared to the experimentally determined values of $\rho - \rho_o$.

Another approach to examining the data is to use the Bloch-Gruneisen calculation of ρ_P and the experimental ρ values to calculate ρ_I and observe its deviation from Matthiessen's rule. Thus

$$\rho_I = \rho - \rho_P \ , \tag{41}$$

where ρ_P is calculated from the Bloch-Gruneisen equation. The results of this calculation are shown in Figure 33 and tabulated in Table B6, Appendix B.

A better calculation for θ was achieved using the high temperature ρ data taken by Kollie,[51] which was used to calculate a high temperature value for θ of 532 °K. It should be noted that this is an unusually high value for θ. This calculation was made by least squares fitting the data to a series solution to the Bloch-Gruneisen equation. Using the value for θ derived from these experimental results instead of the low temperature specific heat value for θ derived by de Novion, the Bloch-Gruneisen calculation was repeated and used to calculate with ρ_I as shown in Figure 33 and Table B6, Appendix B. The positive deviation from Matthiessen's rule is the expected behavior and these results appear qualitatively correct, whereas, the negative deviation from Matthiessen's rule calculated from the low temperature specific heat value for θ is unexpected.

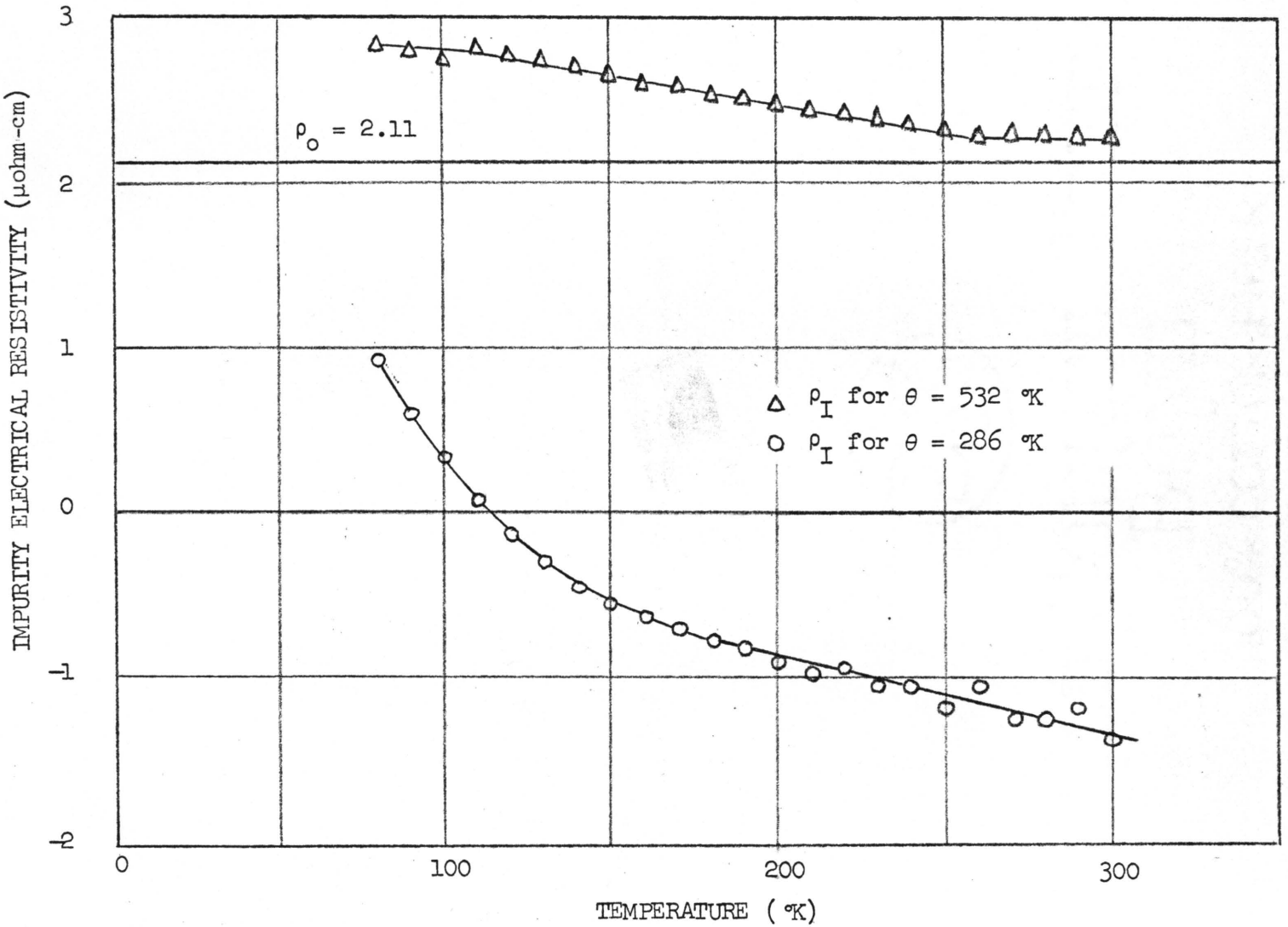

Figure 33. Residual Resistivity of ThN as Function of Temperature as Calculated from Bloch-Gruneisen Equation. These calculations show the deviation from Matthiessen's rule.

Another explanation for the behavior of ρ which would make it difficult to calculate a value for θ is that ρ_o for the alloys is greater than $\rho - \rho_o$. This means that the results were obtained from a small difference of two large numbers. Thus, the electrical resistivity due to the impurities may not exhibit a Matthiessen behavior (i.e., is not constant with temperature). The possibility of non-Mattheissen behavior is examined in a little more detail under the discussion of thermal conductivity.

Thorium nitride shows values for ρ nearly the same as for thorium metal as determined by H. G. Schettler[54] (Figure 34). The curves shown in Figure 34 labeled Th_{30} and Th500 correspond to thorium samples which exhibited resistivity ratios of 30 and 500 respectively. The ρ curve for thorium metal becomes linear at a much lower temperature (20–30 °K) but has a slope of 0.0477 μohm-cm/°K, which is 25% less than the slope for ThN. At 300 °K ThN has a value 17.04 μohm-cm while thorium metal showed values ranging from 15.3 to 17.05 μohm-cm. The range of values is consistent with the range of values for the residual resistivity of the various thorium samples measured. The value of 17.05 μohm-cm corresponds to measurements made on a material with a residual resistivity of 1.7 μohm-cm. The similar behavior of thorium and ThN is consistent with the observation that there is only a 4% change in the atomic arrangement of the thorium atoms in going from thorium to ThN. There is apparently very little change in the electronic and magnetic properties as well. From these observations, one would predict a very similar behavior of λ fpr ThN and thorium. An additional bonus effect from this observation is that the presence of any residual free metal in a ThN sample would not cause a significant error in either ρ or λ measurements.

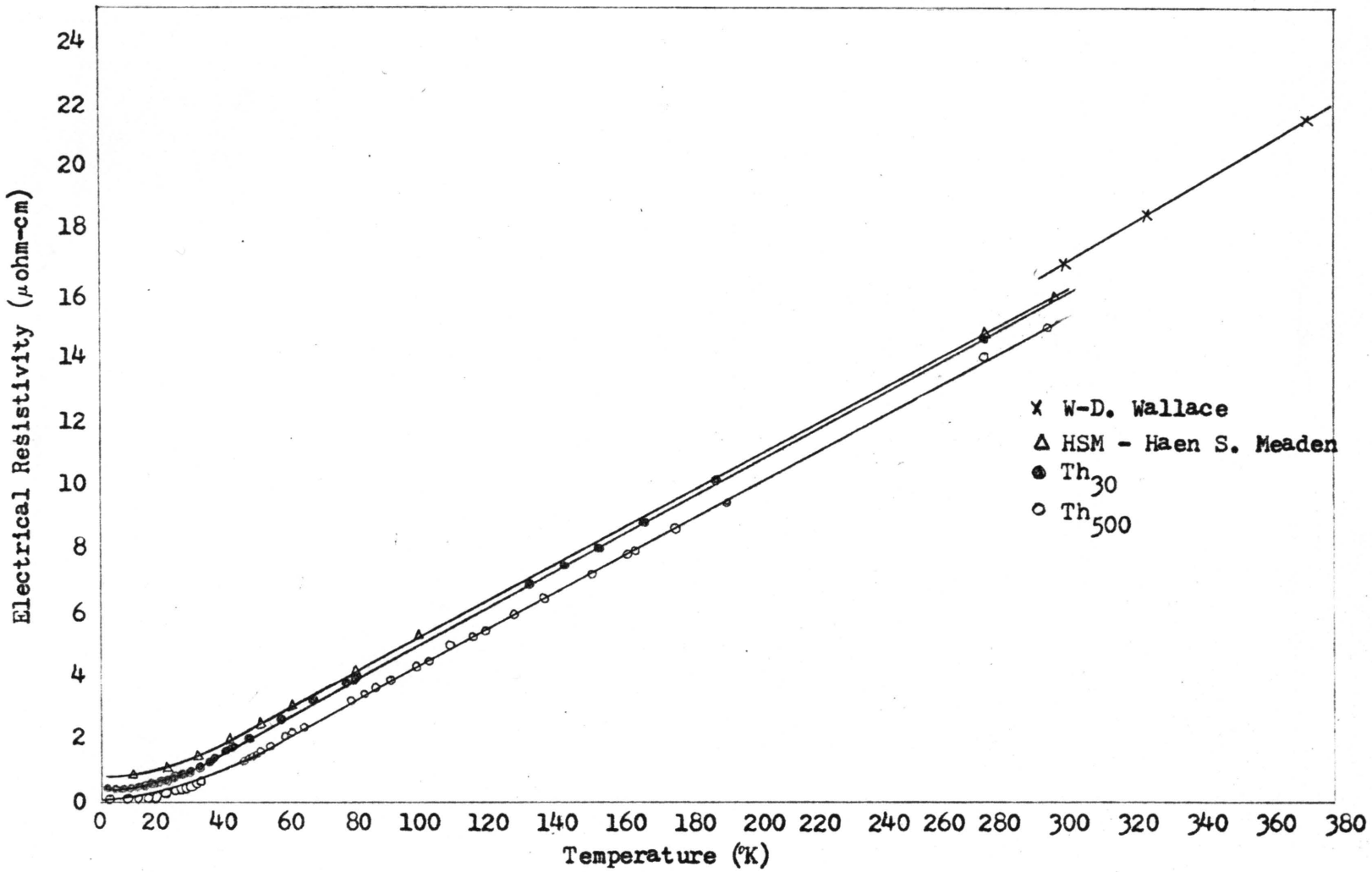

Figure 34. Electrical Resistivity of Thorium Metal.

Source: H. C. Schettler, "Thermal Conductivity of Thorium," M. S. Thesis, Iowa State University, Ames, Iowa, February 1969.

A straightforward comparison of ThN with the UN ρ data is not possible because of the very large magnetic contribution to ρ which is dominant at all temperatures. Bloch-Gruneisen calculations of UN to try to determine the magnetic contribution to ρ were presented by Moore et al.[17] in which they calculated a value for ρ_θ of 8.2 μohm-cm. This compares with a value calculated for ThN of 17.3 μohm-cm.

III. THERMAL CONDUCTIVITY

Total Thermal Conductivity

Thermal conductivity measurements were made on the zone melted (Th-U)N samples over the temperature range 80 to 400 °K in the guarded longitudinal heat flow apparatus. These results are shown as a function of temperature in Figures 35–37 and the data are tabulated in Tables A7–A10, Appendix A.

The data on ThN show a rapid nearly linear decrease in λ from 80 to 140 °K where the curve exhibits a change of slope. In the temperature range of 80 to 140 °K, the slope of the thermal conductivity curve is −0.00261 W/cm-°K^2. Above about 140 °K the slope becomes −0.00031 W/cm-°K^2.

The (Th–2% U)N sample showed a minimum in λ at about 110 °K while the two (Th–5% U)N samples showed minimums about 150 °K. Above 175 °K the slope of the λ versus T curves for (Th–2% U)N appeared to be linear with a positive slope of 0.00024 W/cm-°K^2. The slope of sample Th-15 containing (Th–5% U)N was linear and positive above 250 °K with a slope of 0.00029 W/cm-°K^2. Smoothed values for λ are shown in Table B7, Appendix B. The merging of the λ values on the (Th–5% U)N alloys

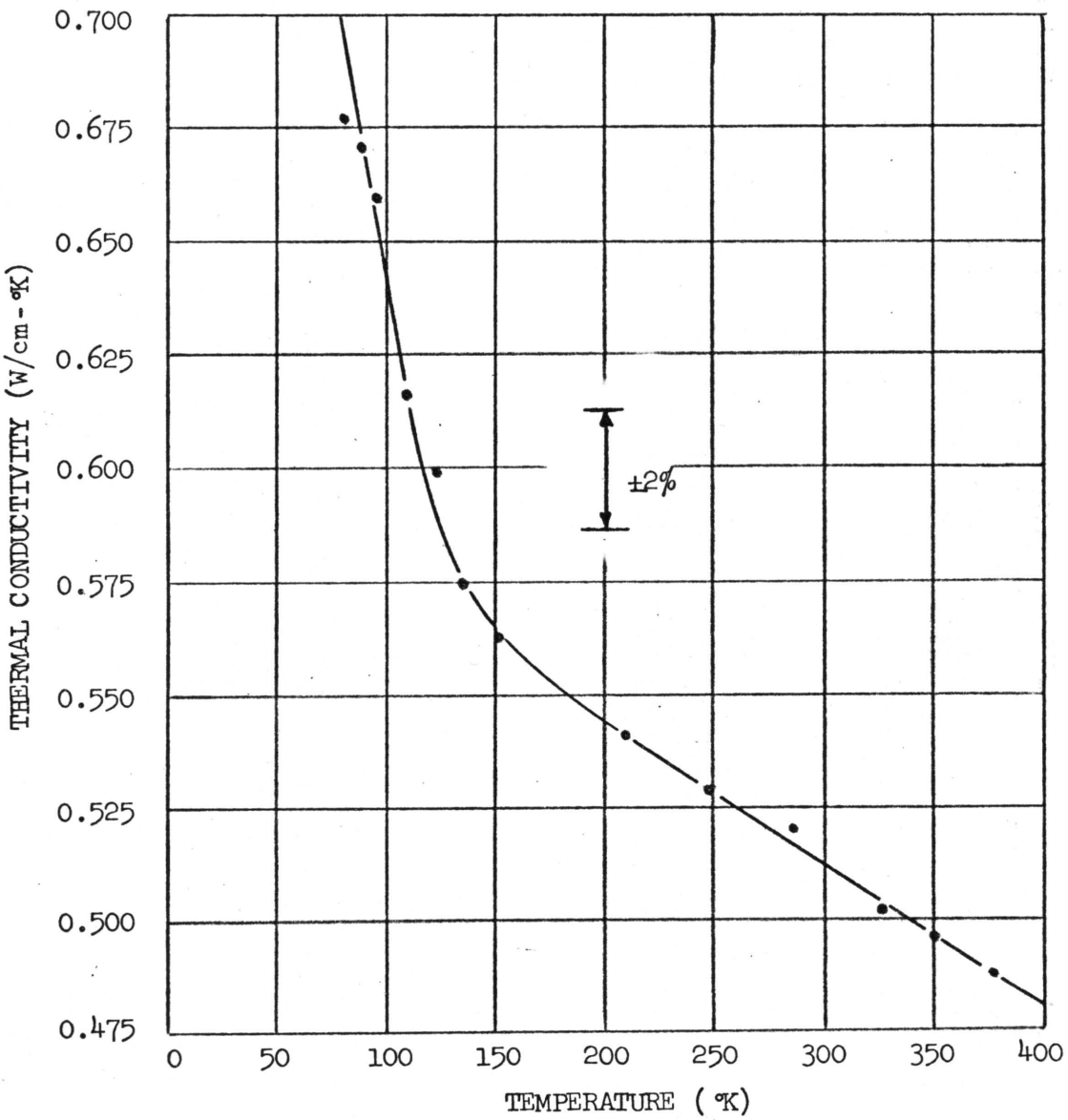

Figure 35. Thermal Conductivity of ThN.

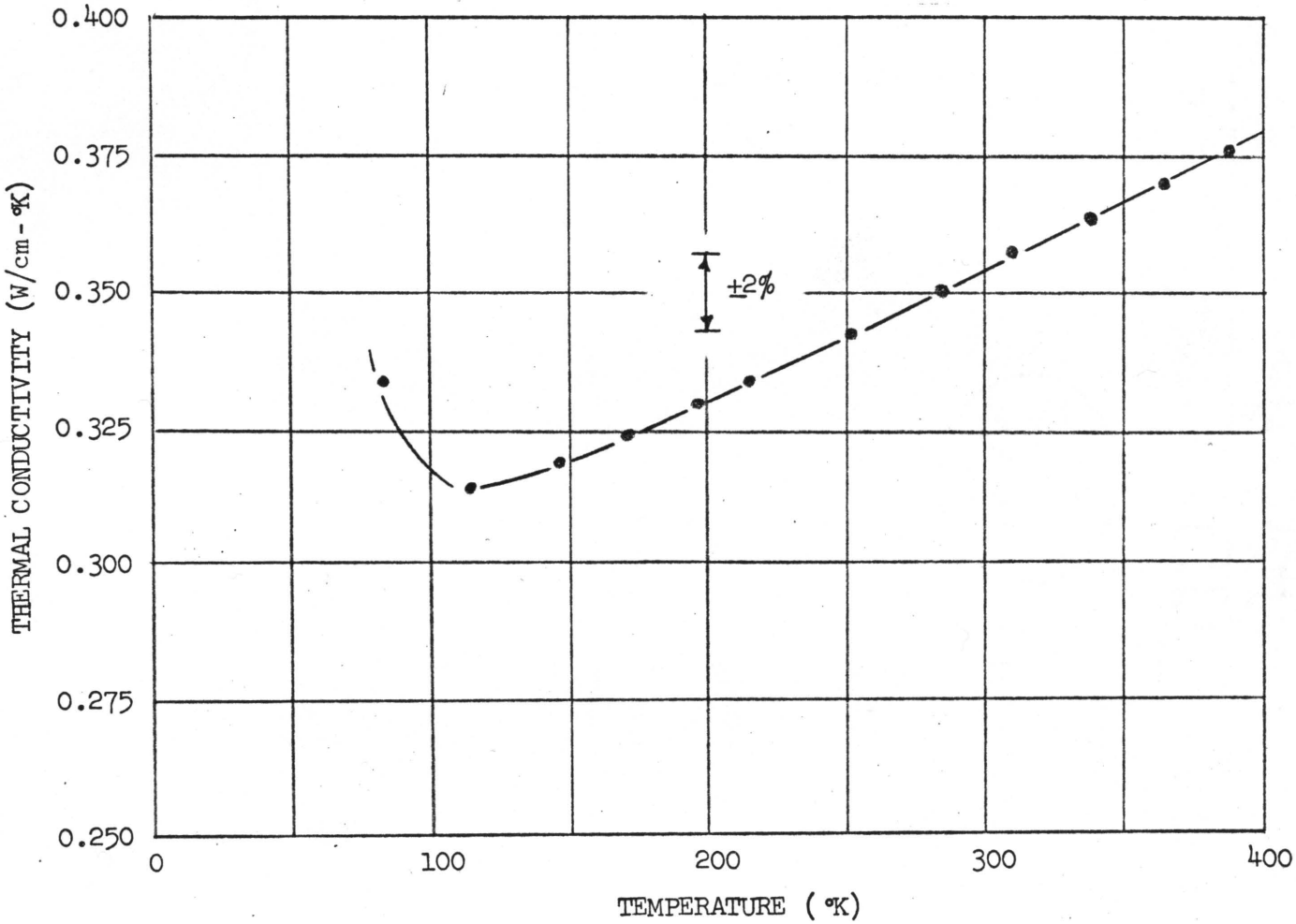

Figure 36. Thermal Conductivity of (Th-2% U)N.

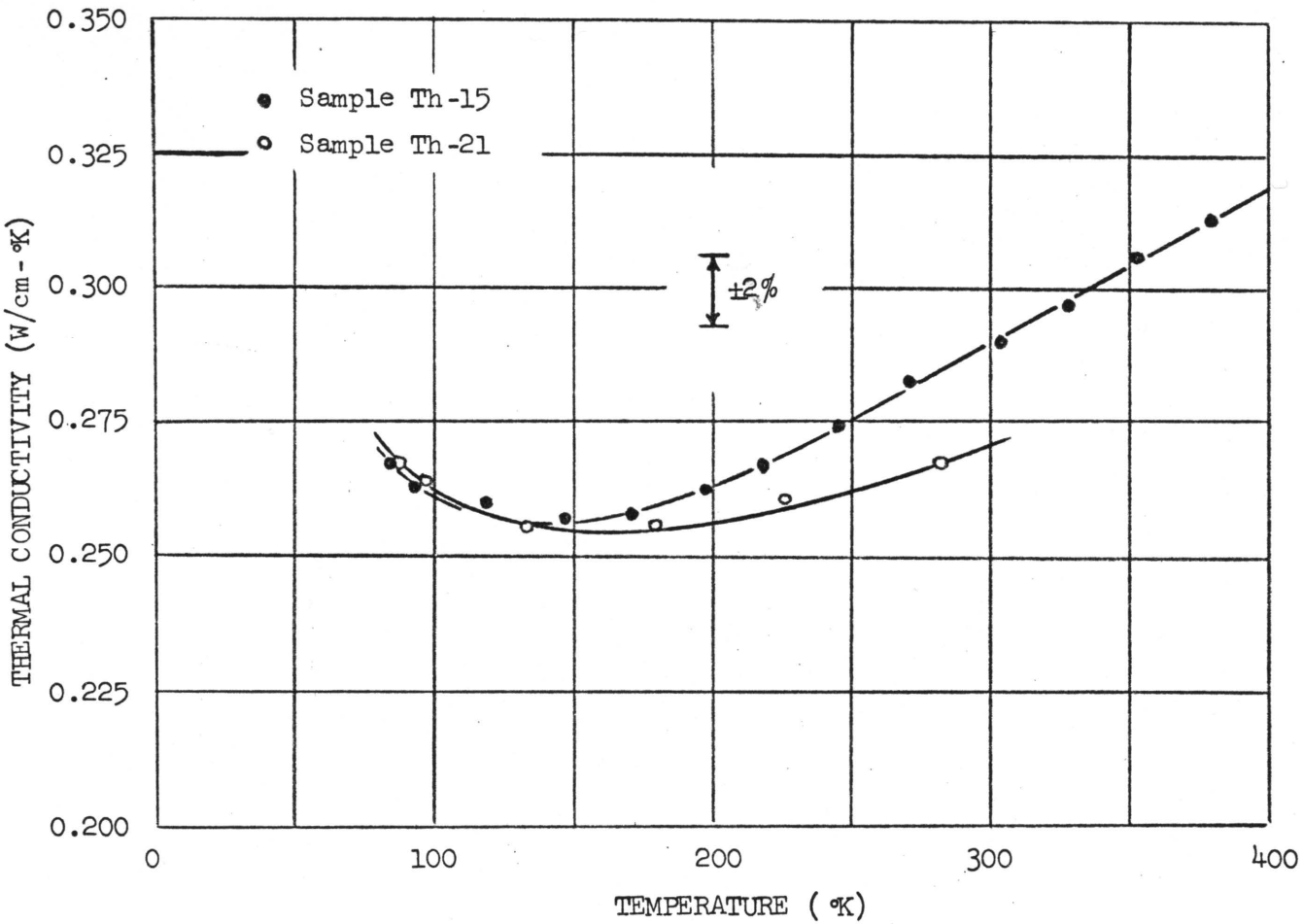

Figure 37. Thermal Conductivity of (Th-5% U)N.

at low temperatures was unexpected as the values of ρ are different. The difference between the observed and expected behavior, however, is within experimental error.

An interesting aspect of these data is that at 80 °K, the lowest temperature which could be measured with this equipment, all of the λ versus T relationships had a negative slope with respect to temperature. This means that somewhere between zero and 80 °K, λ must reach a maximum and then go to zero at absolute zero.

The relatively high thermal conductivity of ThN and (Th-U)N alloys is apparent when compared with UO_2. At 300 °K for instance, λ for ThN is more than six times that of UO_2. With increasing temperature, the factored difference between ThN and UO_2 becomes even larger as the value of λ for UO_2 drops to about 0.02 W/cm-°K at 1000 °C (Figure 1). The addition of UN to ThN decreases λ, as expected but the values are still significantly larger than, for instance, $(U\text{-}Pu)O_2$. The greatest potential use of nitrides as a fuel probably lies in the use of (Th-Pu)N which should have conductivities very similar to (Th-U)N.

These λ measurements indicate that the assumptions for the reactor analysis calculations presented in Chapter I were well justified. Ceramic alloys of ThN should indeed have very high thermal conductivities and exhibit some significant advantages from the standpoint of performance in a reactor. As fuel in any current reactor concept, the operating temperature of the fuel could be kept so low that very good fuel performance would be expected. Low migration rates of fission products, particularly fission gases, would be expected to keep the swelling rate of the fuel very minimal. This is of great importance in a fast

breeder reactor fuel since it is fuel swelling which generally regulates the reactor lifetime of the fuel and therefore the efficiency of the reactor.

Lattice Thermal Conductivity

To examine the fundamental behavior of λ in (Th-U)N alloys, the "alloy-separation" and "curve-fitting" techniques were used to separate and study the lattice and electronic contributions to λ.

The first technique used was the "alloy-separation" of Williams and Fulkerson.[5] This technique assumes that alloying of UN in ThN produces a large effect on λ_e but has no effect on λ_L. The equations used were:

$$\lambda_1 = \lambda_{e1} + \lambda_L = \frac{L_m T}{\rho_m}\left(\frac{1}{1 + \alpha_1 \gamma}\right) + \lambda_L \ , \tag{42}$$

$$\lambda_2 = \lambda_{e2} + \lambda_L = \frac{L_m T}{\rho_m}\left(\frac{1}{1 + \alpha_2 \gamma}\right) + \lambda_L \ , \tag{43}$$

$$L_m = \frac{(\lambda_1 - \lambda_2)(\alpha_1 + \alpha_2) L_o \rho_m}{2(\alpha_2 - \alpha_1) L_o T - (\lambda_1 - \lambda_2)\alpha_1 \alpha_2 \rho_m} \times$$

$$\left\{1 + \left[1 + \frac{4L_o(\alpha_2 - \alpha_1)T}{(\alpha_2 + \alpha_1)^2(\lambda_1 - \lambda_2)\rho_m} - \frac{4\alpha_1\alpha_2}{(\alpha_1 + \alpha_2)^2}\right]^{1/2}\right\} \ , \tag{44}$$

where, λ_1 = total thermal conductivity of pure material,

λ_{e1} = electronic thermal conductivity of pure material,

λ_L = lattice thermal conductivity,

L_m = Lorenz function of pure material,

T = temperature,

ρ_m = electrical resistivity of pure material ($\rho_T - \rho_I$),

λ_e = total thermal conductivity of alloy,

λ_{e2} = electronic thermal conductivity of alloy,

$\alpha_i = \frac{\rho}{\rho_m}$,

L_o = Sommerfeld value of Lorenz function,

$\gamma = \frac{L_m}{L_o}$.

These equations result from the assumptions that: (a) the electronic thermal resistivity is comprised of the electronic thermal resistivity of the pure material, W_m, and the impurity electronic thermal resistivity, W_I, which are additive; (b) W_I is calculated from the equation

$$W_I = \frac{\rho_I}{L_o T} , \tag{45}$$

where, ρ_I = impurity electrical resistivity; (c) the lattice and electronic thermal conductivities are additive; (d) the electronic thermal resistivity of the pure metal, W_m, is given by the equation

$$W_m = \frac{\rho_m}{L_m T} ; \tag{46}$$

(e) the Lorenz function and electrical resistivity of the pure metal are assumed to be unchanged by the solute additions; and (f) the lattice thermal conductivity is not affected by impurity additions.

The measured thermal conductivity and electrical resistivity data were fitted to curves and smoothed values of λ and ρ selected at fixed temperature increments. These values were then used in Equations (42)–(44) yielding the results for λ_L, λ_e, and L_m as tabulated in Tables B8–

B10, Appendix B. Values for the total thermal conductivities, λ_T, and the calculated values for λ_L are shown in Figure 38 for a comparison of results. The calculated values for λ_L show very good agreement between each data set.

Superimposing the error band over the data showed the calculated values of λ_L for the alloys to be in much closer agreement than would be predicted by assuming errors of 0.50 °K, 0.5% in ρ, and 2.1% in λ. The errors in L and λ_L, calculated for each data point are shown in Tables B11-B13, Appendix B. The error calculated for L will also show up in λ_e since $\lambda_e = \frac{LT}{\rho}$.

A temperature dependence of λ_L is expected because the phonon-phonon Umklapp scattering phenomenon increases with temperature, that is,

$$\lambda_L \propto \frac{\eta_1}{T}, \tag{47}$$

where, η_1 = constant.

To determine the value of η_1, the calculated values of λ_L were used to calculate a thermal resistivity (Table B14, Appendix B), which was plotted versus temperature (Figure 39). The resulting slopes yielded values of η_1 of 39.94, 42.24, and 47.71 for an average value of 43.30 W/cm. This compares with a value of 47.40 to 52.50 W/cm for UN as calculated by Moore et al.[17] The intercept of the curves at approximately 3 cm-°K/W is related to the phonon scattering by electrons. The low positive intercept observed in ThN indicates a significant amount of electron-phonon scattering. Uranium dioxide has

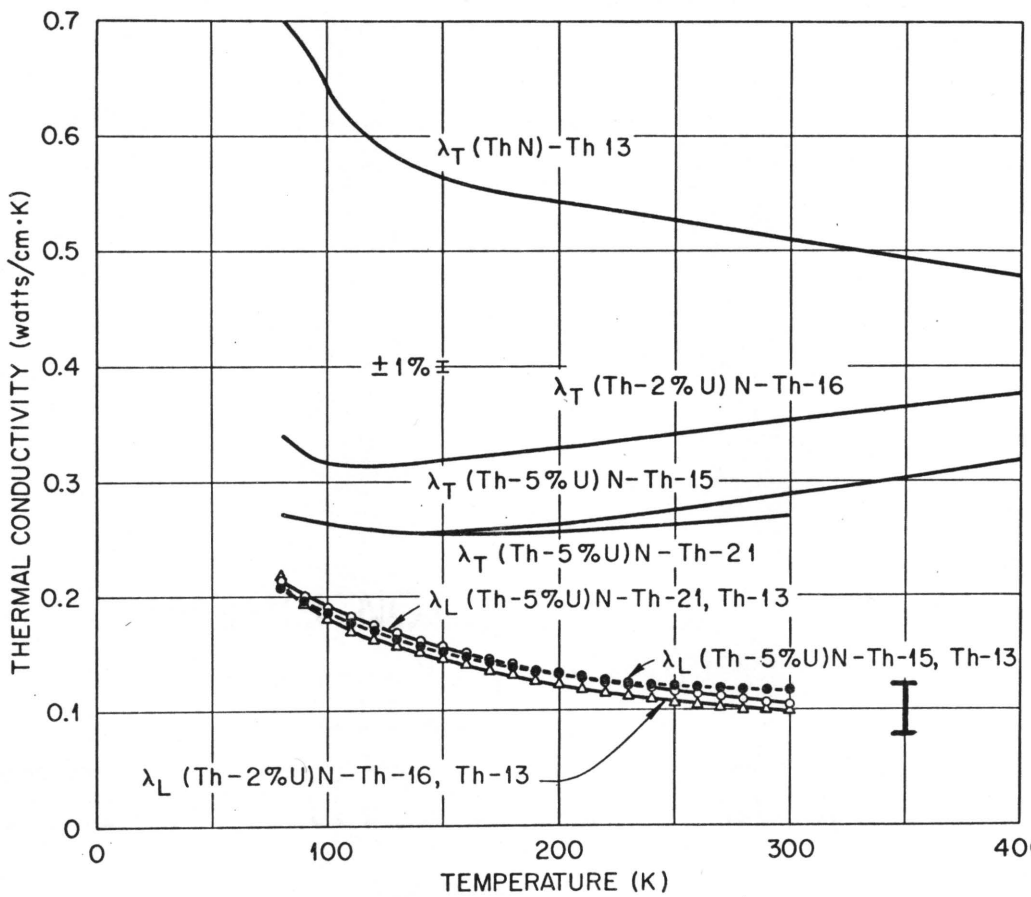

Figure 38. Total Thermal Conductivity and Lattice Contribution to Thermal Conductivity.

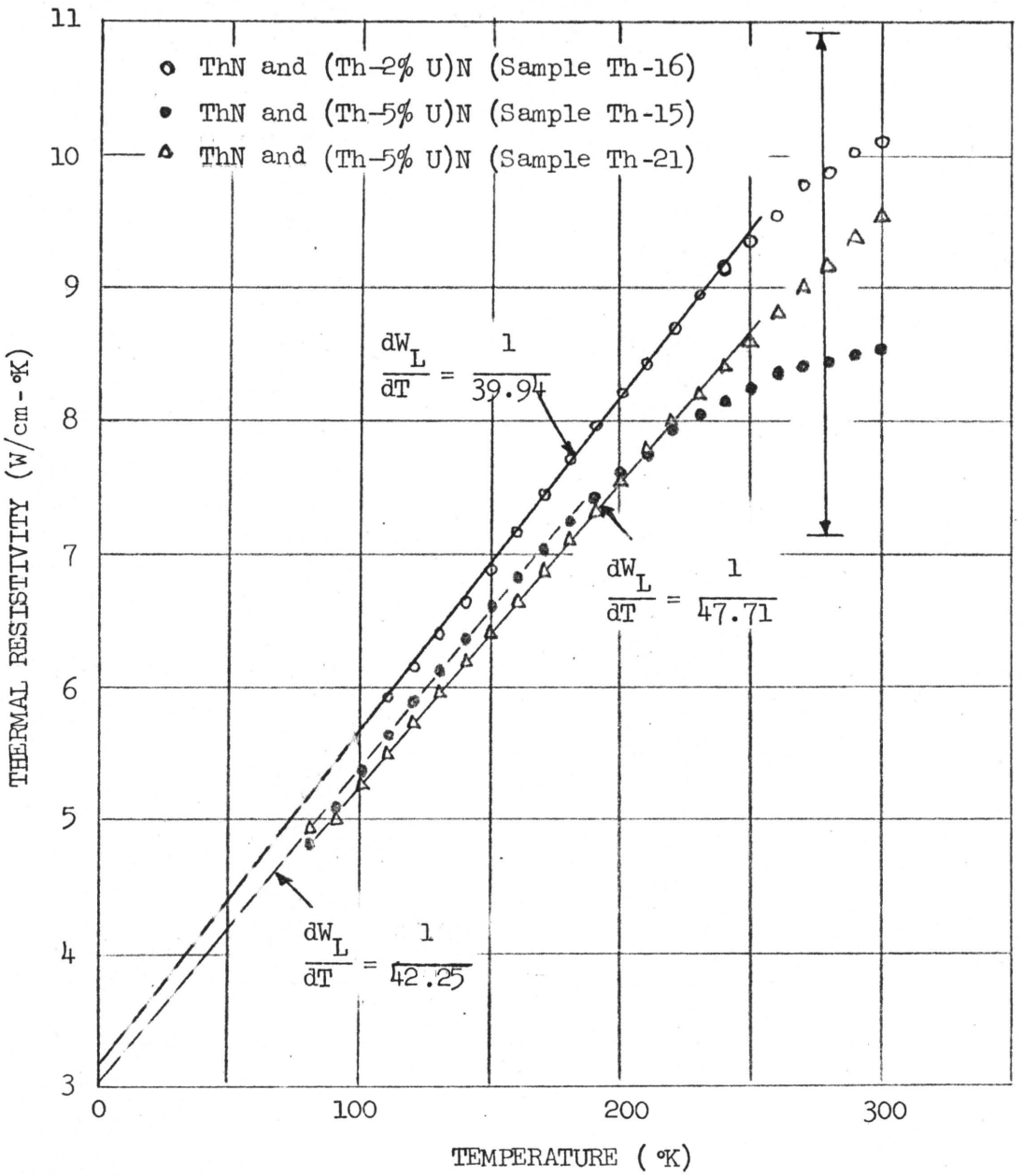

Figure 39. Lattice Component of Thermal Resistivity as Function of Temperature.

an intercept of 4.4 W/cm-°K due to phonon-magnon resistivity, while BeO has an intercept of -2.68 W/cm-°K due to phonon-phonon scattering.

The $\frac{d\rho}{dT}$ value for ThN is about twice that of UN and most of the transition metals which are about 0.03 μohm-cm/°K. With this relatively large $\frac{d\rho}{dT}$, a significant electron-phonon contribution is expected in λ_L. This contribution is given by the equation[4]

$$W_{ep} = \left(\frac{e}{k}\right)^2 N_e^{\frac{2}{3}} \frac{\rho}{T} \quad , \tag{48}$$

where, W_{ep} = thermal resistivity due to electron-phonon collisions,

N_e = effective number of free electrons per atom,

e = electronic charge.

If N_e is assumed to be 1.0 then W_{ep} would be 8 W/cm-°K. Since W_{ep} is experimentally determined to be three then a value of $N_e = 0.6$ is expected.

A comparison of the experimental η_i values can be made to the value of η_1 calculated from the Liebfried-Schlomann[55] equation as modified by Steigmeier and Kudman[56] for deviations of the Gruneisen constant γ from 2.0. The equation is

$$\eta_1 = \frac{\frac{24}{10}(4)^{1/3}\left(1 + \frac{1}{2\gamma}\right)^2 \left(\frac{k}{h}\right)^3 m\delta\theta^3}{\gamma^2} \tag{49}$$

where, k = Boltzmann's Constant,

h = Plank's Constant,

m = average mass per atom = 2.042×10^{-22} gram,

δ^3 = average volume per atom = 1.717×10^{-23} m/cm^3,

θ = Debye temperature = 286 °K,

γ = Gruneisen constant = 1.60.

From this equation a value for η_1 of 168 W/cm was calculated, which is 3.88 times the measured value. Most experimental values are less than calculated from this equation by a factor of 3 to 4 (ref. 16). Thus the values appear to be qualitatively accurate.

A calculation was made using Abeles[57] formula to determine the effect on the lattice thermal conductivity of adding UN to ThN. Unfortunately, some of the data needed in the Abeles equation were not available for ThN and estimates for some of the values were made. The results of the calculation predict at 300 °K a concentration dependency of the lattice thermal conductivity which would reduce λ_L by approximately 5% or 0.01 W/cm-°K for each atomic percent of UN added to ThN. At lower temperatures the predicted change would be even larger. The experimental results actually showed a negligible effect of alloying on the lattice thermal conductivity as illustrated in Figure 38.

The second technique used to evaluate the ThN results was the curve fitting separation also developed by Williams and Fulkerson.[4] The data were fitted to the following equations.

$$\lambda = \frac{TL_\infty}{\rho}\left[1 - \exp\left(-\frac{T}{\Delta} + 0.2138\right)\right], \tag{50}$$

$$\lambda = \frac{TL_\infty}{\rho}\left[1 - \exp\left(-\frac{T}{\Delta} + 0.2138\right)\right] + \frac{\eta_1}{T}, \tag{51}$$

$$\lambda = \frac{TL_\infty}{\rho}\left[1 - \exp\left(-\frac{T}{\Delta} + 0.2138\right)\right] + \frac{\eta_1}{T} + \frac{\eta_2}{T^2}. \tag{52}$$

These equations were developed by examining the lattice and electronic thermal conductivity components and assuming that they use additive. Assumptions for the lattice conductivity were

$$\lambda_L = 0 \ , \tag{53}$$

$$\lambda_L = \frac{\eta_1}{T} \ , \tag{54}$$

$$\lambda_L = \frac{\eta_1}{T} + \frac{\eta_1}{T^2} \ . \tag{55}$$

Equation (53) assumes no lattice thermal conductivity which approximates the case where there is a very high electronic thermal conductivity or a very low lattice conductivity. Equation (54) is based on the observation that at some fraction of the Debye temperature the lattice conductivity should peak and above that temperature phonon-phonon scattering should vary roughly as $1/T$. Equation (55) is an attempt to approximate the case where there is a constant in the thermal resistivity term expressed in the form

$$W_L = A + BT \ . \tag{56}$$

where, A and B are constants. A represents the thermal resistivity due to electron-phonon interactions (see Figure 39).

For the electronic thermal conductivity L was treated by letting the Lorenz function vary as

$$L = L\infty \left[1 - \exp\left(-\frac{T}{\Delta} + 0.2138\right)\right] \ . \tag{57}$$

This expression was derived from Wilson's theoretical expression[5] for L and assumes a spherical Fermi surface, N processes, longitudinal mode scattering, and a Debye spectrum for phonons. There have been more advanced theories than that of Wilson's but they are mathematically complex, do not easily lend themselves to numerical calculations, and are not completely successful. This same equation is a good approximation to the more complicated numerical calculations of Ziman.

The curve fitting method utilizes a least squares fit of the ThN data to Equations (50)–(52) using assumed values of Δ obtaining $L\infty$ and η_1 and η_2 from the analysis. The numerical calculations were carried out using the IBM 360-75 computer at Oak Ridge National Laboratory. The range of data used was from 80 to 300 °K. This is justified from the standpoint that the $\frac{\theta}{3}$ is approximately 90 °K. This L equation is not justified below $\frac{\theta}{3}$. If the value of θ = 532 °K calculated from the ρ data is used, then the curve fitting data would have to be rejected below 177 °K. Values for Δ were assumed from 10 to 1000 °K in 10 °K increments. From the printouts of these calculations, a range of 20 °K was found which produced the minimum standard deviation in the overall fit of the data. The calculations were then repeated using increments of 1 °K over this 20 °K range. Results of the calculations showed no reasonable fit of the data except for Equations (51) and (52). Equation (52) produced an unreasonably low value for η_1 of 10.33 W/cm and a high value for $L\infty = 2.73 \times 10^{-8}$ $V^2/°K^2$ or 12% higher than the Sommerfeld value of 2.443×10^{-8} $V^2/°K^2$. Equation (51) produced a very good fit to the ThN data. The results of the calculation gave values of

$$L = 2.611 \times 10^{-8}\ V^2/°K^2,$$

$$\Delta = 164\ °K\ ,$$

$$\eta_1 = 44.78\ W/cm\ .$$

The calculated standard deviations were 0.48% of $L\infty$ and 0.48% of η_1. The results of this fit are illustrated graphically in Figure 40.

The quality of the fit of this equation is generally judged by how much the values deviate if the data are truncated at either end. The data were initially fitted over the range 80–300 °K. Fits of these data for the ranges 80–250 °K, 110–300 °K, and 150–300 °K are shown in Table 10. These comparisons show the fit to be quite excellent. The value for η_1 of 44.78 W/cm agrees very well with the 43.3 W/cm from the alloy separation and from results expected from the Leibfried-Schlomann Equation.

In spite of the agreement between the calculated values of η_1 for the curve fitting and alloy separation techniques and the fit of the curve to the total λ data, a close look at the curve fitting results indicate they are probably incorrect. The error becomes apparent when the λ_L and λ_e components are calculated and compared. At 80 °K, for instance, the curve fitting results predict a $\lambda_L = 0.5598$ and a $\lambda_e = 0.1403$. The alloy separation results calculate $\lambda_L = 0.22$ and $\lambda_e = 0.48$. Over the entire temperature range, the curve fitting data predict higher values for λ_L. This is due almost exclusively to the fact that the curve fitting λ_L equation does not incorporate the possibility of electron-phonon scattering. Yet the two alloy separation shows an intercept on the lattice thermal resistivity curve of

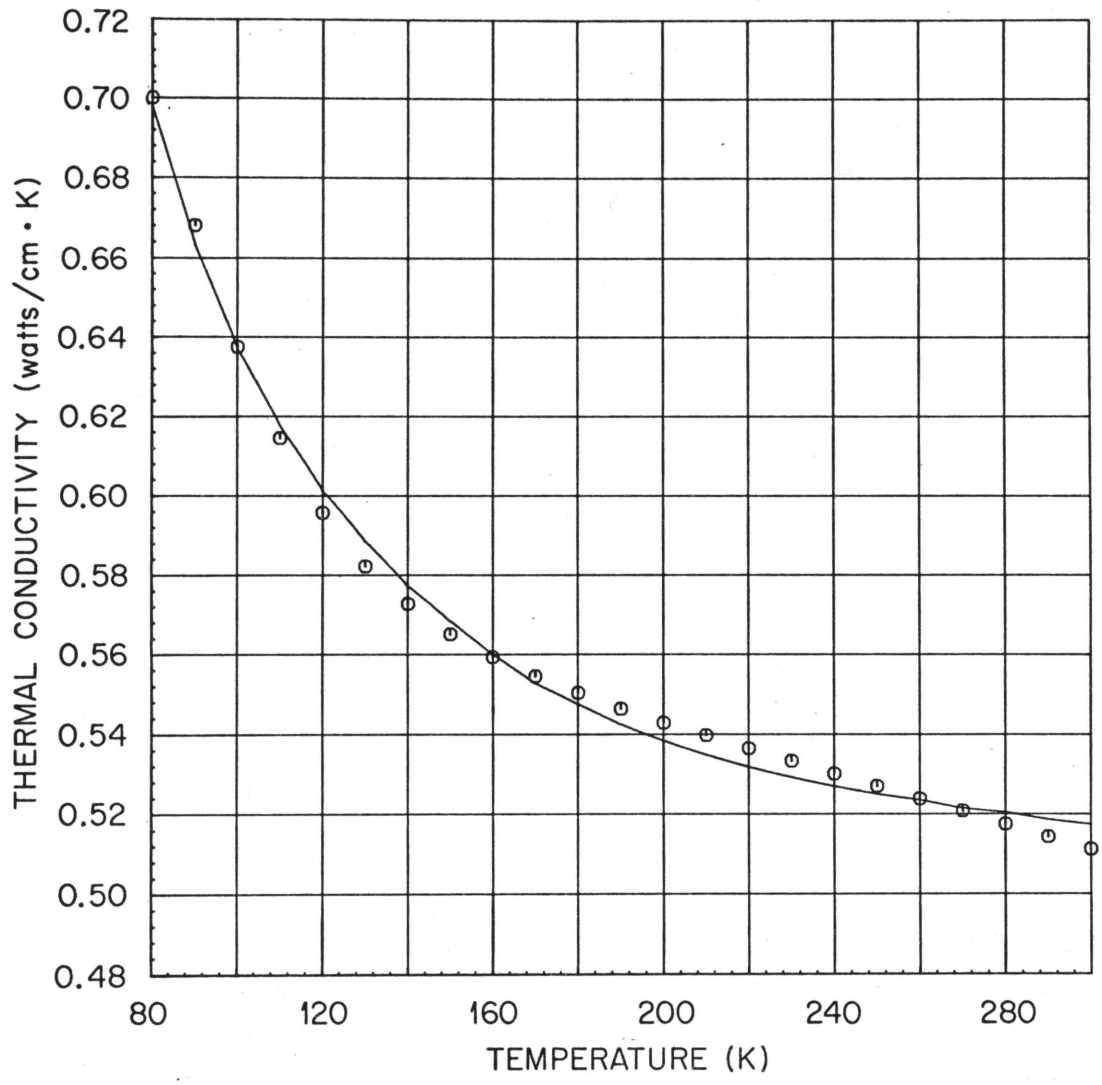

Figure 40. Results of Curve Fit to Equation

$$\lambda = \frac{L\omega T}{\rho}\left[1 - \exp\left(-\frac{T}{\Delta} + 0.2138\right)\right] + \frac{\eta_1}{T} \quad .$$

TABLE 10

COMPARISON OF RESULTS FOR CURVE FITTING OF ThN DATA USING VARIOUS TEMPERATURE RANGES

Temperature Range (°K)	$L_\infty \times 10^8 \left(\frac{V^2}{K^2}\right)$	η_1 (W/cm)	Standard Deviation (%)	
			L_∞	η_1
80–300	2.611	44.78	0.48	0.48
80–250	2.635	44.53	0.59	0.52
110–300	2.634	44.19	0.62	0.79
150–300	2.592	45.45	0.91	1.36

3 W/cm-°K, which indicates a significant electron-phonon resistivity effect. Furthermore the very low electrical resistivity of ThN suggests that a significant portion of the heat should be transferred by electrons and that one would expect an electron-phonon scattering contribution to the lattice thermal resistivity.

Electronic Thermal Conductivity

The calculation of the various components of λ also yields values for λ_e, which are tabulated in Tables B8-B10, Appendix B, and compared graphically in Figure 41. Since each calculation yields a value of λ_e for ThN, we have three sets of ThN values to compare with each of the alloys. It is significant to note the excellent agreement of the calculated λ_e values of ThN with each other and the calculated (Th-5% U)N values with each other. This indicates that the samples were very consistently pure except for the chosen alloy additions of UN to ThN. It further indicates that the measurement errors were indeed small and the alloy separation approach is quite good in this system.

The electronic contribution to λ for ThN is very large and dominant over the entire temperature range that was measured. The curve appears to be relatively flat above 130 °K to at least 300 °K. The electronic thermal conductivity for (Th-2% U)N and (Th-5% U)N are significant and increase with temperature but λ_e is not the dominant term at low temperatures.

Figures 42 and 43 show a comparison of the contributions of λ_e and λ_L to the total thermal conductivity. In the alloys lattice conductivity is dominant at the lower temperatures with λ_e becoming more important at high temperatures, very much like a metallic alloy. In the (Th-5% U)N

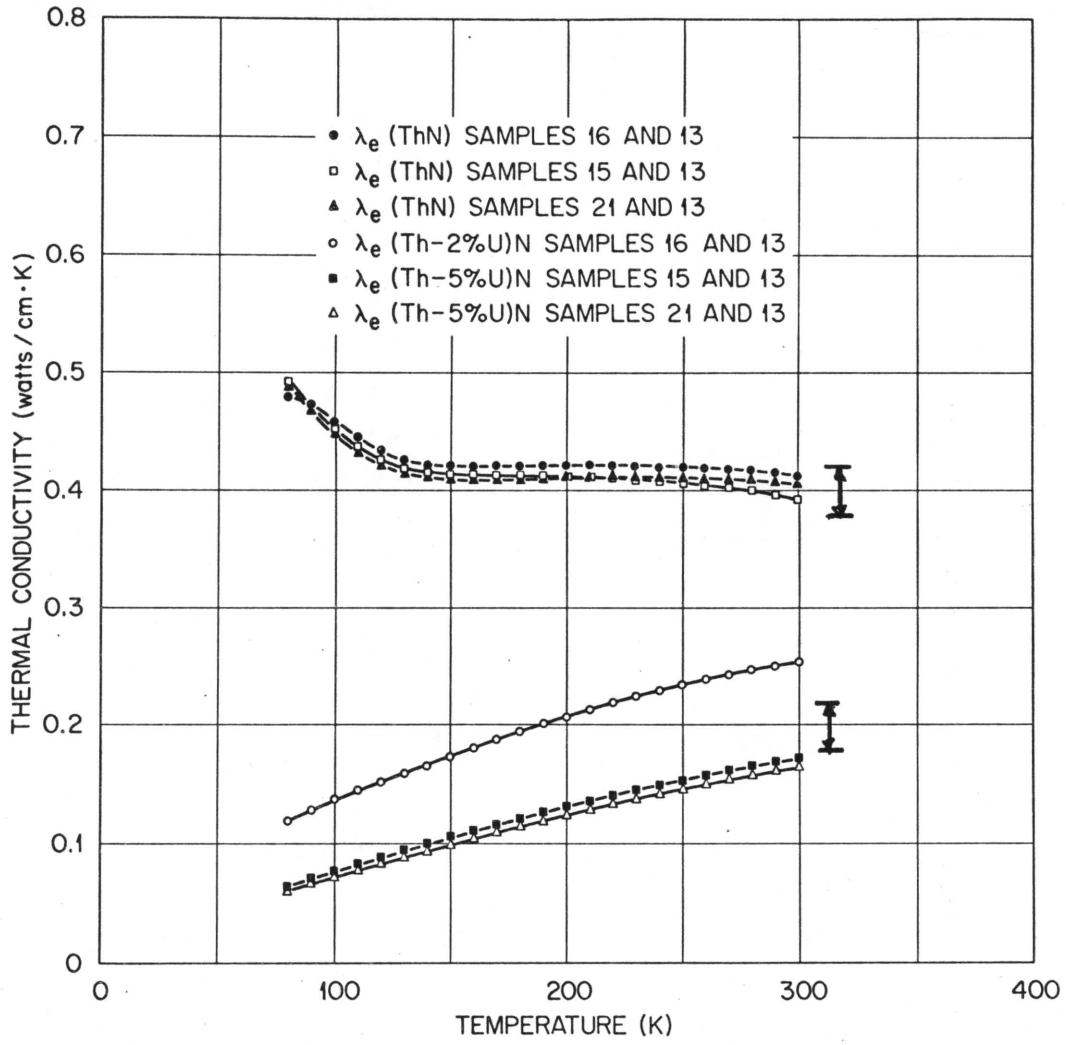

Figure 41. Electronic Contribution to Thermal Conductivity of (Th-U)N.

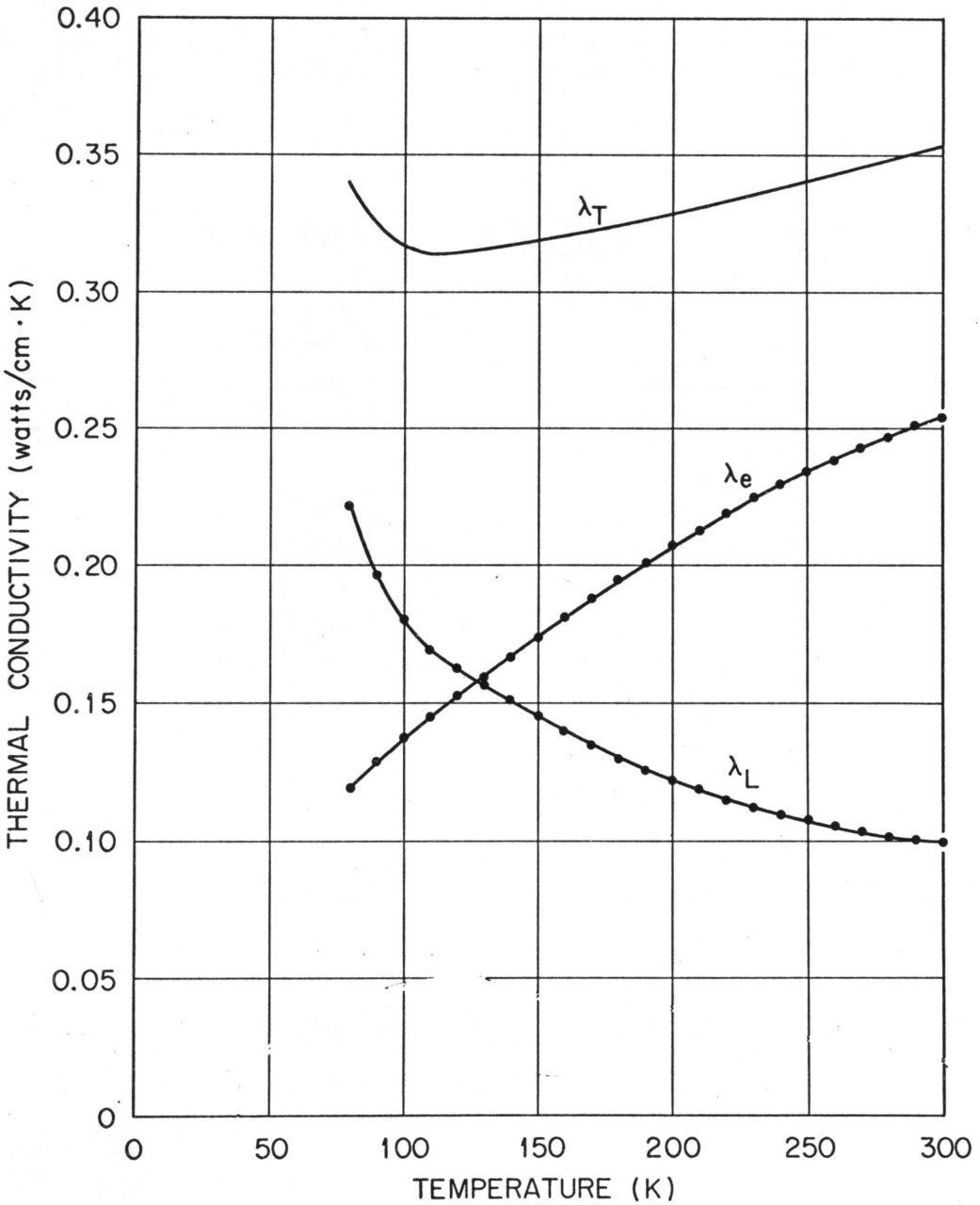

Figure 42. Thermal Conductivity of (Th-2% U)N, Sample Th-16.

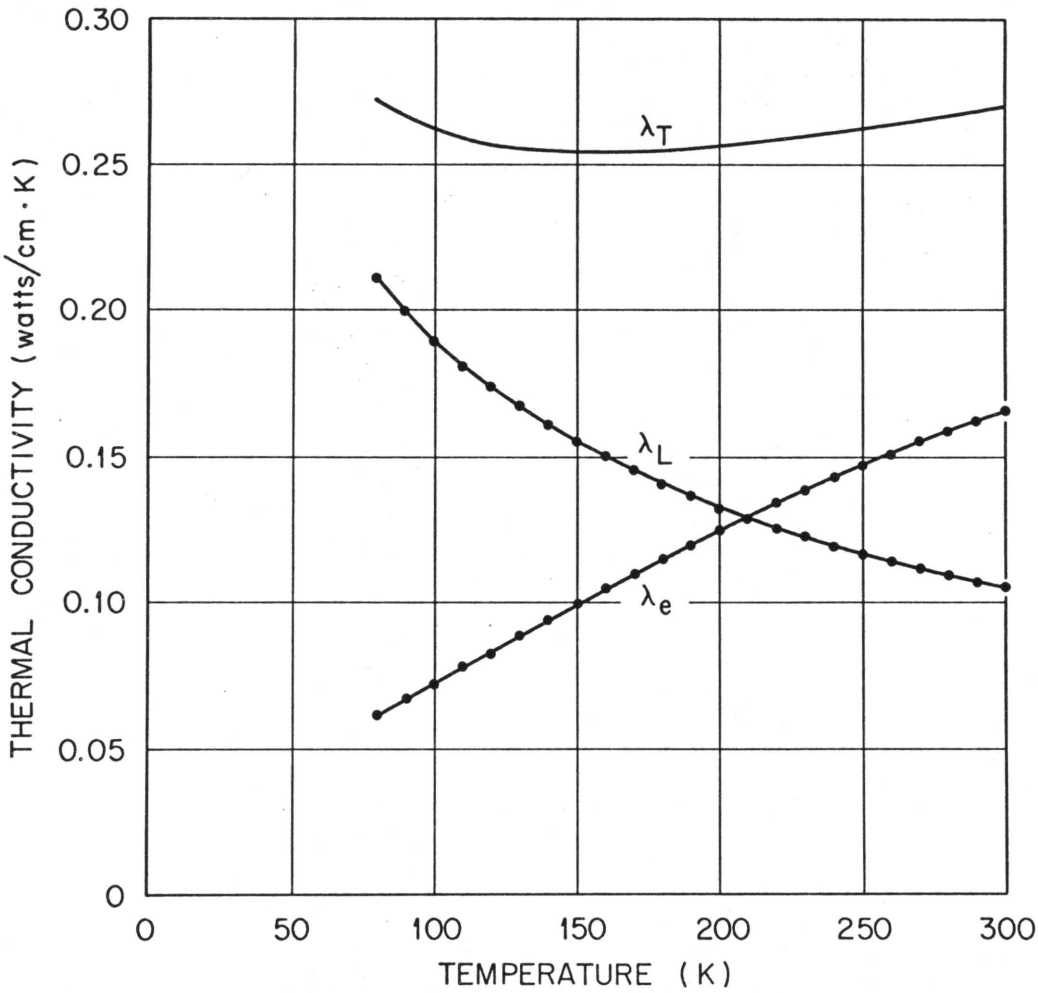

Figure 43. Thermal Conductivity of (Th-5% U)N, Sample Th-15.

alloy the decreasing λ_L term crosses the increasing λ_e at 210°K. In ThN and (Th-2% U)N λ_e becomes dominant at even lower temperatures.

Another important result of this calculation is the Lorenz function which appears to approach the Sommerfeld value 2.443×10^{-8} $V^2/°K$ at high temperatures (Figure 44). Values of 2.22×10^{-8}, 2.33×10^{-8}, and $2.29 \times 10^{-8} V^2/°K$ were calculated with an average value of $2.26 \times 10^{-8} V^2/°K$ calculated for $UC_{1.0}$, a refractory hard metal with the same structure.

A Lorenz function near L_o indicates that the ceramic ThN behaves very much like an ideal metal suggesting that ThN has a degenerate electron gas and that the second term in the theoretical calculation of L is probably not significant. Additional support for this contention comes from the experimental measurements of the thermoelectric power since

$$L = \frac{\lambda_e \rho}{T} - S^2 \quad . \tag{58}$$

As will be shown later in the text, the measured values for S are very nearly zero which supports the observation of an L nearly equal to the Sommerfeld value, L_o. An unexpected result was a calculated upswing of L below 100°K. Since the calculations separate out the residual resistivity of the pure alloy, the curve is expected to go to zero at 0°K. This reflects the decrease in the heat capacity of the electrons at lower temperatures and a decrease in elastic scattering. If the value of the residual resistivity of ThN had not be subtracted out, the curve would have been expected to take this shape and curve back up to the Sommerfeld value because of impurity scattering which is inherently elastic. The

upswing in the curve can be explained by a deviation from Matthiessen's rule (i.e., that the resistivity due to impurities not constant with temperature). To evaluate this possibility, values for ρ of the pure metal were calculated from the Bloch-Gruneisen formula from high temperature ρ data as discussed previously. A new ρ_I value was then calculated at each temperature. With this information the two alloy calculations were repeated. The results showed no change in the calculated values for either λ_e or λ_L even in the fourth significant figure, but it did change the value of L and eliminated the upswing on the low temperature end of the curve as shown in Figure 44. The results of these calculations also show a positive deviation from Matthiessen's rule and the resultant ρ_I as a function of temperature is shown in Figure 33 and tabulated in Table B16, Appendix B. The value for θ of 532 °K calculated from the Bloch-Gruneisen is unusually large value. Whether the value for θ is correct or not does not effect the conclusion that a positive deviation from Matthiessen's rule will explain the apparent upswing in the L curve.

Thermal Conductivity Extrapolated to High Temperatures

The results of the alloy separation were used to extrapolate values for λ to 2000 °K. The basis for the extrapolation was the equation

$$\lambda = \frac{TL_o}{\rho} + \frac{1}{3.0 + 0.023T} \quad . \tag{59}$$

The results of this extrapolation are shown in Table B15, Appendix B, and Figure 45. The extrapolation obviously becomes suspect at temperatures very much larger than the original data because small

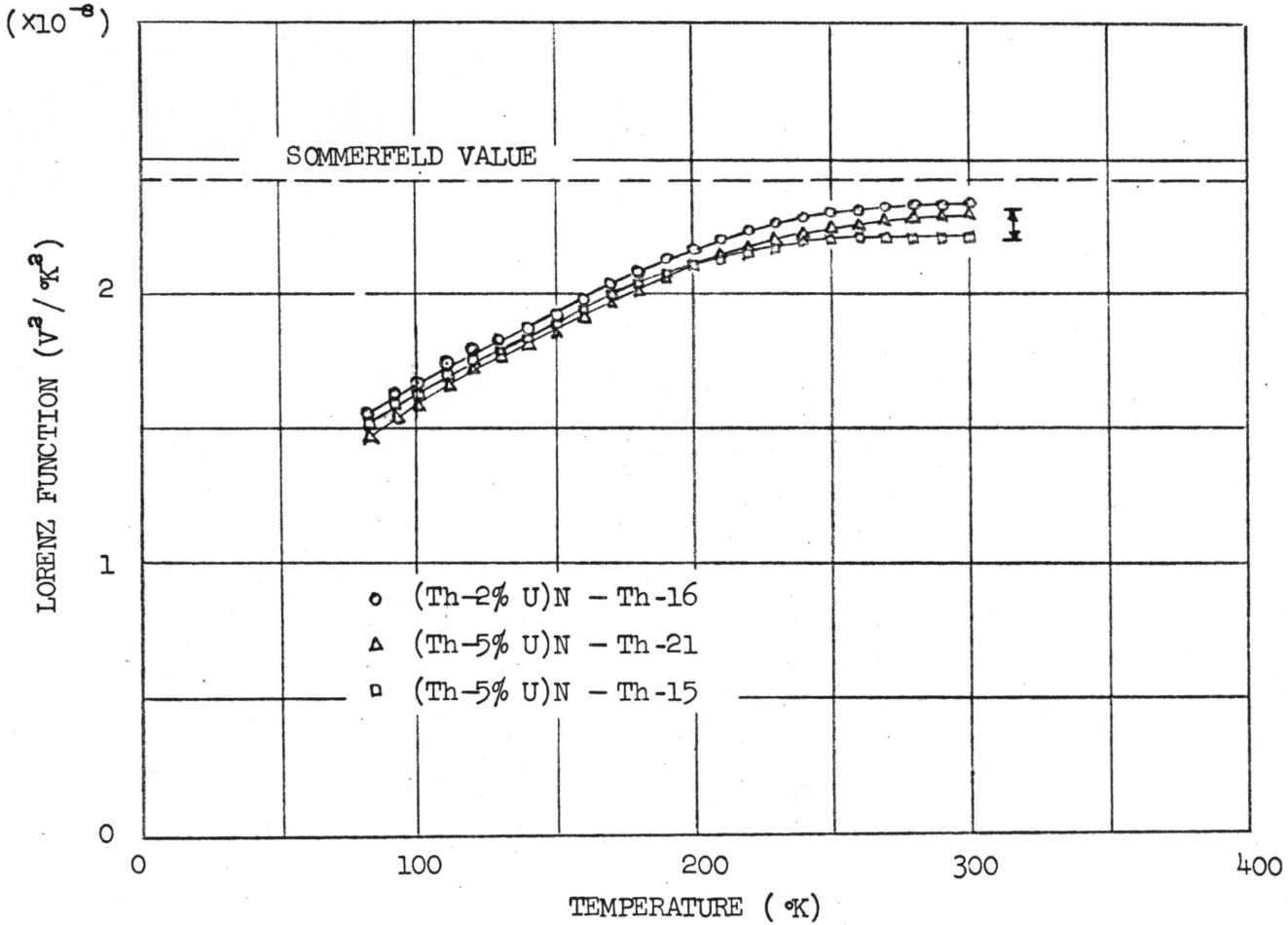

Figure 44. Lorenz Function as Calculated from Two Component Separation.

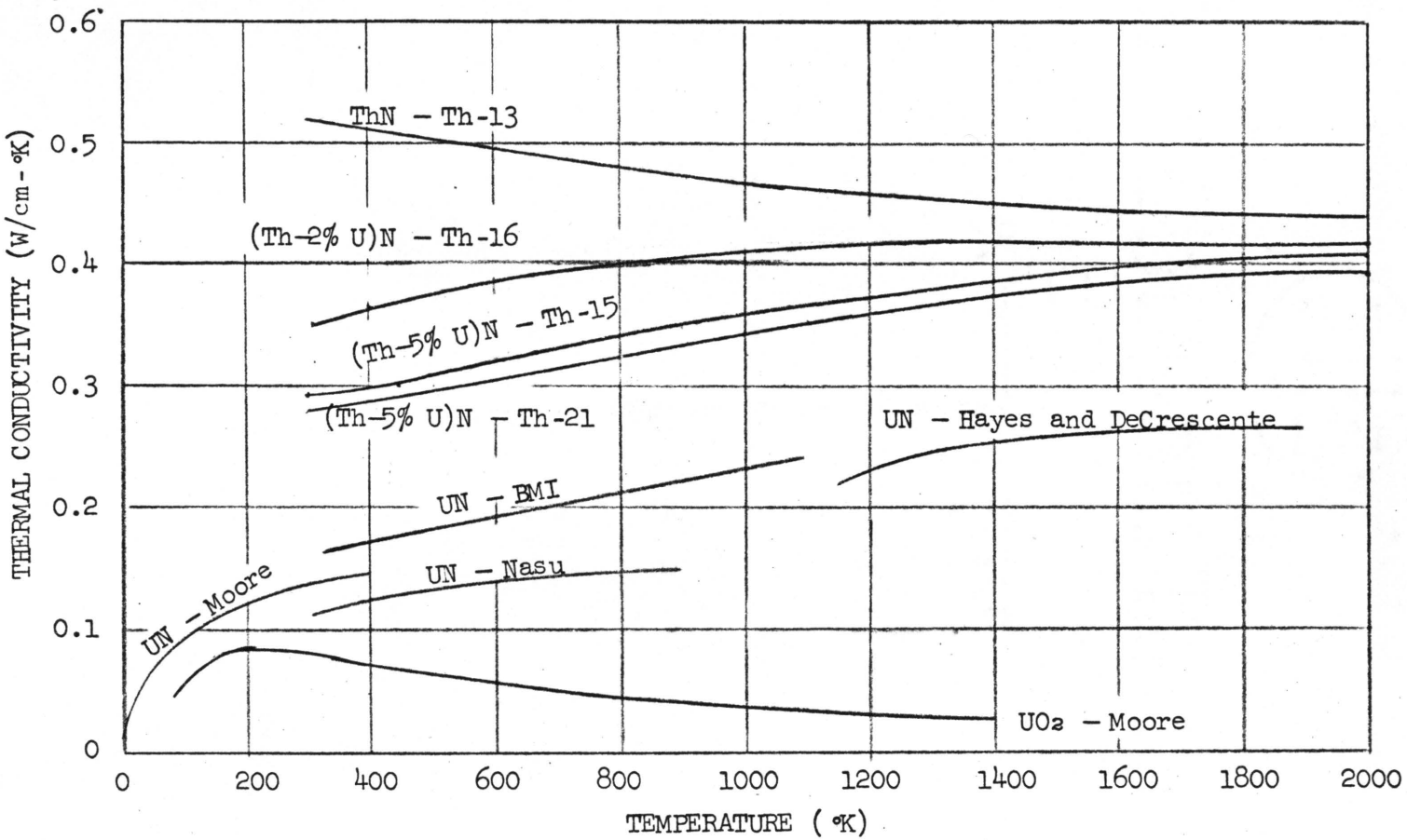

Figure 45. Thermal Conductivity of (Th-U)N Extrapolated to High Temperatures.

errors at low temperatures will have a much larger effect at high temperatures; however, the results should be qualitatively accurate.

The theoretical extrapolations show (Th-U)N alloy thermal conductivities to be roughly 20 times that of UO_2 at temperatures of interest in a reactor system. In addition, they show a thermal conductivity approximately 60% greater than that observed in UN.

The very high thermal conductivities of ThN and its ceramic alloys could well make it the most attractive fuel yet investigated from a reactor performance standpoint. The high thermal conductivity values would probably permit the fuel to operate at much higher power rates than any auxiliary coolant system yet devised could handle. The fuel, in effect, could operate at conditions which far outstrip the auxiliary reactor technology. This is in significant contrast to the existing $(U\text{-}Pu)O_2$ fuel system in which the low thermal conductivity of the fuel restricts the power and operating efficiency of the reactor.

Weidemann-Franz-Lorenz Ratio

The Weidemann-Franz-Lorenz (W-F-L) ratio as a fraction of the Sommerfeld value $\left(\frac{\lambda\rho}{TL_o}\right)$ was plotted versus temperature for both the zone cast alloys (Figure 46 and Tables B16 and B17, Appendix B) where good λ and ρ data are available and for the arc cast alloys (Figure 47 and Tables B18 and B19, Appendix B) where the entrapped porosity prevented accurate calculations of λ and ρ. For the arc cast alloys, the W-F-L ratio was calculated from the thermal conductance and electrical resistance data obtained on the samples since the geometric terms in λ and ρ cancel each other. The calculated W-F-L curves show a very consistent set of results between the two fabrication techniques. The

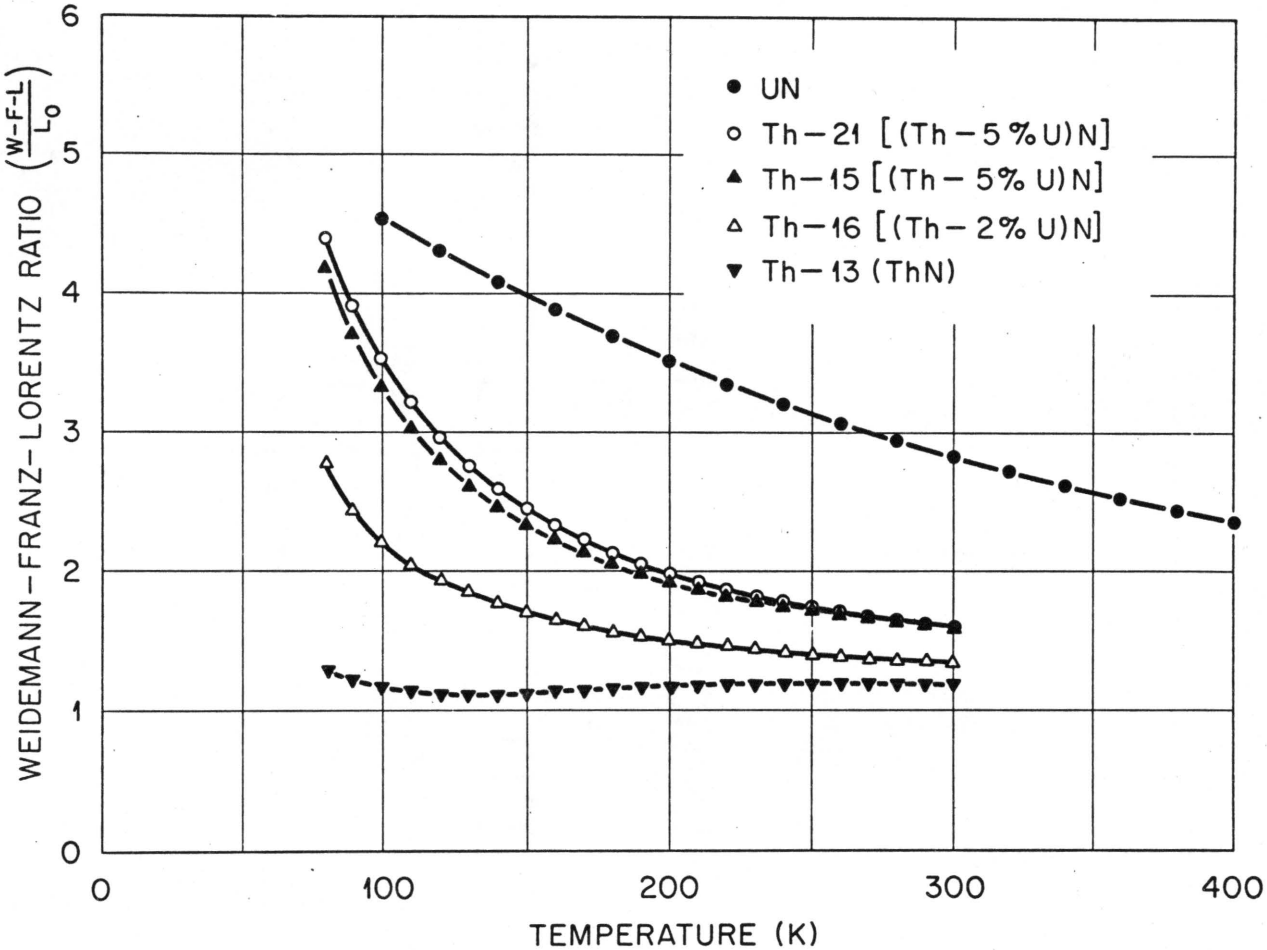

Figure 46. Weidemann-Franz-Lorenz Ratio for Zone Melted Samples Expressed as Fraction of Sommerfeld Value.

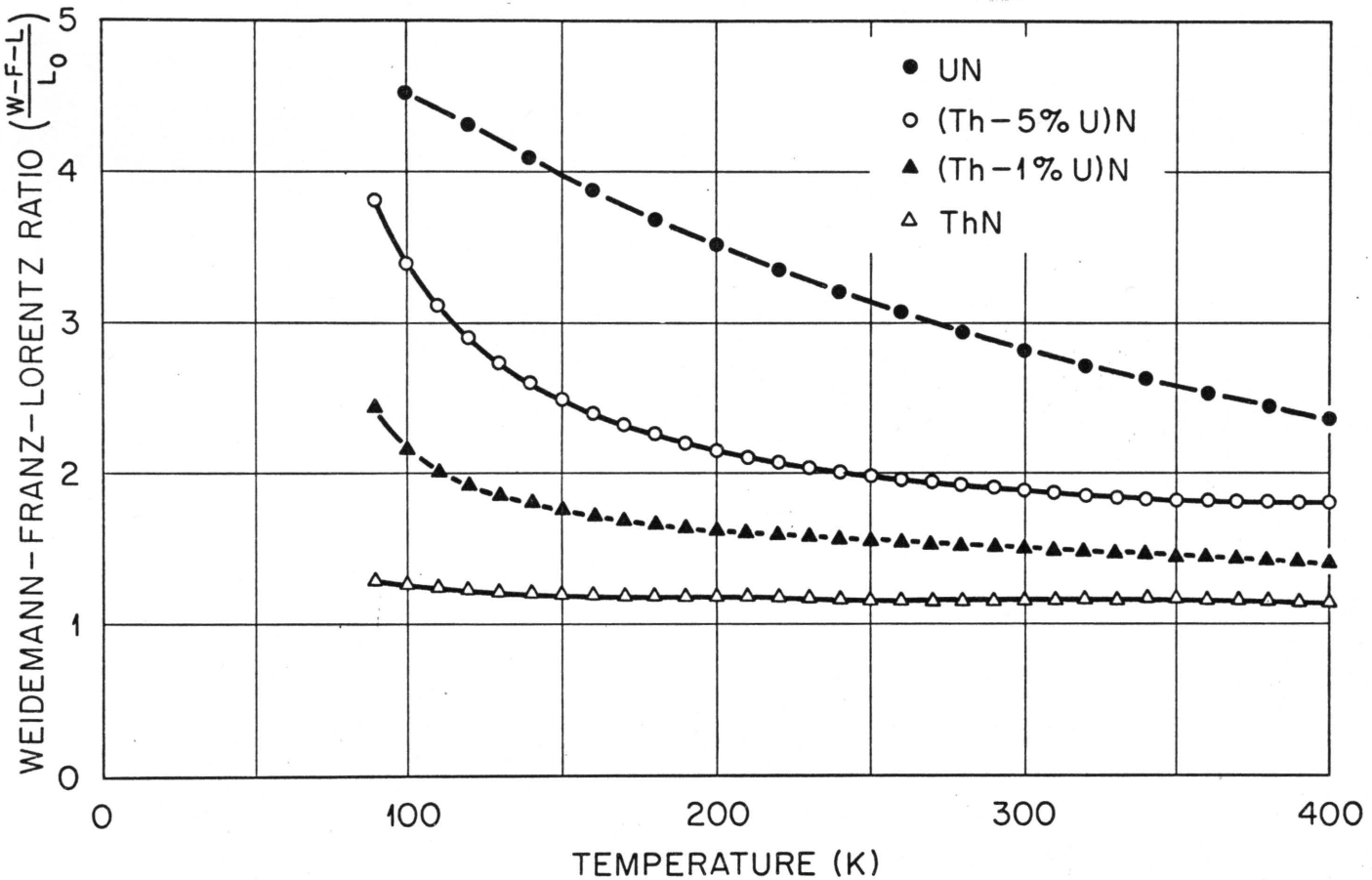

Figure 47. Weidemann-Franz-Lorenz Ratio of Arc Cast Samples Expressed as Fraction of Sommerfeld Value.

W-F-L values should approach the Sommerfeld value at high temperatures as the lattice contribution to the thermal conductivity becomes smaller. A significant contribution of λ_L to λ makes the W-F-L ratio high with respect to the Sommerfeld value.

IV. THERMOELECTRIC POWER

Thermoelectric power (S) measurements were made on the UN sample using the CODAS system at the same time the high temperature ρ data were obtained. Data were taken at 200 °K intervals starting at 466.9 °K. Data points were taken for three different temperature gradients at each temperature. The values for S (Table A11, Appendix A) were calculated by drawing a curve through the data and measuring the slope of E versus ΔT. Data for both tungsten and W-25% Re were measured to calculate the value for S. These two values were then used to calculate absolute S values from both the tungsten and W/W-25% Re data. The final data points plotted in Figure 48 constitute an average of the two points at each temperature. Smoothed values for S_{UN} are tabulated in Table B20, Appendix B.

Arc cast samples of ThN, (Th-2% U)N, and (Th-5% U)N were assembled in the glove boxes and measurements of λ, ρ, and S were made in the longitudinal heat flow apparatus (Tables A12-A15, Appendix A). Because of the nonuniformly distributed porosity in the samples, the λ and ρ data were disregarded and only the S data were assumed to be correct. A plot of the relative measurements of the thermoelectric power of (Th-U)N alloys versus constantan as a function of temperature is shown in Figure 49. This set of data has a very slight but interesting dip at about 305 °K. The magnitude of this dip appears to increase as the

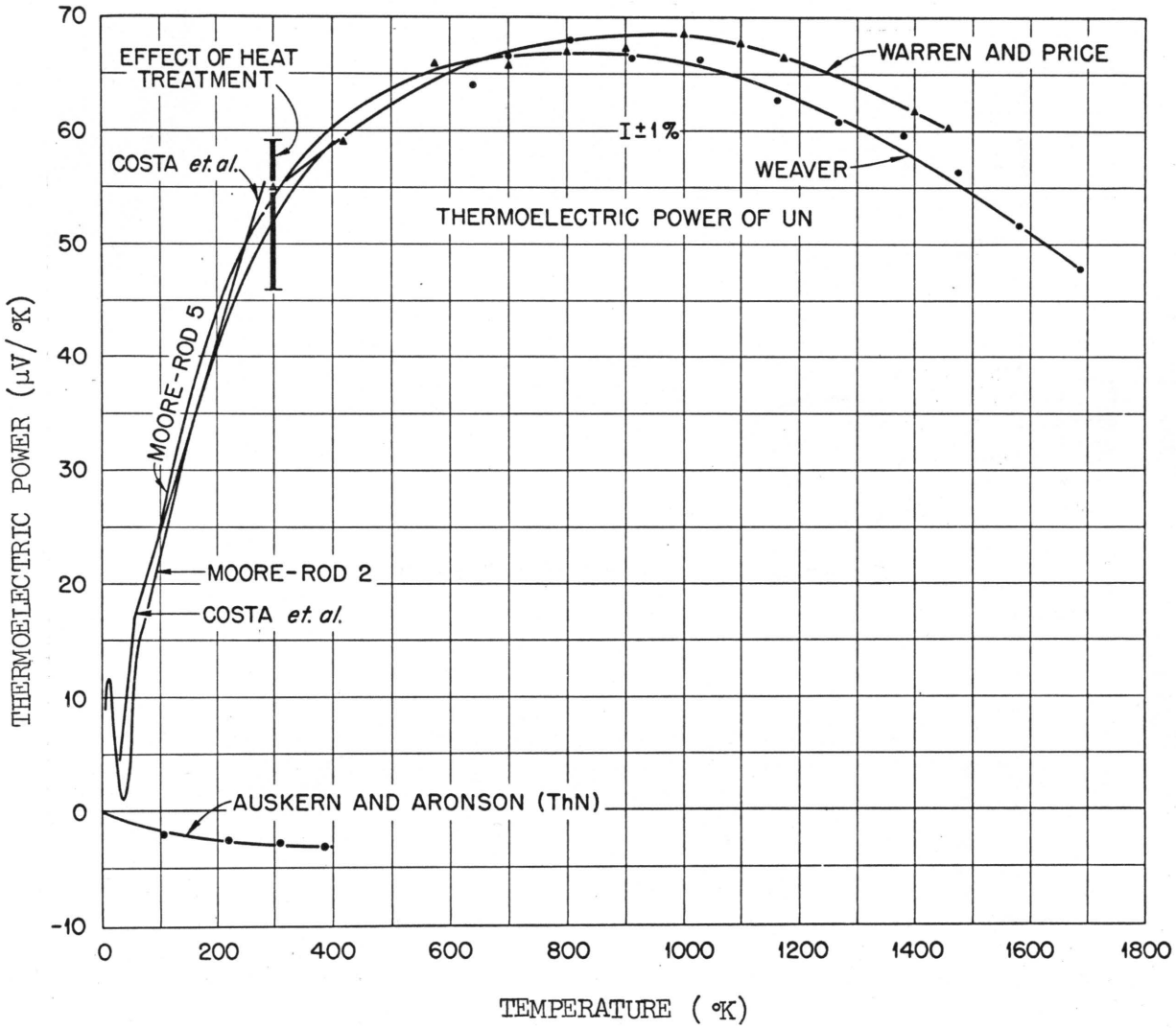

Figure 48. Comparison of Thermoelectric Power Data with Previous Experimenters.

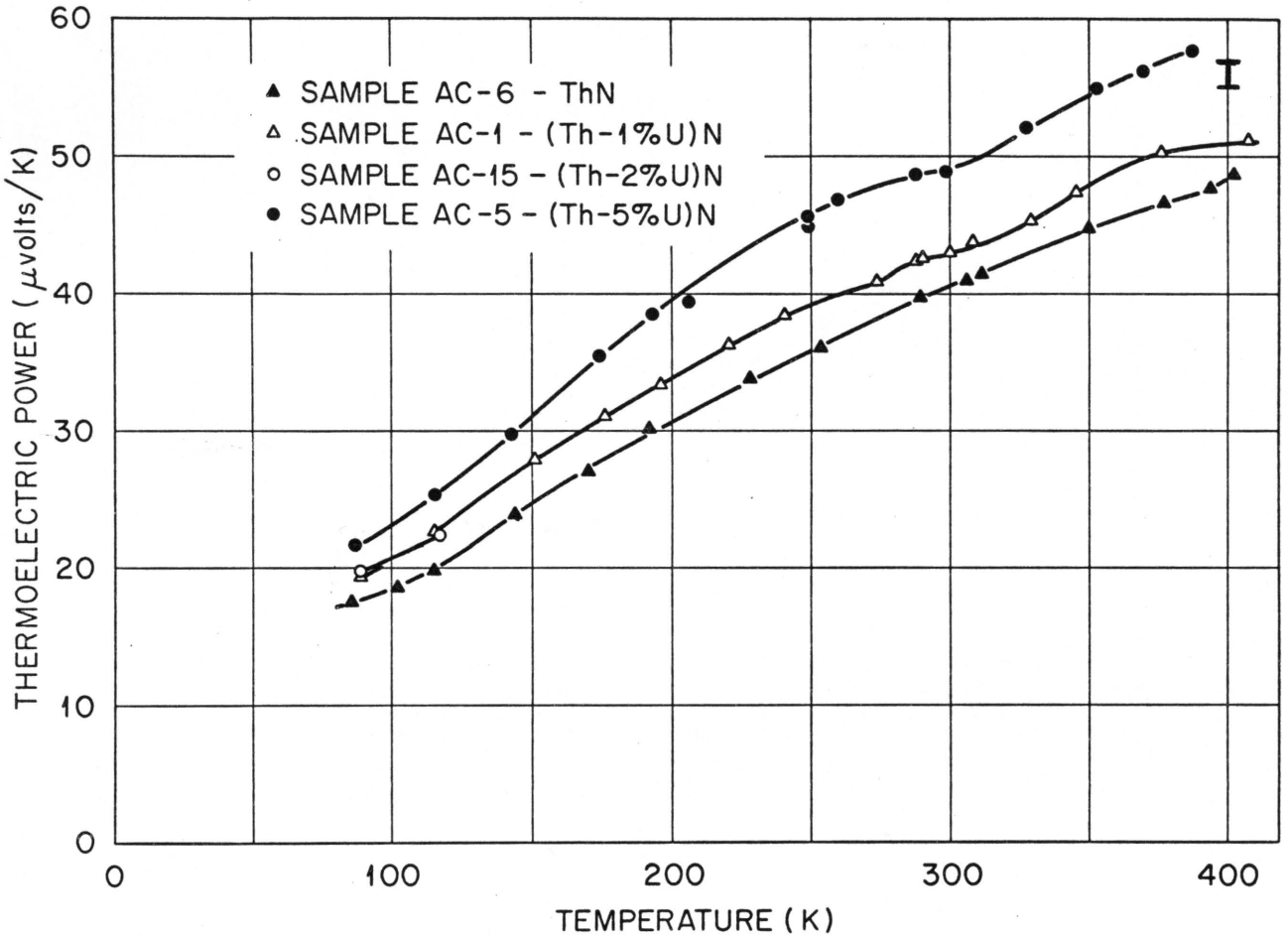

Figure 49. Thermoelectric Power of (Th-U)N Alloys Versus Constantan for Arc Cast Samples.

uranium content increases in the (Th-U)N alloys. The ThN samples show only a very small, almost imperceptible dip, while the (Th–5% U)N sample suggests a decrease in S of about 2 μV/°K at this temperature. The possibility exists that this dip may be the result of the thermocouple tables generated from the calibration of the Chromel-P versus constantan wires which were used. This does not seem likely, however, since an error in the thermocouple calibration should be reflected in both of the other curves by an equal magnitude which they are not.

The data were replotted (Figure 50) in terms of the absolute thermoelectric power, which has more fundamental significance. These were calculated as follows:

$$S^{abs}_{(Th-U)N} = S\left[(Th-U)N \text{ vs constantan}\right] - S^{abs}_{constantan} . \qquad (60)$$

The values for $S^{abs}_{constantan}$ were obtained from J. P. Moore.[58] Plotted this way, the dip in the curve at 305 °K becomes more apparent. It is significant to note that S_{ThN} is nearly zero over the entire temperature range from 80 to 400 °K.

Data were obtained on the zone cast alloys for thermoelectric power over the temperature range 80–400 °K. Data were obtained on four samples, ThN, (Th–2% U)N, and two samples of (Th–5% U)N. The data, shown in Figures 51 and 52, and Tables A16–A19, Appendix A, showed very close agreement with the previous measurements on the arc cast alloys. The alloys again showed a dip in the curve of S versus T, at 305 °K. Smoothed values for S are shown in Tables B21 and B22, Appendix B.

The dip in the S curve is very small and could probably justifiably be ignored by the extent of the error band. It occurs at the temperature

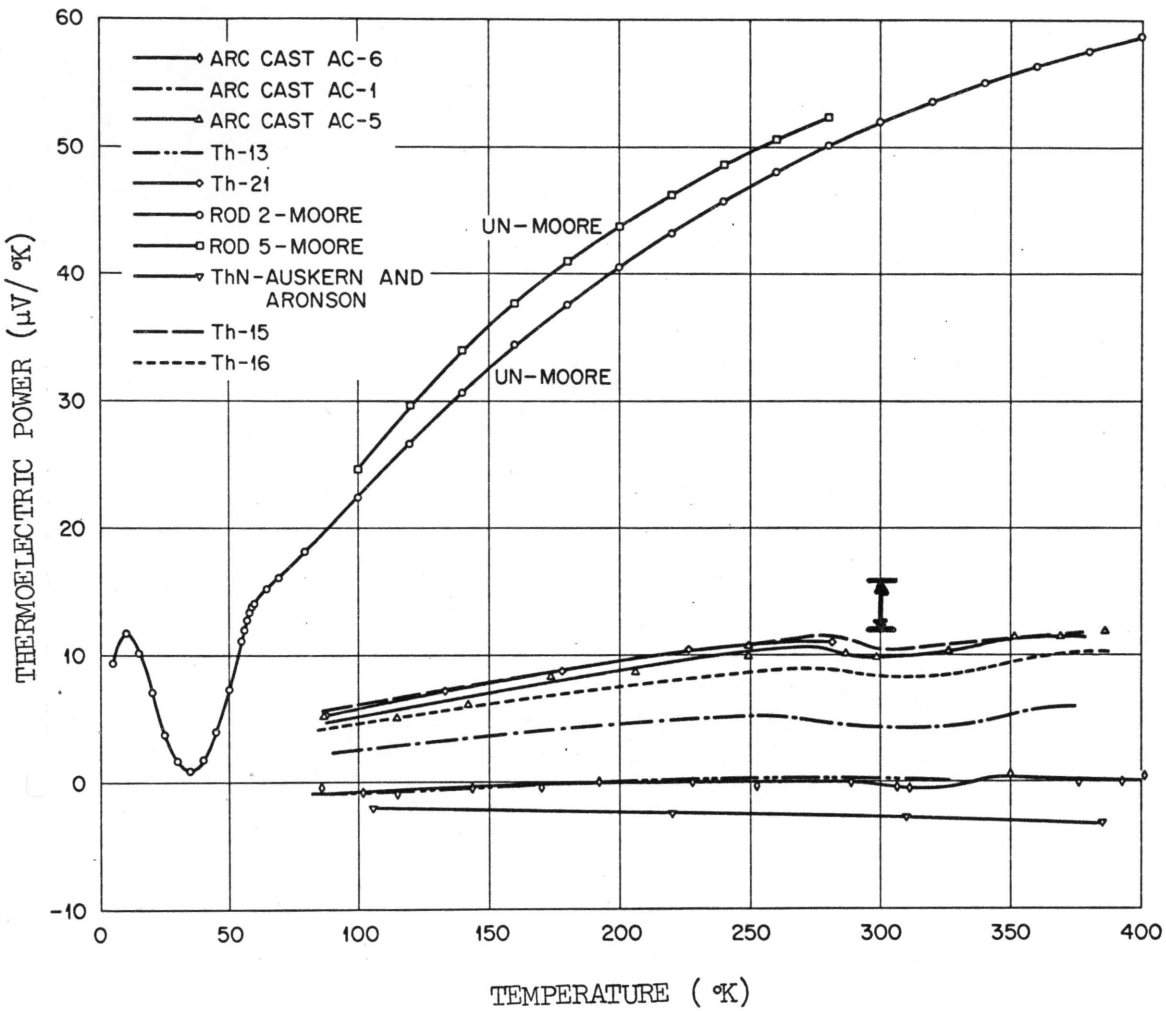

Figure 50. Thermoelectric Power of (Th-U)N Alloys.

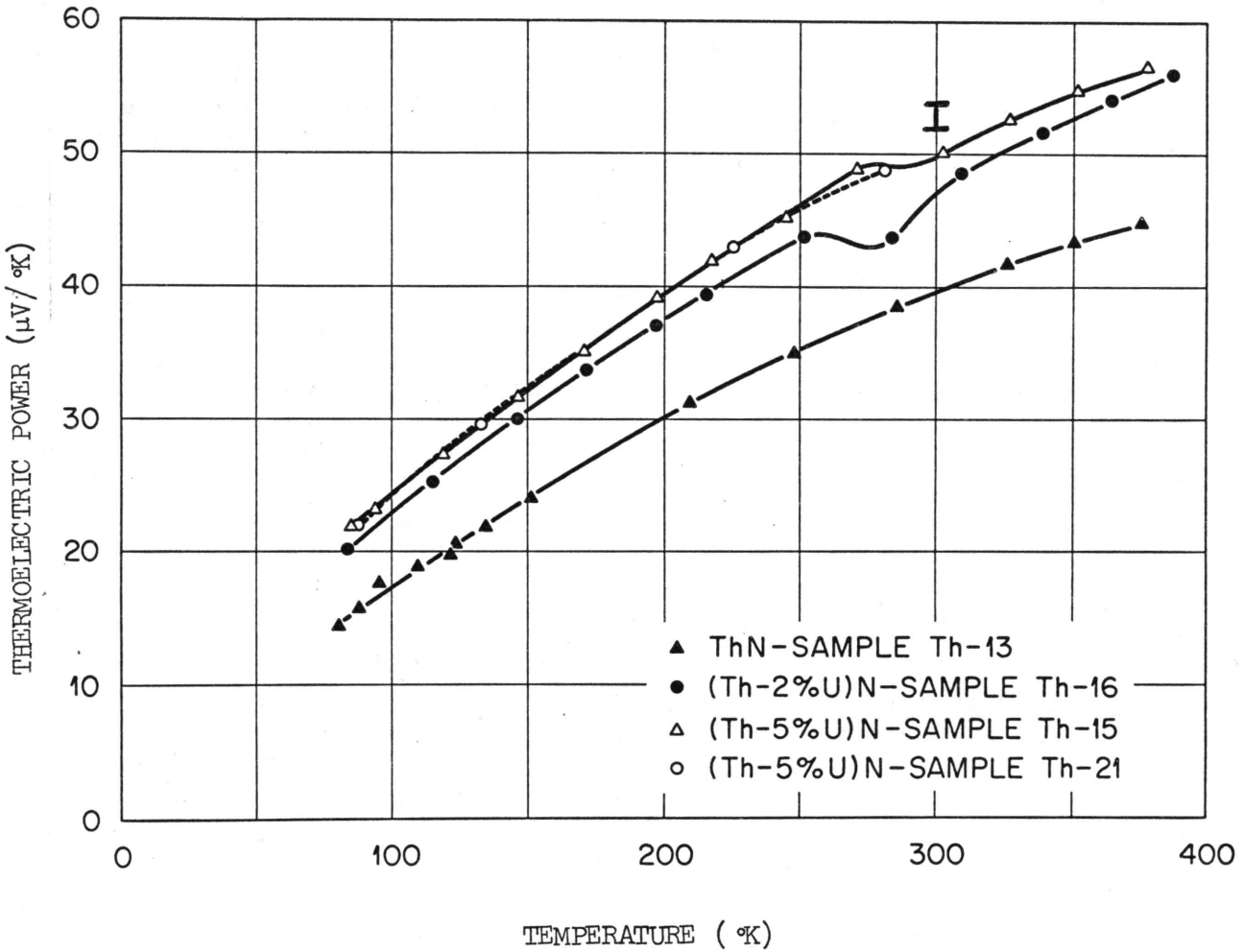

Figure 51. Thermoelectric Power of (Th-U)N Versus Constantan for Zone Cast Alloys.

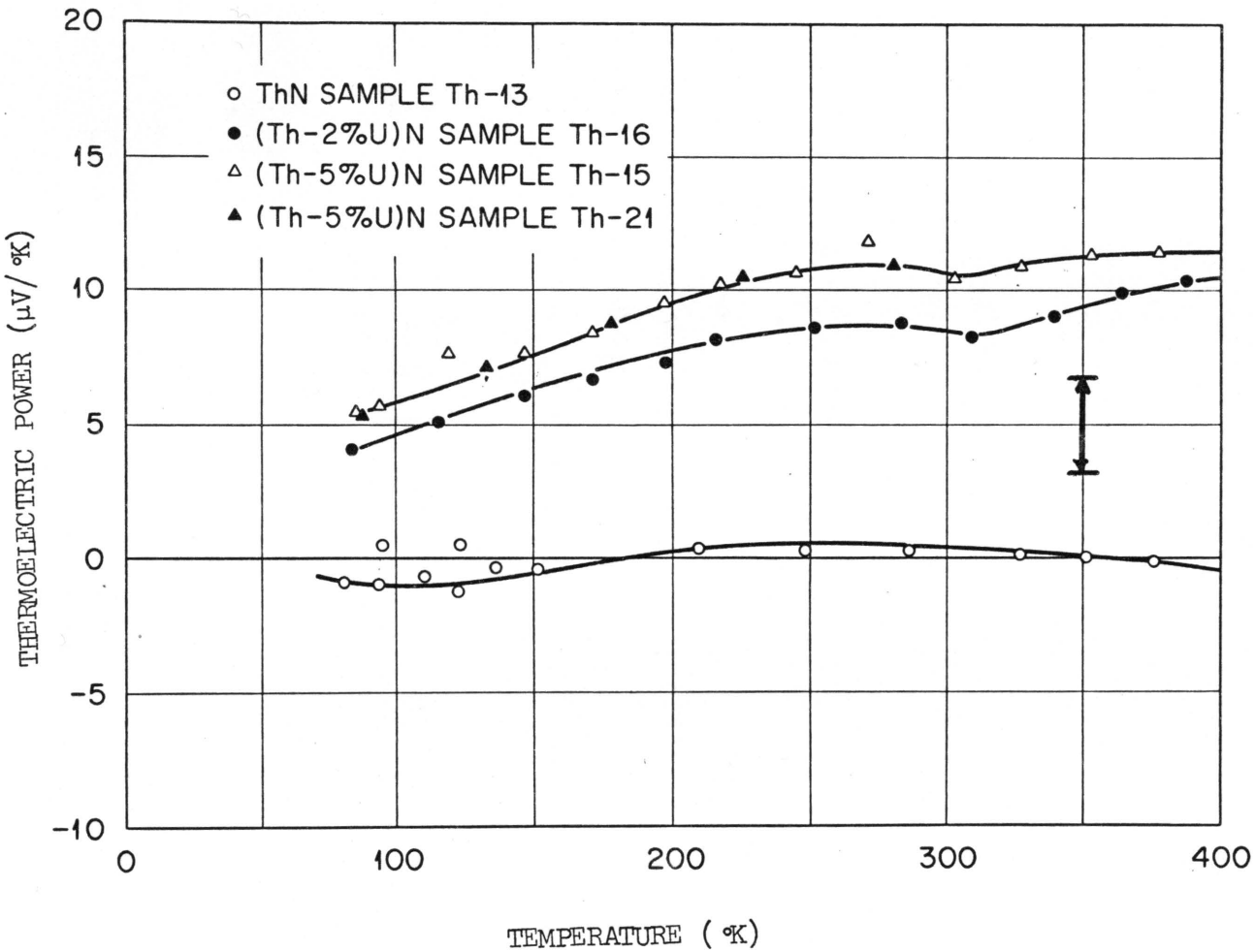

Figure 52. Thermoelectric Power of Zone Melted (Th-U)N.

where a switch is made from the liquid nitrogen bath to the ice-water bath. Also the value for S is obtained by taking a small difference of two large numbers.

CHAPTER V

CONCLUSIONS AND RECOMMENDATIONS

This work resulted in a number of significant conclusions and recommendations for future work in this area which are listed below.

I. CONCLUSIONS

(1) Thorium nitride and (Th-U)N alloys to 5% UN in ThN have high λ values, higher than any other ceramic fuel being considered for reactor use. At reactor operating temperatures of interest, λ for ThN is approximately 20 times that of UO_2. Calculations were presented which suggested that ThN should have a significant economic advantage and a predicted fuel performance which exceeds any other fuel being considered.

(2) A technique was developed for fabricating nitride samples of thorium, uranium, and thorium-uranium alloys directly from the metals by passing a molten zone along the length of a sample in a nitrogen atmosphere. This technique produced high-purity, high density samples 100 times as fast as any of the other more conventional techniques. The fabricated samples were nearly 100% dense with very large grains of approximately 0.3 cm diameter. High-density, large-grained samples would be expected to show superior in-reactor performance to either small-grained or low-density samples.

(3) Alloying of ThN with UN reduces the thermal conductivity but it is still higher than any other ceramic fuels being considered.

Furthermore, $\frac{d\lambda}{dT}$ is positive which results in high values for λ at reactor temperatures.

(4) Alloying of ThN with UN increases the residual resistivity significantly, but reduces the slope of the ρ versus T curve slightly at temperatures above 100 °K.

(5) Alloying of ThN with UN increases S significantly as S of ThN is nearly zero and S of UN is very large (50–60 $\mu V/°K$).

(6) The alloy separation showed only a very small effect on λ_L of adding UN to ThN. Most of the change in λ resulted from the significant increase in ρ from alloying.

(7) The Lorenz function calculated from both the curve fitting and the alloy separation are within 7% of the Sommerfeld value at 300 °K and the alloy separation results suggest L is continuing to approach L_o.

(8) The CODAS system was employed to speed up the data taking process for measuring ρ at high temperatures. This significantly reduced the time required to take data and in the case of UN increased the accuracy of the data.

(9) This is the first attempt at applying the alloy separation for ceramic alloys and the results indicate that it works.

II. RECOMMENDATIONS

The following recommendations are suggestions of work that could be of interest.

(1) A wider composition range of (Th-U)N should be studied to determine where the effect of the antiferromagnetic behavior of UN becomes

dominant in the alloy. This could result in a thermal conductivity at some composition less than that of either UN or ThN.

(2) Alloys of (Th-Pu)N should be studied to determine their thermal conductivities since this is the reactor fuel alloy which shows the most promise as a high performance fuel.

(3) Electrical resistivity values should be extended to 1700 °K for all of the alloys. This will permit a more accurate high temperature λ calculation than the projections presented in this work.

(4) The effect of various heat treatments of the samples in a nitrogen atmosphere should be studied. A variation in the nitrogen activity of the samples could result in a significant change in ρ and therefore λ.

(5) Irradiation tests should be performed on (Th-U)N and (Th-Pu)N fuels to determine their irradiation stability.

BIBLIOGRAPHY

BIBLIOGRAPHY

1. Schwarykopf, P. and R. Kieffer, Refractory Hard Metals. New York: MacMillan, 1953.

2. Weaver, S. C., "Helium Gas Bubble Migration in Uranium Mononitride in a Temperature Gradient," M. S. Thesis, The University of Tennessee, December 1967.

3. Auskern, A. B. and S. Aronson, Electrical Properties of Thorium Nitrides, Brookhaven National Laboratory, BNL-10620R, March 1967.

4. Kittel, C., Introduction to Solid State Physics, 3rd Ed. New York: Wiley, December 1968.

5. Williams, R. K. and W. Fulkerson, "Separation of the Electronic and Lattice Contribution to the Thermal Conductivity of Metals and Alloys," Proceedings of the Eighth Conference on Thermal Conductivity, October 1968.

6. Ziman, J. M., "The Thermal Properties of Materials," Scientific American, 217: 180–188, September 1967.

7. Ziman, J. M., Electrons and Phonons. Oxford University Press, 1963.

8. MacDonald, D.K.C., Thermoelectricity: An Introduction to the Principles. New York: Wiley, 1962.

9. Lorenz, L., Annalen der Physik, Leipzig, 147(2): 429, 1872.

10. Weidemann, G. and R. Franz, Annalen der Physik, Leipzig, 89(2): 497, 1853.

11. Sommerfeld, A., Zeitschrift fur Physik, 47: 1, 1928.

12. Gallo, C. F., "On the Thermal Conductivity of Tungsten and Molybdenum," Journal of Applied Physics, 36: 3410, 1963.

13. MacDonald, D.K.C., "Electrical Conductivity of Metals and Alloys at Low Temperatures," Handbook der Physik Vol. 14. Berlin: Springer, 1956.

14. Meaden, G. T., Electrical Resistance of Metals. New York: Plenum, 1965.

15. Sandheimer, E. H. and A. H. Wilson, Proceedings of the Royal Society (London) Series A, 190: 435, 1947.

16. Ziman, J. M., Principles of the Theory of Solids. Cambridge: University Press, 1964.

17. Moore, J. P., W. Fulkerson, and D. L. McElroy, "Thermal Conductivity, Electrical Resistivity, and Seebeck Coefficient of Uranium Mononitride," Journal of the American Ceramic Society, 53(2): February 1970.

18. Benz, R. and M. G. Bowman, "Some Phase Equilibria in the Uranium-Nitrogen System," Journal of the American Chemistry Society, 88(2): 264-268, 1966.

19. Benz, R., C. G. Hoffman, and G. N. Rupert, "Some Phase Equilibria in the Thorium-Nitrogen System," Journal of the American Chemistry Society, 89: 191-197, 1967.

20. Carlson, O. N. and E. R. Stevens, A Compilation of Thorium Binary Phase Diagrams, IS-1752, January 1968.

21. Venard, J. T. and J. E. Spruiell, "Phase Relations in the Th-U-N Ternary System at 1000 ℃," Journal of Nuclear Material, 27: 257-263, 1968.

22. Venard, J. T., J. E. Spruiell, and O. B. Cavin, "Lattice Parameters Across the UN-ThN Pseudobinary," Journal of Nuclear Material, 24: 245-246, 1967.

23. Auskern, A. B. and S. Aronson, "Electrical Properties of Nonstoichiometric Thorium Carbides," Journal of Applied Physics, 38(9): 3508-3514, August 1967.

24. Auskern, A. B. and S. Aronson, "Electrical Properties of Thorium Carbonitrides," Journal of Applied Physics, 41(1): January 1970.

25. Costa, B., R. Lallement, F. Anselin, and D. Rossignol, "Magnetic Transitions in Uranium and Plutonium Mononitrides, Monocarbides and Sesquicarbides," Compounds of Interest in Nuclear Reactor Technology, J. T. Waber, P. Chiotti, and W. N. Miner, editors. American Institute of Mining, Metallurgical, and Petroleum Engineers, New York, 1964.

26. Olson, W. M. and R.N.R. Mulford, "The Decomposition Pressure and Melting Point of Thorium Mononitride," Journal of Physical Chemistry, 69: 1223-1226, 1965.

27. Benz, R., "Melting Point Maxima of ThC-ThN and of UC-UN Solid Solutions," Journal of Nuclear Material, 31: 93-98, 1969.

28. Street, R. S. and T. N. Waters, The Thermal Expansion of ThC and ThN, AERE-M-1115, October 1962.

29. Aronson, S., E. Cisney, and K. A. Gingerich, "Thermal Expansion of Some Cubic Refractory Compounds of Thorium," Journal of the American Ceramic Society, 50: 248-252, 1967.

30. Chiotti, P., "Experimental Refractory Bodies of High-Melting Nitrides, Carbides, and Uranium Dioxide," Journal of the American Ceramic Society, 35: 123–130, 1952.

31. Aronson, S. and A. B. Auskern, "Vapor Pressure Measurements on Thorium Nitrides," Journal of Physical Chemistry, 70: 3937–3941, 1966.

32. Hayes, B. A. and M. A. DeCrescente, Thermal Conductivity and Electrical Resistivity of Uranium Mononitride, Pratt and Whitney – CANEL, PWAC-481, October 1965.

33. Van Craeynest, J. C., J. C. Weilbacher, and J. C. Salbreux, "Thermal Conductivity of Mixed Uranium and Plutonium Carbides, Nitrides, and Carbonitrides," Proceedings of the Eighth Conference on Thermal Conductivity, C. Y. Ho and R. E. Taylor, editors. New York: Plenum, 1969.

34. Speidel, E. and D. L. Keller, Fabrication and Properties of Uranium Mononitride, Battelle Memorial Institute, BMI-1633, 1963.

35. Endebrock, R. W., E. L. Foster, Jr., and D. L. Keller, Preparation and Properties of Case UN, Battelle Memorial Institute, BMI-1690, August 1964.

36. Warren, I. H. and C. E. Price, "Thermoelectric Properties of Cubic Uranium Monocompounds," Canadian Journal of Physics, 3: 183, 1964.

37. Ohmichi, T. and T. Kikuchi, "Electrical Properties of Uranium Carbonitride," Journal of Nuclear Science Technology (Tokyo), 6(2): 101–102, 1969.

38. Auskern, A. B. and S. Aronson, "Electrical Properties of Thorium Nitrides," Journal of Physics and Chemistry of Solids, 28: 1069–1071, 1967.

39. Fulkerson, W., T. G. Kollie, S. C. Weaver, J. P. Moore, and R. K. Williams, "Electrical and Thermal Properties of the NaCl Structured Metallic Actinide Compounds," Nuclear Metallurgy, 7(1): 374, October 1970.

40. Takahasi, Y., M. Murabayashi, Y. Akimoto, and T. Mukaibo, to be published in Journal of Nuclear Materials.

41. Fauxinstier, J. and J. C. Van Craeynest, Compte Rendu d'Essai No. 475, Centre d'Etudes Nucleaires, de Fontenya-aux-Roses, France, July 1967.

42. Taylor, K. M. and C. H. McMurtry, ORO-400, February 1961.

43. Pascard, R., International Symposium Plutonium Fuels, Technology, Scottsdale, Arizona, 1967, Nuclear Metals, Vol. 13, K. E. Horton, R. E. Macherey, and R. J. Allio, editors. American Institute of Mining, Metallurgical, and Petroleum Engineers, New York, 1968, p. 345.

44. Nasu, S. and T. Kikuchi, Journal of Nuclear Science Technology (Tokyo), 5: 318, 1968.

45. Radosevich, L. G. and W. S. Williams, Journal of American Ceramic Society, 52: 514, 1969.

46. Sturiale, T. J. and M. A. DeCrescente, Self-Diffusion of Nitrogen in Uranium Mononitride, Pratt and Whitney – CANEL, PWAC-482, October 1965.

47. Moore, J. P., D. L. McElroy, and R. S. Graves, "Thermal Conductivity and Electrical Resistivity of High-Purity Copper from 78 to 400 °K," Canadian Journal of Physics, 45: 3849–3865, 1967.

48. Moore, J. P., Oak Ridge National Laboratory, private communication, September 1969.

49. Kollie, T. G., D. L. McElroy, J. M. Jansen, and R. K. Adams, "Measurement Accuracy of a Computer Operated Data Acquisition System," Proceedings of the Fifth Symposium on Temperature, Its Measurement and Control in Science and Industry, June 1971.

50. Moore, J. P., Oak Ridge National Laboratory, private communication, January 1972.

51. Kollie, T. G., Oak Ridge National Laboratory, private communication, November 1971.

52. Fulkerson, W., T. G. Kollie, and T. G. Godfrey, Oak Ridge National Laboratory, private communication (to be published), March 1971.

53. de Novion, C. H., private communication with S. Peterson, Oak Ridge National Laboratory, August 24, 1970.

54. Schettler, H. G., "Thermal Conductivity of Thorium," M. S. Thesis, Iowa State University, Ames, Iowa, February 1969.

55. Leibfried, G. and E. Schlomann, Nachr. Akad. Wiss. Gottingen Math-Physik Kl.IIa, 71: 1954.

56. Steigmer, E. F. and I. Kudman, Physical Review, 132: 508, 1963.

57. Abeles, B., "Lattice Thermal Conductivity of Disordered Semiconductor Alloys at High Temperatures," Physical Review, 131(5): September 1963.

58. Moore, J. P., Oak Ridge National Laboratory, private communication, September 1969.

APPENDIXES

APPENDIX A

The following tables are a compilation of the calculated values for λ, ρ, and S versus T from the actual data. Smoothed values of these data are presented in Appendix B.

TABLE A1

ELECTRICAL RESISTIVITY OF UN AS TAKEN FROM THE 6-DIAL POTENTIOMETER

Temperature (°K)	ρ (μohm-cm)
295.025	148.60
322.376	150.38
376.207	153.26
422.966	155.06
471.358	157.04
527.939	158.51
574.398	160.02
620.816	161.63
672.801	163.17
724.732	164.59
768.174	165.93
823.674	167.50
871.787	168.84
919.916	170.19

TABLE A2

ELECTRICAL RESISTIVITY OF UN FROM ROOM TEMPERATURE TO 1700 °K USING CODAS

Temperature (°K)	ρ (Without Length Correction) (μohm-cm)	$\rho_{Corrected}$ (μohm-cm)
295.689	148.80	148.80
296.928	148.82	148.82
416.3	154.58	154.78
429.1	155.07	155.25
466.6	156.36	156.63
523.2	157.59	157.96
530.2	157.95	158.36
666.2	162.24	162.84
683.8	162.42	163.05
762.6	163.94	164.70
911.6	168.39	169.42
969.4	169.27	170.41
1023.8	171.38	172.62
1069.0	172.05	173.38
1153.1	174.67	176.16
1162.3	175.59	177.11
1224.2	177.08	178.72
1267.1	178.72	180.46
1333.3	180.55	182.60
1374.8	182.23	184.20
1437.1	184.31	186.41
1472.1	185.36	187.54
1477.7	185.72	187.91
1521.6	186.82	189.11
1563.1	188.14	190.52
1610.3	189.33	191.82
1672.7	191.44	194.07

TABLE A3

ELECTRICAL RESISTIVITY DATA FOR ThN,
SAMPLE Th-13

Temperature (°K)	ρ (μohm-cm)
4.2	2.109
98.072	4.425
123.344	5.646
148.164	7.251
148.392	7.112
190.338	9.749
211.377	10.98
234.012	12.92
274.199	15.27
296.376	16.96

The equation for the linear portion of the above data is

$$\rho = -2.122 + 0.063571T \qquad (61)$$

to within ±0.3%.

TABLE A4

ELECTRICAL RESISTIVITY DATA FOR (Th-2% U)N
SAMPLE Th-16

Temperature (°K)	ρ (μohm-cm)
4.2	14.42
103.3	17.30
126.00	18.42
148.74	19.66
172.42	20.99
195.54	22.30
219.396	23.65
247.788	25.26
273.876	26.68
296.441	27.908

The equation for the linear portion of the above data is

$$\rho = 11.385 + 0.055646T \qquad (62)$$

to within ±0.3%.

TABLE A5

ELECTRICAL RESISTIVITY DATA FOR (Th-5% U)N
SAMPLE Th-15

Temperature (°K)	ρ (μohm-cm)
4.2	28.51
78.0	30.09
89.1	30.50
114.3	31.56
115.5	31.62
141.9	32.91
166.4	34.15
171.4	34.45
192.5	35.52
212.8	36.56
241.9	37.97
268.1	39.26
297.1	40.71
323.0	41.93
348.1	43.07
374.0	43.92

The equation for the linear portion of the above data is

$$\rho = 25.946 + 0.049625T \qquad (63)$$

to within ±0.3%.

TABLE A6

ELECTRICAL RESISTIVITY DATA FOR (Th–5% U)N
SAMPLE Th-21

Temperature (°K)	ρ (μohm-cm)
78.531	31.64
79.478	31.69
219.846	39.00
275.774	41.99
296.495	43.06

The equation for the linear portion of the above data is

$$\rho = 27.494 + 0.052377T \qquad (64)$$

to within ±0.3%.

TABLE A7

THERMAL CONDUCTIVITY DATA FOR ThN
SAMPLE Th-13

Temperature (°K)	λ (W/cm-°K)
80.321	0.6774
88.541	0.6711
95.800	0.6601
109.975	0.6164
123.641	0.5993
135.643	0.5752
151.750	0.5632
209.903	0.5407
248.627	0.5295
286.709	0.5199
326.775	0.5021
350.730	0.4961
376.390	0.4872

TABLE A8

THERMAL CONDUCTIVITY DATA FOR (Th-2% U)N
SAMPLE Th-16

Temperature (°K)	λ (W/cm-°K)
84.159	0.3237
115.460	0.3136
146.725	0.3177
171.759	0.3229
197.870	0.3285
215.867	0.3329
252.260	0.3417
284.548	0.3495
310.106	0.3561
339.623	0.3620
364.998	0.3682
388.234	0.3750

TABLE A9

THERMAL CONDUCTIVITY DATA FOR (Th–5% U)N
SAMPLE Th-15

Temperature (°K)	λ (W/cm-°K)
85.843	0.2679
94.080	0.2636
119.240	0.2604
146.705	0.2573
171.110	0.2578
197.560	0.2627
218.401	0.2669
245.392	0.2741
271.648	0.2826
303.691	0.2903
328.051	0.2975
353.116	0.3063
378.491	0.3132

TABLE A10

THERMAL CONDUCTIVITY DATA FOR (Th-5% U)N
SAMPLE Th-21

Temperature (°K)	λ (W/cm-°K)
87.556	0.2679
97.283	0.2647
133.168	0.2555
178.778	0.2554
226.350	0.2606
281.734	0.2673

TABLE A11

THERMOELECTRIC POWER MEASUREMENTS OF URANIUM NITRIDE

Temperature (°K)	S_{UN} vs W (μV/°K)	S_{UN} vs W-26% Re (μV/°K)	S_{UN} From W (μV/°K)	S_{UN} From W-26% Re (μV/°K)	S_{UN} avg. (μV/°K)
466.9	44.16	51.18	47.16	49.46	48.31
638.8	49.70		63.88		63.88
699.3	53.30	68.24	66.33	66.51	66.42
910.9	48.75	67.16	66.11	66.33	66.22
1027.6	46.92	66.84	65.93	66.26	66.10
1162.2	42.45	62.86	62.79	62.50	62.64
1267.2	40.02	62.16	60.82	60.72	60.77
1380.2	38.67	59.70	59.60	59.39	59.50
1472.0	35.70	57.34	56.40	56.36	56.38
1578.0	31.53	52.13	51.53	51.52	51.52
1683.5	28.66	48.83	47.96	47.81	47.88

TABLE A12

THERMOELECTRIC POWER OF ThN, SAMPLE AC-6

Temperature (°K)	S_{ThN} (μV/°K)	S_{UN} vs Constantan (μV/°K)
86.009	-0.39	17.01
101.591	-0.76	18.05
114.985	-0.94	19.36
143.715	-0.45	23.25
170.032	-0.46	26.20
192.119	0.01	29.11
227.645	-0.03	32.75
252.650	-0.37	34.83
288.878	-0.00	38.60
306.497	-0.41	39.69
311.185	-0.48	40.00
349.980	0.07	43.39
376.208	-0.04	45.02
392.780	0.14	46.16
402.396	0.56	47.16

TABLE A13

THERMOELECTRIC POWER OF (Th–1% U)N, SAMPLE AC-1

Temperature (°K)	S (μV/°K)	S (Th-U)N vs Constantan (μV/°K)
89.510	2.33	19.98
115.713	2.60	22.97
150.936	3.78	28.76
175.816	4.32	31.62
196.173	4.49	34.01
220.353	4.85	36.88
240.419	5.10	39.16
274.356	4.42	41.68
287.312	4.78	43.23
289.191	4.76	43.39
299.798	4.23	43.78
308.029	4.48	44.69
329.454	4.31	46.21
345.481	5.26	48.33
376.437	6.06	51.13
407.081	5.20	52.05

TABLE A14

THERMOELECTRIC POWER OF (Th-2% U)N, SAMPLE AC-15

Temperature (°K)	$S_{(Th-U)N}$ vs Constantan ($\mu V/°K$)	$S_{(Th-2\%\ U)N}$ ($\mu V/°K$)
89.12	19.382	1.74
116.704	20.870[a]	0.47[a]

[a]The accuracy of these numbers is questionable because only one isothermal correction was obtained on this sample before a thermocouple came off.

TABLE A15

THERMOELECTRIC POWER OF (Th-5% U)N, SAMPLE AC-5

Temperature (°K)	$S_{(Th-U)N}$ vs Constantan (μV/°K)	$S_{(Th-U)N}$ (μV/°K)
86.749	21.69	5.15
115.043	25.36	5.06
141.754	29.60	6.14
173.841	35.35	8.29
192.829	38.36	9.19
205.747	39.17	8.60
249.434	44.86	9.92
249.484	45.64	10.70
260.254	46.70	10.70
286.820	48.52	10.12
298.651	48.72	9.30
327.327	52.03	10.29
351.518	54.94	11.46
369.308	56.12	11.49
387.264	57.66	11.94

TABLE A16

THERMOELECTRIC POWER OF ThN, SAMPLE Th-13

Temperature (°K)	S ThN vs Constantan (μV/°K)	S_{ThN} (μV/°K)
80.321	14.66	-0.91
88.541	15.86	-0.94
95.800	17.72	0.50
109.975	18.98	-0.70
122.037	19.86	-1.24
123.641	20.66	0.56
135.643	21.85	-0.40
151.750	24.10	-0.48
209.903	31.37	0.39
248.627	35.12	0.24
286.709	38.70	0.30
326.775	41.84	0.14
350.730	43.37	-0.03
376.390	44.99	-0.09

TABLE A17

THERMOELECTRIC POWER OF (Th-2% U)N, SAMPLE Th-16

Temperature (°K)	$S_{(Th-U)N}$ vs Constantan (μV/°K)	$S_{(Th-U)N}$ (μV/°K)
84.159	20.22	4.02
115.460	25.38	5.05
146.725	30.06	6.06
171.759	33.58	6.70
197.870	37.06	7.36
215.867	39.42	8.19
252.260	43.83	8.63
284.548	43.74	8.79
310.106	48.61	8.22
339.623	51.70	9.02
364.998	54.33	9.98
388.234	56.15	10.37

TABLE A18

THERMOELECTRIC POWER OF (Th-5% U)N, SAMPLE Th-15

Temperature (°K)	$S_{(Th-U)N}$ vs Constantan (μV/°K)	$S_{(Th-U)N}$ (μV/°K)
85.843	21.88	5.48
94.080	23.26	5.68
119.240	27.27	7.70
146.705	31.66	7.63
171.110	35.19	8.40
197.560	39.18	9.53
218.401	42.14	10.29
245.392	45.38	10.71
271.648	48.89	11.87
303.691	50.33	10.46
328.051	52.70	10.91
353.116	54.93	11.36
378.491	56.63	11.43

TABLE A19

THERMOELECTRIC POWER OF (Th–5% U)N, SAMPLE Th-21

Temperature (°K)	$S_{(Th-5\%\ U)N}$ vs Constantan (μV/°K)	S_{ThN} (μV/°K)
87.556	21.98	5.28
133.168	29.60	7.15
177.976	36.29	8.69
226.350	43.17	10.55
281.734	48.93	11.00

APPENDIX B

Contained in Appendix B are tables of calculated results based on the experimental data evaluation discussed in the text.

TABLE B1

SMOOTHED ELECTRICAL RESISTIVITY VALUES FOR UN

Temperature (°K)	ρ (μohm-cm)	Temperature (°K)	ρ (μohm-cm)
0	5.65	70	102.30
1	5.67	75	104.95
2	5.73	77.7	106.40
3	5.825	80	107.17
4	5.955	80	108.0
4.2	5.992	100	116.4
5	6.110	120	123.2
6	6.285	140	128.6
7	6.496	160	133.1
8	6.762	180	136.9
9	7.080	200	140.0
10	7.470	220	142.5
15	9.75	240	144.6
20	13.45	260	146.3
25	18.45	280	147.8
30	25.55	300	149.1
35	35.12	300	149.0
40	47.35	320	149.9
45	61.80	340	151.0
50	79.00	360	151.8
51	82.75	380	152.8
52	86.20	400	153.6
53	89.25	400	154.1
54	91.65	500	157.7
55	93.65	600	160.6
56	95.35	700	163.4
57	96.35	800	166.1
58	96.50	900	168.9
59	96.90	1000	171.5
60	97.30	1100	174.6
61	97.80	1200	177.9
62	98.25	1300	181.2
63	98.75	1400	185.0
64	99.25	1500	188.3
65	99.75	1600	191.5

TABLE B2

SMOOTHED ELECTRICAL RESISTIVITY VALUES OF ThN FROM 298 TO 1273 °K

Temperature (°K)	ρ (μohm-cm)
298	16.98
323	18.48
373	21.51
423	24.57
473	27.37
523	30.27
573	33.12
623	35.96
673	39.01
723	41.63
773	44.49
823	47.34
873	50.13
923	52.93
973	55.89
1023	58.83
1073	61.81
1123	64.76
1173	67.72
1223	70.64
1273	73.67

TABLE B3

SMOOTHED VALUES OF ELECTRICAL RESISTIVITY

Temperature (°K)	ρ (μohm-cm) ThN Th-13	(Th-2% U)N Th-16	(Th-5% U)N Th-15	(Th-5% U)N Th-21
4.2	2.11	14.40	28.5	
10	2.2	14.40	28.5	
20	2.2	14.43	28.6	
30	2.3	14.6	28.75	
40	2.5	14.75	29.0	
50	2.7	15.00	29.2	
60	3.0	15.3	29.5	
70	3.3	15.6	29.8	
80	3.63	16.02	30.20	31.70
90	4.04	16.48	30.58	32.22
100	4.51	16.98	30.98	32.74
110	5.0	17.52	31.38	33.28
120	5.55	18.07	31.88	33.79
130	6.11	18.62	32.38	34.31
140	6.71	19.19	32.88	34.82
150	7.31	19.72	33.38	35.34
160	7.95	20.28	33.88	35.87
170	8.60	20.82	34.38	36.38
180	9.23	21.38	34.88	36.91
190	9.88	21.93	35.38	37.44
200	10.53	22.50	35.88	37.96
210	11.18	23.07	36.37	38.49
220	11.83	23.62	36.86	39.00
230	12.48	24.18	37.36	39.54
240	13.13	24.73	37.86	40.07
250	13.78	25.31	38.35	40.60
260	14.42	25.86	38.85	41.11
270	15.09	26.41	39.34	41.63
280	15.72	26.98	39.84	42.18
290	16.39	27.52	40.34	42.68
300	17.04	28.10	40.84	43.22
310			41.34	
320			41.84	
330			42.28	
340			42.70	
350			43.11	
360			43.47	
370			43.80	
380			44.07	
390			44.30	
400			44.53	

TABLE B4

EXTRAPOLATED ELECTRICAL RESISTIVITY DATA

Temperature (°K)	ρ (μohm-cm) ThN Th-13	(Th-2% U)N Th-16	(Th-5% U)N Th-15	(Th-5% U)N Th-21
300	17.10	28.18	40.84	43.22
350	19.99	30.86	43.31	45.83
400	22.91	33.64	45.80	48.44
450	25.80	36.43	48.28	51.06
500	28.73	39.21	50.76	53.68
550	31.63	41.99	53.24	56.30
600	34.54	44.77	55.72	58.92
650	37.45	47.55	58.20	61.54
700	40.35	50.34	60.68	64.16
750	43.26	53.12	63.16	66.78
800	46.17	55.90	65.65	69.40
850	49.08	58.68	68.13	72.01
900	51.98	61.47	70.61	74.63
950	54.89	64.25	73.09	77.25
1000	57.80	67.03	75.57	79.87
1050	60.70	69.81	78.05	82.49
1100	63.61	72.60	80.53	85.11
1150	66.52	75.38	83.01	87.73
1200	69.43	78.16	85.50	90.35
1250	72.33	80.94	87.98	92.97
1300	75.24	83.72	90.46	95.58
1350	78.15	86.51	92.94	98.20
1400	81.05	89.29	95.42	100.82
1450	83.96	92.07	97.90	103.44
1500	86.87	94.85	100.38	106.06
1550	89.78	97.64	102.86	108.68
1600	92.68	100.42	105.35	111.30
1650	95.59	103.20	107.83	113.92
1700	98.50	105.98	110.31	116.53
1750	101.41	108.77	112.79	119.15
1800	104.31	111.55	115.27	121.77
1850	107.22	114.33	117.75	124.39
1900	110.13	117.11	120.23	127.01
1950	113.03	119.89	122.71	129.63
2000	115.94	122.68	125.20	132.25

TABLE B5

COMPARISON OF ELECTRICAL RESISTIVITY VALUES WITH THAT CALCULATED FROM THE BLOCH-GRUNEISEN EQUATION, ASSUMING θ = 286 °K

Temperature (°K)	Th (μohm-cm)		(Th–2% U)N (μohm-cm)		(Th–5% U)N (μohm-cm)	
	$\rho - \rho_o$	ρ_{BG}	$\rho - \rho_o$	ρ_{BG}	$\rho - \rho_o$	ρ_{BG}
80	1.52	2.70	1.62	2.36	1.70	2.17
90	1.93	3.43	2.08	3.00	2.08	2.75
100	2.30	4.18	2.58	3.66	2.48	3.35
110	2.89	4.91	3.12	4.30	2.88	3.94
120	3.44	5.67	3.67	4.96	3.38	4.55
130	4.00	6.40	4.22	5.60	3.88	5.13
140	4.60	7.15	4.79	6.26	4.38	5.74
150	5.20	7.86	5.32	6.88	4.88	6.31
160	5.84	8.59	5.88	7.52	5.38	6.89
170	6.49	9.30	6.42	8.14	5.88	7.46
180	7.12	10.01	6.98	8.76	6.38	8.03
190	7.77	10.69	7.53	9.36	6.88	8.58
200	8.42	11.44	8.10	10.01	7.38	9.18
210	9.07	12.16	8.67	10.64	7.87	9.76
220	9.72	12.76	9.22	11.17	8.36	10.24
230	10.37	13.54	9.78	11.85	8.86	10.86
240	11.02	14.18	10.33	12.41	9.36	11.38
250	11.67	14.96	10.91	13.10	9.85	12.00
260	12.31	15.48	11.46	13.55	10.35	12.42
270	12.98	16.33	12.01	14.30	10.84	13.10
280	13.61	16.95	12.58	14.84	11.34	13.60
290	14.28	17.57	13.12	15.38	11.84	14.10
300	14.93	18.41	13.70	16.12	12.34	14.77
310					12.84	15.31
320					13.34	15.72
330					13.78	16.44
340					14.20	17.00
350					14.61	17.43
360					14.93	17.79
370					15.30	18.61
380					15.57	19.30
390					15.80	19.75
400					16.03	20.15

TABLE B6

CHANGE IN IMPURITY ELECTRICAL RESISTIVITY AS CALCULATED FROM BLOCH-GRUNEISEN EQUATION

Temperature (°K)	$\rho - \rho_P$ (θ = 286 °K) (μohm-cm)	$\rho - \rho_P$ (θ = 532 °K) (μohm-cm)
80	0.93	2.84
90	0.61	2.80
100	0.33	2.75
110	0.09	2.81
120	-0.12	2.78
130	-0.29	2.73
140	-0.44	2.70
150	-0.55	2.64
160	-0.64	2.60
170	-0.70	2.59
180	-0.78	2.54
190	-0.81	2.51
200	-0.91	2.47
210	-0.98	2.45
220	-0.93	2.42
230	-1.06	2.39
240	-1.05	2.36
250	-1.18	2.32
260	-1.06	2.29
270	-1.24	2.30
280	-1.23	2.30
290	-1.18	2.27
300	-1.37	2.27

TABLE B7

SMOOTHED VALUES OF THERMAL CONDUCTIVITY

Temperature (°K)	λ (W/cm-°K) ThN Th-13	(Th-2% U)N Th-16	(Th-5% U)N Th-15	(Th-5% U)N Th-21
80	0.7000	0.3400	0.2715	0.2727
90	0.6680	0.3246	0.2660	0.2668
100	0.6375	0.3176	0.2624	0.2627
110	0.6145	0.3138	0.2598	0.2596
120	0.5957	0.3145	0.2581	0.2574
130	0.5822	0.3155	0.2570	0.2560
140	0.5727	0.3168	0.2565	0.2551
150	0.5651	0.3184	0.2565	0.2548
160	0.5593	0.3202	0.2571	0.2546
170	0.5545	0.3221	0.2580	0.2548
180	0.5503	0.3242	0.2593	0.2552
190	0.5463	0.3265	0.2609	0.2558
200	0.5428	0.3290	0.2628	0.2565
210	0.5397	0.3314	0.2650	0.2575
220	0.5364	0.3338	0.2673	0.2587
230	0.5333	0.3362	0.2698	0.2598
240	0.5301	0.3386	0.2726	0.2611
250	0.5270	0.3410	0.2754	0.2626
260	0.5238	0.3435	0.2778	0.2640
270	0.5208	0.3458	0.2813	0.2656
280	0.5175	0.3482	0.2842	0.2672
290	0.5143	0.3507	0.2871	0.2688
300	0.5112	0.3530	0.2900	0.2706
310	0.5080	0.3555	0.2929	
320	0.5048	0.3580	0.2958	
330	0.5015	0.3605	0.2987	
340	0.4985	0.3629	0.3016	
350	0.4954	0.3653	0.3044	
360	0.4922	0.3678	0.3073	
370	0.4890	0.3702	0.3102	
380	0.4860	0.3727	0.3131	
390	0.4827	0.3750	0.3159	
400	0.4797	0.3775	0.3188	

TABLE B8

TWO COMPONENT SEPARATION OF (Th-2% U)N AND ThN
SAMPLES Th-16 AND Th-13

Temperature (°K)	L($\times 10^8$ $V^2/°K^2$)	λ_L (W/cm-°K)	λ_e (W/cm-°K)	
			ThN	(Th-2% U)N
80	1.882	0.2214	0.4786	0.1186
90	1.850	0.1960	0.4720	0.1286
100	1.812	0.1805	0.4570	0.1371
110	1.800	0.1689	0.4456	0.1449
120	1.804	0.1625	0.4332	0.1520
130	1.827	0.1565	0.4257	0.1590
140	1.875	0.1506	0.4221	0.1661
150	1.921	0.1450	0.4201	0.1734
160	1.981	0.1396	0.4197	0.1806
170	2.040	0.1342	0.4203	0.1879
180	2.085	0.1297	0.4206	0.1945
190	2.129	0.1254	0.4209	0.2011
200	2.167	0.1217	0.4211	0.2073
210	2.202	0.1182	0.4215	0.2132
220	2.232	0.1148	0.4216	0.2190
230	2.258	0.1117	0.4216	0.2245
240	2.280	0.1088	0.4213	0.2298
250	2.296	0.1066	0.4204	0.2344
260	2.305	0.1047	0.4191	0.2388
270	2.324	0.1022	0.4186	0.2436
280	2.322	0.1012	0.4163	0.2470
290	2.330	0.0996	0.4147	0.2511
300	2.329	0.0988	0.4124	0.2542

TABLE B9

TWO COMPONENT SEPARATION OF (Th-5% U)N AND ThN
SAMPLES Th-15 AND Th-13

Temperature (°K)	L($\times 10^8$ $V^2/°K^2$)	λ_L (W/cm-°K)	λ_e (W/cm-°K)	
			ThN	(Th-5% U)N
80	1.998	0.2075	0.4925	0.0640
90	1.854	0.1955	0.4725	0.0705
100	1.778	0.1858	0.4517	0.0766
110	1.750	0.1772	0.4373	0.0826
120	1.760	0.1698	0.4259	0.0883
130	1.788	0.1632	0.4190	0.0938
140	1.837	0.1571	0.4156	0.0994
150	1.881	0.1516	0.4135	0.1049
160	1.938	0.1467	0.4126	0.1104
170	1.991	0.1422	0.4123	0.1158
180	2.032	0.1382	0.4121	0.1211
190	2.071	0.1347	0.4116	0.1262
200	2.105	0.1316	0.4112	0.1312
210	2.135	0.1288	0.4109	0.1362
220	2.159	0.1264	0.4100	0.1409
230	2.179	0.1243	0.4090	0.1455
240	2.192	0.1227	0.4074	0.1499
250	2.203	0.1213	0.4057	0.1541
260	2.211	0.1196	0.4042	0.1582
270	2.216	0.1191	0.4017	0.1622
280	2.212	0.1184	0.3991	0.1658
290	2.215	0.1177	0.3966	0.1694
300	2.212	0.1171	0.3941	0.1729

TABLE B10

TWO COMPONENT SEPARATION OF (Th-5% U)N AND ThN
SAMPLES Th-21 AND Th-13

Temperature (°K)	L($\times 10^8$ $V^2/°K^2$)	λ_L (W/cm-°K)	λ_e (W/cm-°K)	
			ThN	(Th-5% U)N
80	1.962	0.2118	0.4882	0.0609
90	1.822	0.1999	0.4681	0.0669
100	1.749	0.1902	0.4473	0.0725
110	1.723	0.1817	0.4328	0.0779
120	1.735	0.1741	0.4216	0.0833
130	1.762	0.1674	0.4148	0.0886
140	1.812	0.1612	0.4115	0.0939
150	1.857	0.1557	0.4094	0.0991
160	1.916	0.1503	0.4090	0.1043
170	1.972	0.1453	0.4092	0.1095
180	2.016	0.1407	0.4096	0.1145
190	2.060	0.1364	0.4099	0.1194
200	2.101	0.1323	0.4105	0.1242
210	2.137	0.1286	0.4111	0.1289
220	2.167	0.1251	0.4113	0.1336
230	2.194	0.1218	0.4115	0.1380
240	2.217	0.1188	0.4113	0.1423
250	2.236	0.1161	0.4109	0.1465
260	2.250	0.1134	0.4104	0.1506
270	2.268	0.1109	0.4099	0.1547
280	2.273	0.1089	0.4086	0.1583
290	2.285	0.1065	0.4078	0.1623
300	2.290	0.1048	0.4064	0.1658

TABLE B11

ERROR ANALYSIS FOR TWO COMPONENT SEPARATION OF (Th-2% U)N AND ThN SAMPLES Th-16 AND Th-13

	± Error	
Temperature (°K)	$L(\times 10^{8}\ V^2/°K^2)$	λ_L (W/cm-°K)
80	0.078	0.0297
90	0.071	0.0278
100	0.068	0.0262
110	0.067	0.0249
120	0.065	0.0239
130	0.065	0.0231
140	0.065	0.0226
150	0.065	0.0222
160	0.065	0.0218
170	0.066	0.0216
180	0.066	0.0213
190	0.067	0.0211
200	0.067	0.0209
210	0.067	0.0207
220	0.068	0.0206
230	0.068	0.0204
240	0.068	0.0202
250	0.068	0.0201
260	0.068	0.0200
270	0.069	0.0198
280	0.069	0.0197
290	0.069	0.0195
300	0.069	0.0194

TABLE B12

ERROR ANALYSIS FOR TWO COMPONENT SEPARATION OF (Th-5% U)N AND ThN SAMPLES Th-15 AND Th-13

	± Error	
Temperature (°K)	L($\times 10^{8}$ $V^2/°K^2$)	λ_L (W/cm-°K)
80	0.077	0.0302
90	0.072	0.0282
100	0.068	0.0264
110	0.065	0.0251
120	0.064	0.0241
130	0.063	0.0233
140	0.063	0.0227
150	0.063	0.0223
160	0.063	0.0219
170	0.064	0.0216
180	0.064	0.0213
190	0.064	0.0211
200	0.065	0.0209
210	0.065	0.0207
220	0.065	0.0205
230	0.065	0.0204
240	0.066	0.0202
250	0.066	0.0200
260	0.066	0.0199
270	0.066	0.0197
280	0.066	0.0196
290	0.066	0.0194
300	0.066	0.0193

TABLE B13

ERROR ANALYSIS FOR TWO COMPONENT SEPARATION OF (Th-5% U)N AND ThN SAMPLES Th-21 AND Th-13

	± Error	
Temperature (°K)	$L(\times 10^{8} V^2/°K^2)$	λ_L (W/cm-°K)
80	0.077	0.0302
90	0.072	0.0282
100	0.068	0.0264
110	0.065	0.0251
120	0.064	0.0241
130	0.063	0.0233
140	0.063	0.0227
150	0.063	0.0223
160	0.063	0.0219
170	0.064	0.0216
180	0.064	0.0214
190	0.064	0.0211
200	0.065	0.0209
210	0.065	0.0207
220	0.065	0.0205
230	0.065	0.0204
240	0.065	0.0202
250	0.065	0.0200
260	0.065	0.0199
270	0.065	0.0197
280	0.065	0.0196
290	0.065	0.0194
300	0.065	0.0193

TABLE B14

LATTICE COMPONENT OF THERMAL RESISTIVITY OF ThN AND (Th-U)N ALLOYS

Temperature (°K)	Thermal Resistivity (W/cm-°K)		
	(Th-2% U)N Th-16	(Th-5% U)N Th-15	(Th-5% U)N Th-21
80	4.52	4.82	4.721
90	5.10	5.12	5.003
100	5.54	5.38	5.258
110	5.92	5.64	5.504
120	6.15	5.89	5.744
130	6.39	6.13	5.974
140	6.64	6.37	6.203
150	6.89	6.60	6.423
160	7.16	6.82	6.653
170	7.45	7.03	6.882
180	7.71	7.24	7.107
190	7.97	7.42	7.331
200	8.22	7.60	7.559
210	8.46	7.76	7.776
220	8.71	7.91	7.994
230	8.95	8.05	8.210
240	9.19	8.15	8.418
250	9.38	8.24	8.613
260	9.55	8.36	8.818
270	9.78	8.40	9.017
280	9.88	8.45	9.183
290	10.04	8.50	9.390
300	10.12	8.54	9.542

TABLE B15

EXTRAPOLATED THERMAL CONDUCTIVITY DATA

Temperature (°K)	Thermal Conductivity (W/cm-°K)			
	ThN Th-13	(Th-2% U)N Th-16	(Th-5% U)N Th-15	(Th-5% U)N Th-21
350	0.5182	0.3676	0.2879	0.2771
400	0.5085	0.3724	0.2953	0.2837
450	0.5009	0.3766	0.3025	0.2901
500	0.4940	0.3804	0.3095	0.2965
550	0.4885	0.3837	0.3162	0.3024
600	0.4839	0.3870	0.3226	0.3083
650	0.4797	0.3897	0.3286	0.3137
700	0.4762	0.3922	0.3342	0.3189
750	0.4729	0.3943	0.3395	0.3237
800	0.4699	0.3963	0.3443	0.3283
850	0.4675	0.3983	0.3492	0.3327
900	0.4652	0.3999	0.3536	0.3369
950	0.4630	0.4014	0.3578	0.3407
1000	0.4612	0.4030	0.3591	0.3444
1050	0.4594	0.4042	0.3654	0.3477
1100	0.4577	0.4054	0.3690	0.3510
1150	0.4563	0.4066	0.3724	0.3542
1200	0.4550	0.4078	0.3756	0.3572
1250	0.4537	0.4088	0.3786	0.3600
1300	0.4525	0.4098	0.3815	0.3627
1350	0.4514	0.4106	0.3843	0.3652
1400	0.4504	0.4114	0.3868	0.3676
1450	0.4494	0.4122	0.3893	0.3699
1500	0.4486	0.4131	0.3918	0.3723
1550	0.4477	0.4138	0.3941	0.3744
1600	0.4469	0.4144	0.3961	0.3763
1650	0.4461	0.4150	0.3982	0.3782
1700	0.4454	0.4157	0.4003	0.3802
1750	0.4447	0.4161	0.4021	0.3819
1800	0.4440	0.4167	0.4040	0.3836
1850	0.4436	0.4173	0.4059	0.3854
1900	0.4429	0.4178	0.4075	0.3869
1950	0.4424	0.4183	0.4091	0.3884
2000	0.4418	0.4187	0.4107	0.3899

TABLE B16

WEIDEMANN-FRANZ-LORENZ RATIO OF ARC CAST SAMPLES

Temperature (°K)	W-F-L Ratio ($\times 10^8$ $V^2/°K^2$)			
		Rod 1		
	ThN	(Th-2% U)N	(Th-5% U)N	UN
90	3.141	5.960	9.344	
100	3.074	5.279	8.305	11.070
110	3.034	4.923	7.594	
120	3.010	4.693	7.065	10.513
130	2.985	4.540	6.665	
140	2.965	4.417	6.346	9.994
150	2.945	4.309	6.095	
160	2.928	4.221	5.884	9.483
170	2.917	4.142	5.707	
180	2.912	4.075	5.552	9.043
190	2.912	4.019	5.417	
200	2.907	3.969	5.297	8.610
210	2.898	3.927	5.193	
220	2.884	3.888	5.099	8.213
230	2.869	3.854	5.014	
240	2.857	3.821	4.938	7.845
250	2.846	3.794	4.871	
260	2.838	3.766	4.810	7.518
270	2.832	3.742	4.756	
280	2.829	3.717	4.707	7.211
290	2.828	3.695	4.663	
300	2.831	3.671	4.622	6.918
310	2.835	3.648	4.586	
320	2.840	3.624	4.556	6.656
330	2.843	3.599	4.527	
340	2.843	3.574	4.501	6.404
350	2.843	3.546	4.478	
360	2.841	3.517	4.457	6.181
370	2.837	3.489	4.439	
380	2.829	3.463	4.423	5.963
390	2.808	3.437	4.409	
400	2.769	3.414	4.396	5.756

TABLE B17

WEIDEMANN-FRANZ-LORENZ RATIO OF ARC CAST SAMPLE EXPRESSED AS FRACTION OF SOMMERFELD VALUE

Temperature (°K)	W-F-L Ratio $\left(\frac{W\text{-}F\text{-}L}{L_o}\right)$			
	ThN AC-6	(Th-2% U)N AC-1	(Th-5% U)N AC-5	UN
90	1.286	2.440	3.825	
100	1.258	2.161	3.400	4.531
110	1.242	2.015	3.108	
120	1.232	1.921	2.892	4.303
130	1.222	1.858	2.728	
140	1.214	1.808	2.598	4.091
150	1.205	1.764	2.495	
160	1.199	1.728	2.409	3.882
170	1.194	1.695	2.336	
180	1.192	1.668	2.273	3.702
190	1.192	1.645	2.217	
200	1.190	1.625	2.168	3.524
210	1.186	1.607	2.126	
220	1.181	1.591	2.087	3.362
230	1.174	1.578	2.052	
240	1.169	1.564	2.021	3.211
250	1.165	1.553	1.994	
260	1.162	1.542	1.969	3.077
270	1.159	1.532	1.947	
280	1.158	1.521	1.926	2.952
290	1.158	1.512	1.909	
300	1.159	1.503	1.892	2.832
310	1.160	1.493	1.877	
320	1.163	1.483	1.865	2.725
330	1.164	1.473	1.853	
340	1.164	1.463	1.842	2.621
350	1.164	1.451	1.833	
360	1.163	1.440	1.824	2.530
370	1.161	1.428	1.817	
380	1.158	1.418	1.810	2.441
390	1.149	1.407	1.805	
400	1.133	1.397	1.799	2.356

TABLE B18

WEIDEMANN-FRANZ-LORENZ RATIO OF ZONE MELTED SAMPLES

Temperature (°K)	W-F-L Ratio ($\times 10^8$ $V^2/°K^2$)			
	ThN Th-13	(Th-2% U)N Th-16	(Th-5% U)N Th-15	(Th-5% U)N Th-21
80	3.176	6.809	10.25	10.81
90	2.999	5.944	9.038	9.551
100	2.875	5.393	8.129	8.601
110	2.793	4.998	7.411	7.854
120	2.755	4.736	6.857	7.248
130	2.736	4.519	6.401	6.756
140	2.745	4.342	6.024	6.345
150	2.754	4.186	5.708	6.003
160	2.779	4.059	5.444	5.708
170	2.805	3.945	5.218	5.453
180	2.822	3.851	5.025	5.233
190	2.841	3.768	4.858	5.041
200	2.858	3.701	4.715	4.868
210	2.873	3.641	4.590	4.720
220	2.884	3.584	4.478	4.586
230	2.894	3.534	4.352	4.466
240	2.900	3.489	4.300	4.359
250	2.905	3.452	4.225	4.265
260	2.905	3.417	4.151	4.174
270	2.911	3.382	4.099	4.095
280	2.905	3.355	4.044	4.025
290	2.907	3.328	3.994	3.956
300	2.904	3.306	3.948	3.898

TABLE B19

WEIDEMANN-FRANZ-LORENZ RATIO OF ZONE MELTED SAMPLES EXPRESSED FRACTION OF SOMMERFELD VALUE

	W-F-L Ratio $\left(\frac{W\text{-}F\text{-}L}{L_o}\right)$			
Temperature (°K)	ThN Th-13	(Th-2% U)N Th-16	(Th-5% U)N Th-15	(Th-5% U)N Th-21
80	1.300	2.787	4.195	4.423
90	1.227	2.433	3.700	3.910
100	1.177	2.207	3.328	3.521
110	1.142	2.044	3.031	3.215
120	1.127	1.937	2.804	2.967
130	1.119	1.848	2.618	2.766
140	1.123	1.776	2.464	2.597
150	1.126	1.712	2.335	2.457
160	1.137	1.660	2.227	2.336
170	1.147	1.613	2.134	2.232
180	1.154	1.575	2.055	2.142
190	1.162	1.541	1.987	2.063
200	1.169	1.514	1.928	1.993
210	1.175	1.489	1.877	1.932
220	1.180	1.466	1.831	1.877
230	1.184	1.445	1.792	1.828
240	1.186	1.427	1.759	1.784
250	1.188	1.412	1.728	1.746
260	1.188	1.398	1.698	1.709
270	1.191	1.383	1.676	1.676
280	1.188	1.372	1.654	1.648
290	1.189	1.361	1.634	1.619
300	1.188	1.352	1.615	1.596

TABLE B20

SMOOTHED VALUES OF THERMOELECTRIC POWER FOR UN FROM 100 TO 1700 °K

Temperature (°K)	Thermoelectric Power (μV/°K)
100	24.7
150	32.7
200	43.8
250	49.8
300	54.2
350	57.6
400	60.2
450	62.2
500	63.7
550	64.8
600	65.6
650	66.2
700	66.4
750	66.6
800	66.6
850	66.7
900	66.6
950	66.3
1000	65.9
1050	65.3
1100	64.6
1150	63.6
1200	62.6
1250	61.4
1300	60.2
1350	59.0
1400	57.7
1450	56.1
1500	54.5
1550	52.7
1600	51.0
1650	49.1
1700	47.3

TABLE B21

SMOOTHED VALUES OF THERMOELECTRIC POWER FROM ARC CAST SAMPLES

Temperature (°K)	S (μV/°K) ThN AC-6	(Th-1% U)N AC-1	(Th-5% U)N AC-5
90	-0.4	1.4	5.9
100	-0.6	1.5	6.0
110	-0.8	1.6	6.3
120	-0.8	1.8	6.6
130	-0.8	1.9	7.0
140	-0.8	2.0	7.4
150	-0.7	2.1	7.9
160	-0.6	2.2	8.5
170	-0.4	2.3	8.9
180	-0.2	2.4	9.4
190	0	2.5	9.8
200	0.1	2.6	10.2
210	0.3	2.7	10.5
220	0.4	2.7	10.8
230	0.4	2.8	11.1
240	0.5	2.8	11.3
250	0.5	2.8	11.4
260	0.5	2.7	11.5
270	0.5	2.7	11.6
280	0.5	2.5	11.5
290	0.5	2.3	11.4
300	0.5	1.9	11.1
310	0.5	1.7	11.1
320	0.4	1.7	11.4
330	0.3	1.8	11.7
340	0.1	2.1	11.9
350	0	2.4	12.0
360	0	2.6	12.1
370	0	2.7	12.2
380	0	2.8	12.3
390	0.1	2.8	12.4
400	0.3	2.7	12.4

TABLE B22

SMOOTHED VALUES OF THERMOELECTRIC POWER OF (Th-U)N
FOR ZONE MELTED SAMPLES

Temperature (°K)	Thermoelectric Power (μV/°K)		
	ThN	(Th-2% U)N	(Th-5% U)N
80	-0.8	3.8	5.3
90	-0.9	4.2	5.6
100	-1.0	4.6	5.8
110	-1.0	4.9	6.1
120	-1.0	5.3	6.5
130	-0.9	5.6	6.8
140	-0.8	6.0	7.2
150	-0.6	6.3	7.5
160	-0.4	6.6	7.9
170	-0.2	6.9	8.3
180	0	7.2	8.8
190	0.1	7.5	9.2
200	0.3	7.7	9.6
210	0.3	7.9	9.9
220	0.4	8.2	10.2
230	0.5	8.4	10.5
240	0.5	8.5	10.6
250	0.5	8.6	10.8
260	0.5	8.7	10.9
270	0.5	8.7	11.0
280	0.5	8.7	10.9
290	0.4	8.6	10.8
300	0.4	8.5	10.6
310	0.4	8.4	10.5
320	0.3	8.5	10.7
330	0.2	8.8	10.9
340	0.2	9.1	11.1
350	0.1	9.4	11.2
360	0	9.7	11.3
370	-0.1	9.9	11.4
380	-0.2	10.1	11.4
390	-0.3	10.3	11.4
400	-0.4	10.6	11.4

VITA

Samuel Cavin Weaver was born November 10, 1941, in Minot, North Dakota, but lived most of his life in Branson, Missouri. He attended Southwest Missouri State College at Springfield, Missouri, from 1959 to 1961, and graduated from Missouri School of Mines and Metallurgy at Rolla, Missouri, in January 1964, with a Bachelor of Science degree in Metallurgical Engineering. He began his graduate work at Rennsselaer Polytechnical Institute, Windsor, Connecticut, and completed work for a Master of Science degree from the University of Tennessee in December 1968.

He was employed at Pratt and Whitney's Connecticut Advanced Nuclear Engineering Laboratory in Middletown, Connecticut, from January 1964 to August 1965, and at the Oak Ridge National Laboratory from September 1965 to March 1971. He is presently President and a member of the Board of Directors for U. S. Nuclear, Inc., Oak Ridge, Tennessee.

He is married to the former Carol Jane Schwaegler of Zwingle, Iowa. They have two children, Samuel and Daniel.